MAREES TERRESTRES

BULLETIN D'INFORMATIONS

INTERNATIONAL CENTER FOR EARTH TIDES
CENTRE INTERNATIONAL DES MAREES TERRESTRES

Federation of Astronomical and Geophysical Data Analysis Services
(FAGS)

International Association of Geodesy - International Gravity Field Service
(IAG – IGFS)

BIM
1 3 5

15 JUILLET 2002

Editeur: Dr. Bernard DUCARME
Observatoire Royal de Belgique
Avenue Circulaire 3
B-1180 Bruxelles

INTERNATIONAL CENTER FOR EARTH TIDES
CENTRE INTERNATIONAL DES MAREES TERRESTRES

(Federation of Astronomical and Geophysical Data Analysis Services)
(FAGS)

Director: B.DUCARME **Email: ducarme@oma.be**

Observatoire Royal de Belgique **Tel: 32-2-3730211**
Avenue Circulaire, 3 **Fax: 32-2-3749822**
B- 1180 Bruxelles, Belgium http://www.astro.oma.be/ICET/

FOREWORD

As you certainly noticed, the presentation of our publication has been slightly modified to take into account the new organisation of the Services inside the International Association of Geodesy (IAG). The International Center for Earth Tides (ICET), which is publishing this "Bulletin d'Information des Marées Terrestres" (BIM), is a member of the Federation of Astronomical and Geophysical Data Analysis Services (FAGS) and is also an IAG Service.
For efficiency purposes it has been decided to confederate three existing IAG Services (the International Gravimetric Bureau, the International Geoid Service and ICET) into the new International Gravity Field Service (IGFS). This new entity is also welcoming new partners.
ICET will continue to publish regularly the BIM as before. We wish to express here our gratitude to the Royal Observatory of Belgium which is supporting this publication.

We have now the pleasure to publish the Proceedings of two important Earth Tide meetings which took place in Jena in March 2002. The material is so large that we have to split the publication in three successive issues: BIM135, BIM136 and BIM137. However ICET decided to make all the papers directly available from its WEB site. You can access them already now. This is the first time and, to reduce the printing and mailing costs in the future, we are planning to propose next year a kind of electronic journal with the papers directly available on line. A traditional publication will continue for libraries and on request for individual scientists.

B.Ducarme
Editor

BIM 135

15 juillet 2002

Third Workshop of the Global Geodynamics Project (GGP) on Superconducting Gravimetry

WORKSHOP .....
Program of the sessions.....10601

VIRTANEN H.....
Summary of observation in Metsähovi 1994-2001 with SG T020.....10605

NEUMEYER J., BARTHELMES F., COMBRINCK L., DIERKS O., FOURIE P.... .....
Analysis results from the SG registration with the dual sphere superconducting gravimeter at SAGOS (South Africa) 10607

KRONER C, JAHR TH. and JENTZSCH G.....
Comparison of results obtained with a dual sensor superconducting gravimeter.....10617

ALMAVICT, M., HINDERER J., GEGOUT P., ROSAT S. and CROSSLEY D. .....
On the use of AG data to calibrate SG instruments in the GGP network: example of Strasbourg J9.....10621

HARNISCH, M. HARNISCH G. and FALK R.....
Improved scale factors of the BKG superconducting gravimeters, derived from comparisons with absolute gravity measurements.....10627

SUN H-P., HSU H-T. and YONG W.....
On the calibration for GWR superconducting gravimeter GWR-C032 with an absolute.....
gravimeter FG-5 in Wuhan.....10639

MEURERS B.....
Aspects of gravimeter calibration obtained by time domain comparison of gravity records 10643

VENEDIKOV A.P., ARNOSO J. and VIEIRA R.....
VAV: A program for tidal data processing.....10651

HINDERER J., ROSAT S., CROSSLEY D., AMALVICT M., BOY J-P. and GEGOUT P.
Influence of different processing methods on the retrieval of gravity signals from GGP data 10653

DIERKS O. and NEUMEYER J.....
Comparison of Earth tides analysis programme. 10669

ROSAT S., HINDERER J. and CROSSLEY D. .....
A comparison of the seismic noise levels at various GGP stations.....10689

WIDMER-SCHNIDRIG R.....
What can superconducting gravimeters contribute to normal mode seismology?.....10701

LEI X.E., HSU H-T. and SUN H-P. .....
Preliminary results of the Earth's free oscillations after Peru earthquake observed using a SG in China 10713

ZURN W., BAYER B. and WIDMER-SCHNIDRIG R.....
The 3.7 mHz - gravity signal on June 10, 1991 10717

Third Workshop of the Global Geodynamics Project (GGP) on Superconducting Gravimetry

Jena, March 11 - 13, 2002

Program

Monday, 11 March, Session 1 - GGP Business

D. Crossley, Hinderer, J., H., and Ducarme, B.: Introduction, Status of GGP Network and ICET Data

GGP groups: Status of the GGP stations - short reports on the running of the stations, status of the data, processing, future problems, etc.

Ritschel, B. and Palm, H.: Status of GGP-ISDC, report about last year's activities and future plans

Monday, 11 March, Session 2 - Extended Station Reports

H. Virtanen: Summary of observation in Metsähovi 1994 - 2001 with SG T020

J. Neumeyer, Barthelmes, F.,Combrinck L., Dierks, O. and Fourie P.: Analysis results from the SG registration with the dual sphere superconducting gravimeter at SAGOS (South Africa)

C. Kroner, Jahr, Th., and Jentzsch, G.: Comparison of results obtained with a dual sensor superconducting gravimeter

Monday, 11 March, Session 3 - SG Calibration

M. Amalvict, Hinderer, J., Gegout, P., Rosat S. and Crossley, D.: On the use of AG data to calibrate SG instruments in the GGP network : Example of Strasbourg - J9

Richter, B., Harnisch, G. and Nowak, I.: Experimental and computational contributions to estimate the accuracy and reliability of the Frankfurt Calibration System (FCS)

Harnisch, M., Harnisch, G., and Falk, R.: Improved scale factors of the BKG superconducting gravimeters, derived from comparisons with absolute gravity measurements

H.-P. Sun, Hsu, H.-T. and Yong Wang: On the calibration of a superconducting gravimeter GWR-C032 with an absolute gravimeter FG-5 in Wuhan

B. Meurers: Aspects of gravimeter calibration obtained by time domain comparison of gravity records

Monday, 11 March, Session 4 - Data Processing

A.P.Venedikov, Arnoso, J., and Vieira, R.: VAV: A program .. for tidal data processing

J. Hinderer, Rosat S., Crossley D., Amalvict M., Boy J.-P. and Gegout P.: Influence of different processing methods on the retrieval of gravity signals from GGP data

O. Dierks and Neumeyer, J.: Comparison of earth tides analysis programs

Tuesday, 12 March, Session 5 - Free Oscillations

S. Rosat, Hinderer, J. and Crossley D.: A comparison of the seismic noise levels at various GGP stations

R. Widmer-Schnidrig: What can superconducting gravimeters contribute to normal mode seismology?

X.E. Lei, Hsu, H.-T., and Sun, H.-P.: Preliminary results of the Earth's free oscillations after Peru earthquake observed using a SG in China

W. Zürn, Bayer, B., and Widmer-Schnidrig, R.: A 3.7 mHz - gravity signal on June 10, 1991

Tuesday, 12 March, Session 6 - General Applications

H.-P. Sun, Ducarme, B., and Xu, J.-Q.: Preliminary results of the free core nutation eigenperiod obtained by stacking SG observations at GGP stations

H.-P. Sun, Xu, J.-Q. and Ducarme, B.: Experimental earth tidal models of the core resonance obtained by stacking tidal gravity measurements from GGP stations

D. Crossley and Hinderer J..: GGP ground truth for satellite gravity missions

T.F. Baker, Bos, M.S. and Williams, S.D.P.: Confronting superconducting and absolute gravity measurements with models

Tuesday, 12 March, Session 7 - Special Session

T.v. Dam and **Plag, H.-P.**: The IERS Special Bureau for Loading: Tasks and Products Discussion

Tuesday/Wednesday, 12/13 March, Session 8 - Tides

P. Varga: Tidal friction, geodynamical properties and rotation speed in the remote geological past

T. Sato, Y. Tamura, K. Matsumoto, Y. Imanishi and H. McQueen: Parameters of the fluid core resonance estimated from superconducting gravimeter data

B. Ducarme, Sun, H.-P. and Xu, J.-Q.: New investigation of tidal gravity results from the GGP network

B. Richter, Harnisch, M., Harnisch, G., Falk, R.: Long-period tides and absolute gravity measurements

P. Varga, Mentes, Gy. and Eperne Papai, I.: Theoretical description of the extensional and rotational strain tensor components

Tuesday/Wednesday, 12/13 March, Session 9 - GGP Finale

General discussion

Summary of observations in Metsähovi 1994 – 2001 with T020

H. Virtanen
Finnish Geodetic Institute

Extended abstract

We present a short, all-around summary of the registration of superconducting gravimeter T020 (SG) at Metsähovi station for years 1994-2001. The gravity registration started at August 10 1994. The data of 20 days have been lost totally, the longest data gap has been 11 days. Detailed results of present research activities are given below. The studies comprise full gravity spectrum from microseism to Chandlerian periods. Metsähovi is a geodetic laboratory with large number of observation programs: permanent GPS, GLONASS, satellite laser ranging, DORIS beacon, absolute gravity and seismograph station (STS-2). In addition to gravity and air-pressure, various environmental quantities have been recorded. These include e.g. groundwater level, soil moisture, properties of snow, precipitation and other weather parameters. Though the gravimeter stands on the crystalline bedrock, gravity residuals correlate with the groundwater level, as shown in Figure 1. The top panel gives refined gravity record from 1994 to 2001. All known effects on gravity have been removed except the groundwater. Lower panel gives the groundwater level with the range of 2 metres.

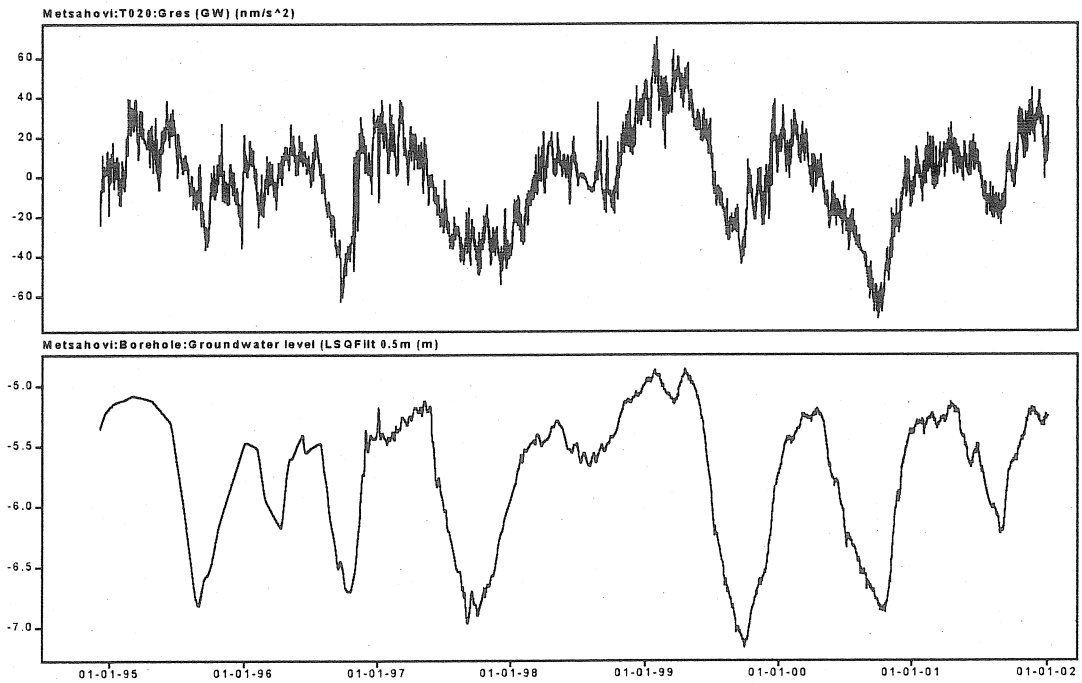

Figure 1. Top: The hourly gravity residuals from 1994 to 2001 excluding correction of groundwater (28 $ms^{-2}m^{-1}$). Bottom: The observed level of groundwater in the borehole near the gravity laboratory.

Results of some loading studies by atmosphere and by Baltic Sea are presented. To improve the correction of air-pressure, we have used regional data instead of single admittance by regression (3.10 $nms^{-2}hPa^{-1}$). For atmospheric loading calculations HIRLAM (High Resolution Limited Area Model) data (2000-2001) for North Europe were used. At the grid-points, spacing 44 km, surface pressure and temperature were given every 6 hours. The pressure field from 0.5° up to 10° was convoluted with the atmospheric load gravity Green's functions. We have applied the surface temperature and topographic corrections. Regional results were interpolated to hourly values. In the

local zone (< 0.5°) hourly local air-pressure observed at Metsähovi was used. The gravity was then corrected with calculated values, without any regression between gravity and local air-pressure.

The gravity station is about 15 km from the Baltic Sea. Metsähovi is 1000 km from the ocean, thus global ocean loading is relatively small. The tidal variation in the Baltic is of the order of centimetres only. The variation in the Baltic sea level is mostly non-tidal and driven internally by wind stress and air-pressure. The nearest tide gauge is in Helsinki at a distance of 30 km. The hourly data by several tide-gauges were available for years 2000-2001. As an example shown in the Figure 2, variation in the Baltic Sea level is directly seen in the gravity residual of the SG at Metsähovi.

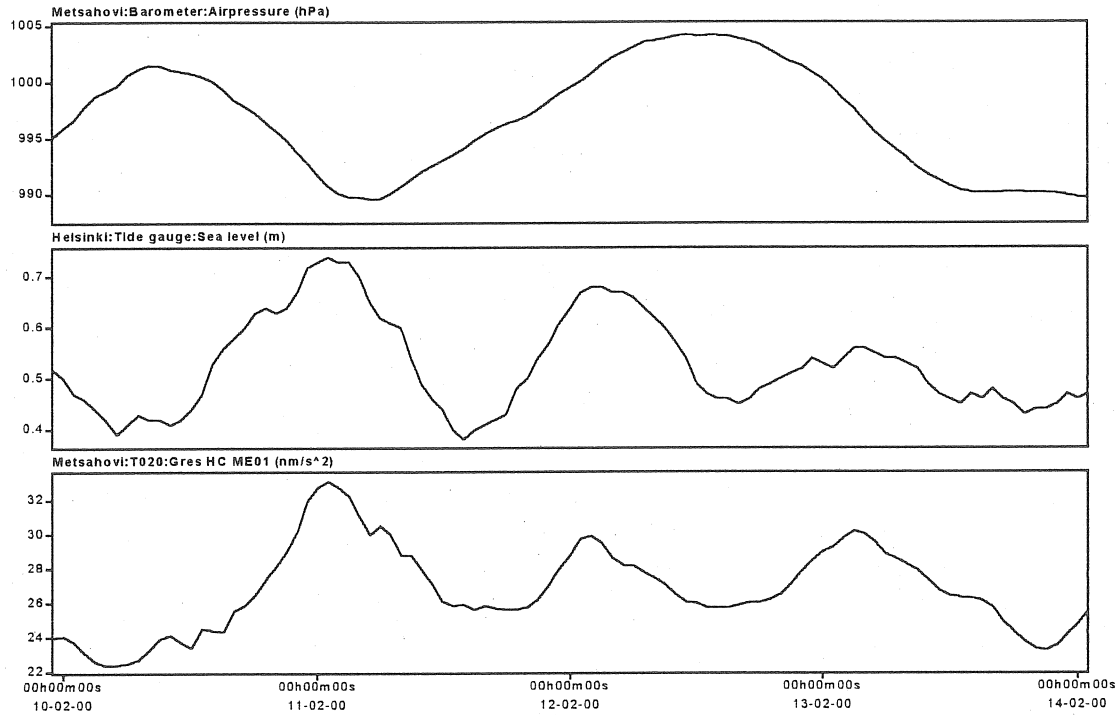

Figure 2. Top: Air-pressure at Metsähovi from 10th to 14th of February 2000 (hPa). Middle: The sea level at Helsinki (m). Bottom: The gravity residuals with HIRLAM corrected air-pressure (nms^{-2}).

Table 1. The effect of sea-level (SL) and air-pressure corrections on the gravity residuals from January 1 2000 to December 31 2001.

	RMS nms^{-2}	Regression $nms^{-2}m^{-1}$	Correlation	Reduction
Gres (Single 3.10)	9.2			0 %
Gres (HIRLAM)	9.5			-3 %
Gres (Single 3.10)/SL	7.9	21.6	0.51	+14 %
Gres (HIRLAM)/SL	7.4	27.6	0.63	+19 %

The standard atmospheric correction to gravity, using coefficient(s) obtained by regression from the local barometer, partly includes the effect of sea level. Independent atmospheric corrections using the pressure field from HIRLAM bring better out the loading effect of Baltic Sea level. The combination of HIRLAM for atmosphere and local tide gauge data for sea level reduces the gravity residual by 19%, compared with just a single admittance for local air pressure, as presented in Table 1.

Analysis Results from the SG registration with the Dual Sphere Superconducting Gravimeter at SAGOS (South Africa)

Jürgen Neumeyer[1)], Franz Barthelmes[1)], Ludwig Combrinck[2)] Olaf Dierks[1)], Piet Fourie[3]
[1)]GeoForschungZentrum Potsdam, Division 1, Telegrafenberg, 14473 Potsdam, Germany
[2)] Hartebeesthoek Radio Astronomy Observatory, Krugersdorp , South Africa
[3)] South African Astronomical Observatory, Sutherland , South Africa

1. Introduction

The "South African Geodynamic Observatory Sutherland of GFZ" (SAGOS) has been constructed by GFZ at the site of the "South African Astronomical Observatory" (SAAO) near Sutherland. The observatory is designed for high precision geodynamic observations of the Earth with ground instruments and space techniques (Neumeyer and Stobie, 2000).

The installed Superconducting Gravimeter (SG) and the environmental sensors are continuously recording data since February 2000 (Neumeyer et al. 2001). These data have been preprocessed and analyzed. In detail the noise at the site, the tidal parameters, the vertical surface shift and the free oscillation of the Earth after the Peru earthquake on June 23rd 2001 have been analyzed.

2. Calibration of the two gravity sensors

For calibration of the two SG gravity sensors three different methods have been selected applied for each sensor. For each sensor the same method has been used. The results are shown in figure 2.

1. The first calibration factors have been determined by least square fit between the tidal prediction (theoretical tides) for the Sutherland site and the output signals of the gravity sensors.
2. Parallel registration of the SG and the LaCoste & Romberg Feedback Gravimeter D02 which has been calibrated at the Hanover calibration line. The calibration factor for each sensor has been determined by changing the SG gravity sensor calibration factor until the amplitude factor for the partial tide O1 had the same value as the O1 amplitude factor determined by the LaCoste & Romberg Gravimeter registration (reference).
3. Parallel registration of the SG and an Absolute Gravimeter (Hinderer et al., 1991, 1998). In February and March 2001 parallel registrations have been carried out with the Absolute Gravimeters
    a) FG5 from "Ecole et Observatoire des Sciences de la Terre"Strasbourg , France from 2001-02-01 to 2001-02-09
    b) JILAg5 FROM " Finnish Geodetic Institute" Masala, Finland from 2001-03-21 to 2001-03-29

    From both time series absolute and SG measurements the outliers and the linear trend have been removed. For determination of the calibration coefficient a linear least square fit has been performed between the Absolute Gravimeter and the SG data.

In a second estimation the method of Fourier coefficients has been used. This method determines the amplitudes for selected frequencies from both data sets. The calibration factor is determined by the amplitude ratio obtained from Absolute Gravimeter and SG measurements at these frequencies. Both methods deliver equivalent results within the required accuracy.

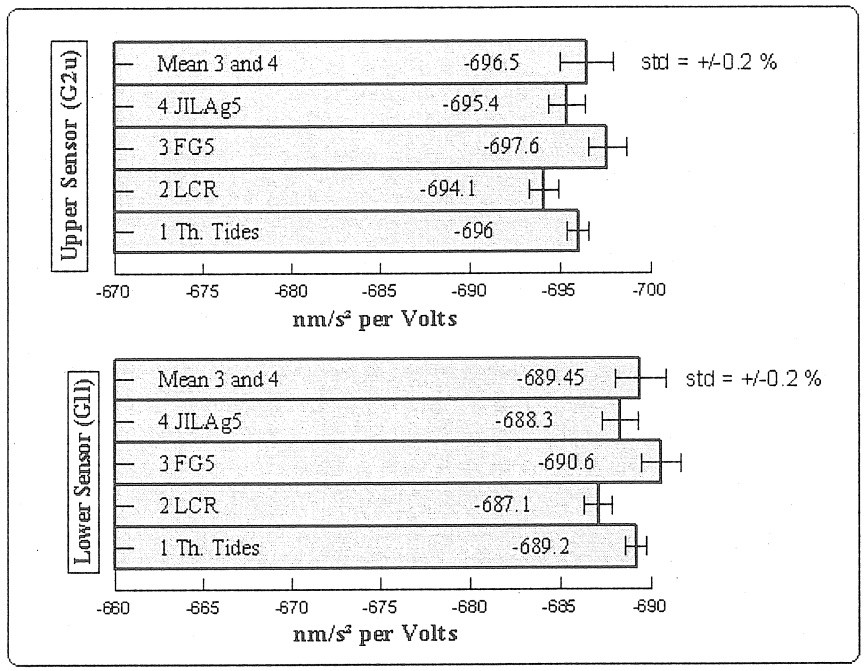

Fig. 2 Calibration results of SG D037

As the final calibration coefficient the mean between the parallel registrations of the Absolute Gravimeters FG5 (3), JILAg5 (4) and the SG is used. The calibration factors have been determined with an standard deviation of 0.2 percent.

In a step response experiment (Van Camp et al., 1999) the time delay of both sensors has been determined to 8.7 seconds for G1l (lower sensor) and to 7.9 seconds for G2u (upper sensor).

3. Noise at the site SAGOS

The investigation of weak gravity effects requires a low noise site. The quality of the recorded gravity data depends on the noise at the site and the noise of the instrument. The noise of the instrument is small in the inspected frequency band.

For estimation of the noise at the site the Noise Magnitude is used (Banka and Crossley, 1999). The Noise Magnitude [NM =10* log(PSD) in dB] is calculated by the Power Spectral Density (PSD) of raw gravity data (1sec sampling rate) with a length of one month (February 2001). In figure 1 the Power Spectral Density (PSD, left axis) and the allocated Noise Magnitude (NM, right axis) are diagrammed as function of the frequency. Additionally the Noise Magnitude according to the „New Low Noise Model" is diagrammed as graph NLNM (gray).

A comparison between the Noise Magnitude and the New Low Noise Model shows that the Noise Magnitude characterizing the quality of the site is close and even smaller as the New Low Noise Model values at frequencies below 1 mHz. This comparison shows that the site offers excellent conditions for high precision gravity measurements and the detection of weak gravity signals. In this frequency range the free oscillations of the Earth have their modes too. Therefore they can be detected very well.

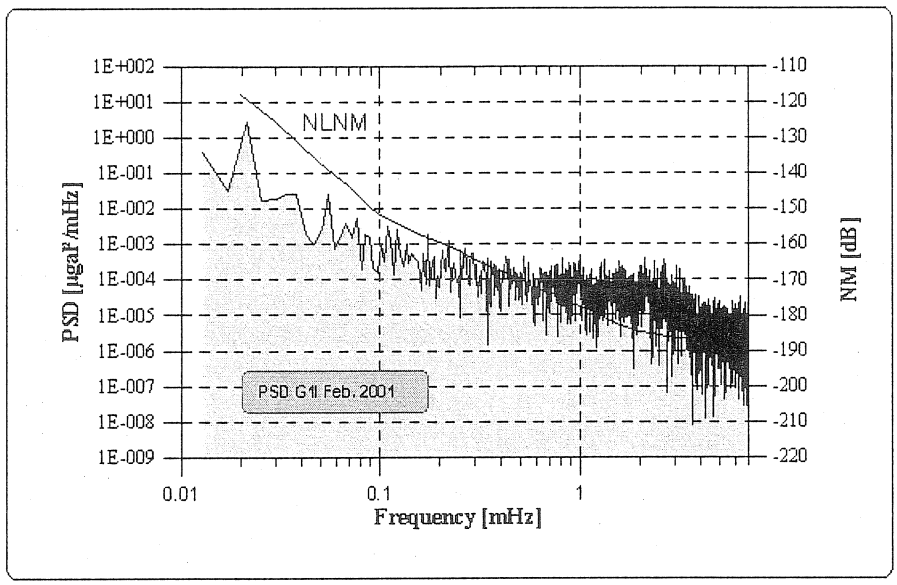

Fig 1 Noise spectra at SAGOS site
Black: Power Spectral Density (PSD) and Noise Magnitude (NM) of lower SG sensor (G11))
Grey: New Low Noise Model (NLNM)

4. Evaluation of gravity and environmental data

For processing of the gravity and atmospheric pressure data the Earth Tide Data Processing Package ETERNA 3.3 (Wenzel, 1996) has been used. The first high precision tidal amplitudes, amplitude factors δ and phase leads κ have been determined for the Sutherland site and the South African region. The tidal analysis has been performed on 18 month SG and atmospheric pressure data. The amplitude factors and the phase leads are in good agreement for both sensors of the SG. The standard deviation of the tidal analysis is ± 0.7 nm/s^2.

Figure 3 shows the Wahr-Dehant model (white columns) and the measured tidal amplitudes (black columns) for Sutherland. The tidal amplitudes are latitude dependent. The long periodic waves MF. MM, SSA und SA are small at Sutherland latitude of 32.38 deg South. The minimum of these waves are about at latitude 35 deg. Therefore seasonal effects (like the atmospheric pressure effect) and the polar motion (like the separation of the annual part of the polar motion from the annual tidal wave SA) can be investigated with small influence of the annual and semiannual tidal waves. The diurnal waves (maximum amplitude at latitude 0 deg) and semidiurnal waves (maximum amplitude at latitude 45 deg) can be observed well.

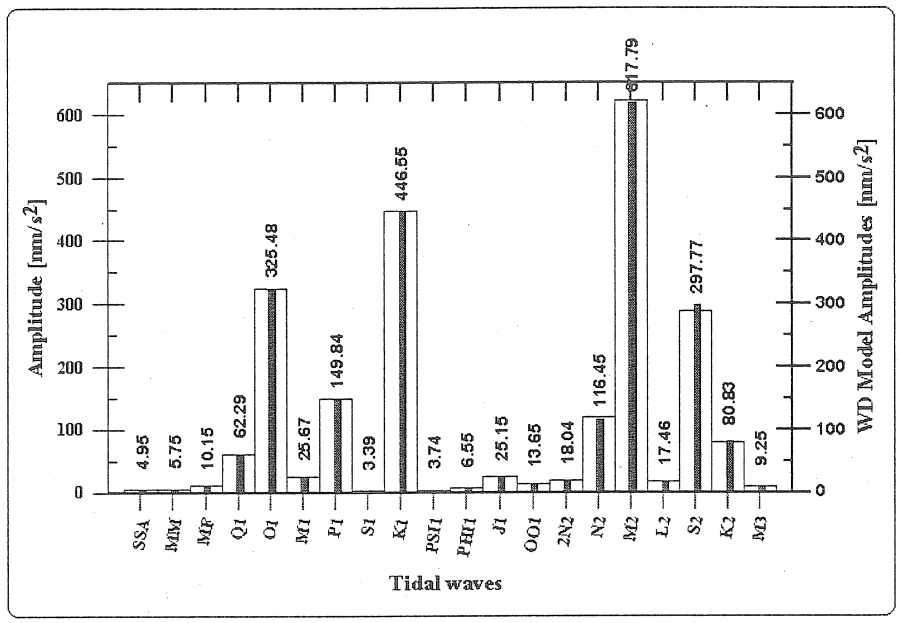

Fig. 3 Tidal amplitudes for SAGOS
White columns: Wahr-Dehant Model amplitudes
Black columns: measured amplitudes

Figure 4 shows the determined tidal parameters. For comparison the Wahr-Dehant model (white columns) and the observed amplitude factors (gray columns) are pictured. The deviations from the model can be seen clear. One reason for the deviations is the influence of the ocean loading. Therefore the ocean loading correction has been calculated for the diurnal partial tides Q1, O1, P1, K1 and the semidiurnal partial tides N2, M2, S2, K2 (Schwiderski model). The black columns show the ocean loading corrected amplitude factors. One can see that the ocean loading corrected amplitude factors come closer to the model values for the semidiurnal waves N2, M2, S2, K2 and the diurnal waves P1 and K1. For the diurnal waves Q1 and O1 the ocean loading corrected amplitude factors depart form the model values. The reason for this behavior is the ocean loading model as shown by Ducarme et. al. 2002.

The model phase is zero. Larger deviations from the model phase show the semidiurnal waves 2N2, N2, M2, L2, S2, K2 and the diurnal wave S1. The ocean corrected phase leads for the diurnal waves N2, M2, S2, K2 give a good improvement close to zero (observed values near 5 deg phase lead). The ocean corrected phase lead for the diurnal waves Q1, O1, P1, K1 become larger than the uncorrected value.

The strong deviation (δ and κ) of the S1 wave to the model my be caused by the influence of the daily variations of the atmospheric pressure. Investigations for a better modeling of the atmospheric pressure influence are necessary. Furthermore the discrepancies between real measurements and the Earth tide and ocean models for the South African region have to be investigated more in detail. These discrepancies have to be abolished by improving the models and data correction for non-tidal induced gravity effects.

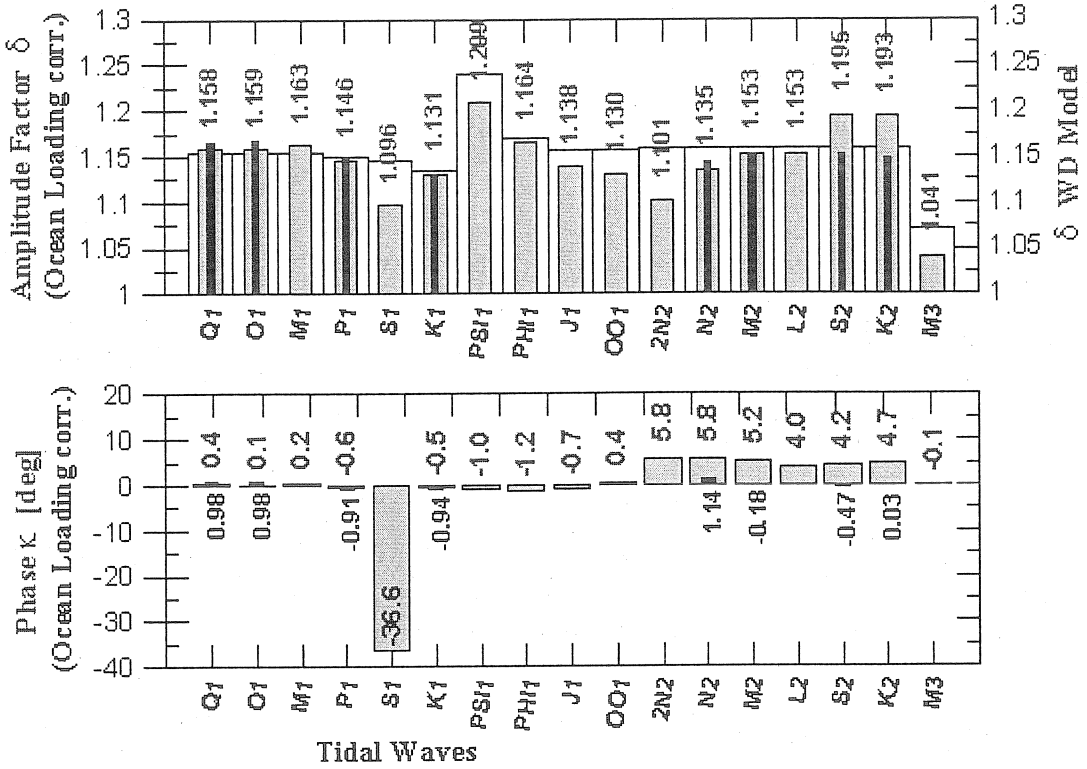

Fig 4 Earth tide parameters δ and κ for SAGOS
White columns: Wahr-Dehant Model parameter δ
Gray columns: calculated parameters δ and κ
Black columns: Ocean loading corrected parameters δ and κ

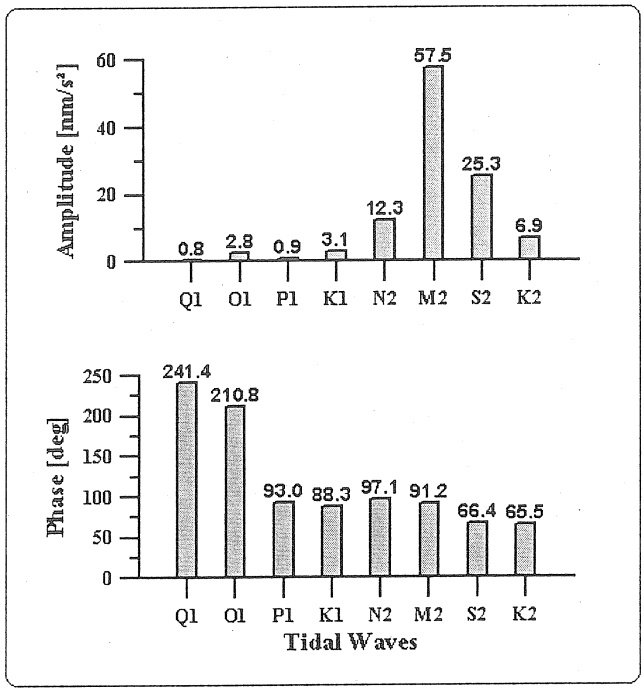

Fig.5 Ocean loading effect at SAGOS for the main tidal waves

The ocean loading effect to gravity has been calculated with the program LOAD97. Figure 5 shows the correction amplitudes and the phases for the main diurnal and semidiurnal tidal waves. The most affected wave is M2 with an amplitude of 57.5 nm/s^2.

5. Vertical surface shift caused by Earth tides and atmospheric pressure

Because of the elastic behaviour of the Earth the tides and changing loading on the Earth (e.g. mass redistributions in the atmosphere measured by the atmospheric pressure) cause vertical surface shift ζc. This shift can be calculated by the following formula

$$\zeta c := \frac{-\Delta g}{g} \cdot \frac{R \cdot h2}{2 \cdot \delta 2 \cdot (1 + k2)}$$

With the elastic parameters of the Earth the Love number for elastic deformation h2 = 0.6137 and the Love number for deformation potential k2 = 0.3041, the gravimetric factor $\delta 2$= 1.159 , the geocentric radius R= 6373830.451m determined with the tidal analysis and g = 9.79079 m/s^2 determined by absolute gravity measurements the elastic deformation coefficient for SAGOS has been determined to Δvs =-1.32 mm/µgal according to the formula

$$\Delta vs := \frac{-R \cdot h2}{2 \cdot \delta 2 \cdot g \cdot (1 + k2)}$$

The vertical shift for SAGOS can be calculated by multiplying Δvs with the measured gravity changes Δg corrected for the atmospheric pressure effect. (Neumeyer, 1995; Kroner and Jentzsch, 1999). The atmospheric pressure correction of the gravity data has been done with the atmospheric pressure admittance coefficient apc = -2.92 µgal/hPa calculated for

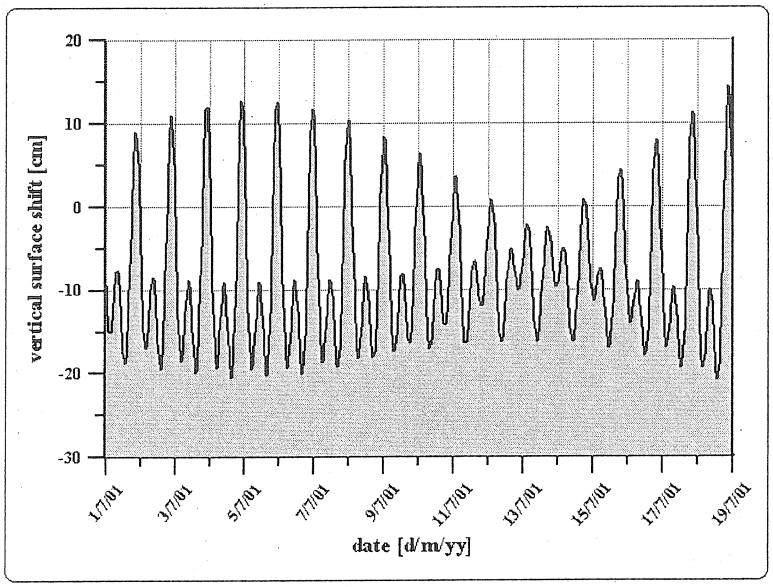

Fig. 6 Vertical surface shift caused by the Earth tides for Sutherland

SAGOS. These determined gravity changes induced by atmospheric pressure changes have been subtracted from the gravity data. Figure 6 shows the vertical surface shift ζc at SAGOS for18 days in July 2001. The maximal vertical shift caused by the Earth tides and mass redistribution in the atmosphere during the time from March 27th 2000 to August 1st 2001 is 41.9 cm.

For separation of the atmospheric pressure influence to the vertical surface shift the Greens function method which calculates the attraction and deformation term separately has to be used (Sun, 1995; Neumeyer et al. 1998). With the deformation term the surface shift induced by atmospheric pressure changes can be calculated. For the Potsdam site this effect is about 2.3 cm (Neumeyer et al., 2001)

These vertical surface shift is derived from gravity measurements only. The gravity signal includes height and mass changes. It is impossible to separate mass and height changes with the gravity measurements. Therefore GPS measurements have been used to calculate the height changes for SAGOS. .

Initial results to determine vertical displacement due to tidal forces using GPS were obtained using the GAMIT (King and Bock, 1999) software package. Additional scripts were developed to allow processing of 24 hour GPS data files using a stepped, sliding window technique. The scripts allow seamless processing over the start and end of the individual 24 hour GPS data files. Alternative processing strategies were used, varying the length of the window, the step size as well as GPS station geometry and station position constrains. No earth-tide and ocean-tide modeling were used during the processing and GPS stations were constrained horizontally but not vertically. ITRF2000 coordinates and velocities were used. The best results were obtained using a four hour window, which is stepped by 30 minutes, followed by a running average procedure to smoothen the results. This results in 48 four hour sessions per day.

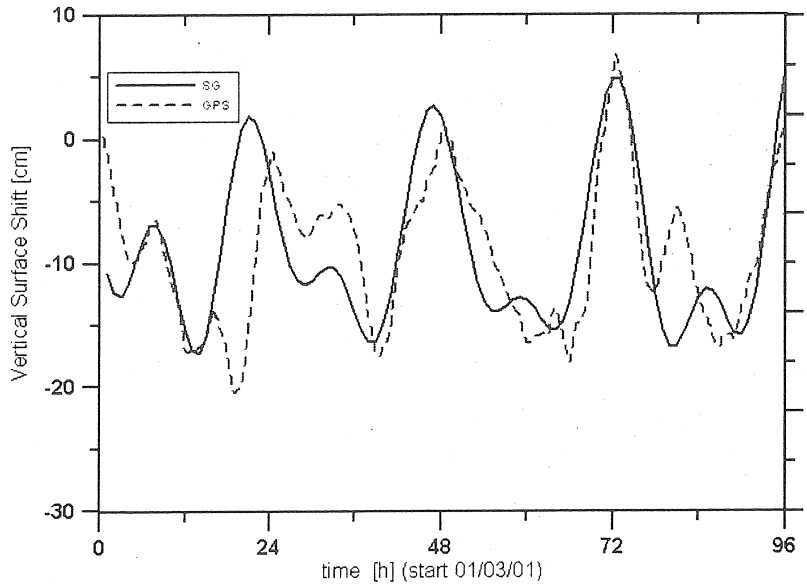

Fig. 7 Vertical surface shift calculated from gravity (black line) and GPS (dashed line)

Only two GPS stations (separated by about 1000 km), the IGS stations HRAO (located at Hartebeesthoek Radio Astronomy Observatory near Pretoria)) and SUTH (located at

Sutherland) were finally used. Another station towards the south (SIMO) located at Simonstown marginally degraded solutions and was therefore not included. This station (SIMO) will be included once a new station has been installed at Windhoek, Namibia, which is towards the north of Sutherland. The degrading effect is probably due to poor network geometry. Including both SIMO and the Windhoek station will improve the network geometry considerably. Improved network geometry in combination with further development of the processing scripts is expected to yield improved results.

The first result of this calculation is shown in Figure 7. The black line shows the vertical surface shift derived from gravity measurements and the dashed line shows the first result from the GPS measurements. There is in some parts already a good agreement of both curves.

6. Analysis of the free oscillation modes after the Peru earthquake on June 23rd 2001

The Earthquake near the coast of Peru (latitude 16.14S, longitude 73.312 W, depth 33 km,) on June 23rd 2001 at 20:33:14.14 with a magnitude of 8.4 has been recorded by the mode channel of the Superconducting Gravimeter at SAGOS site.

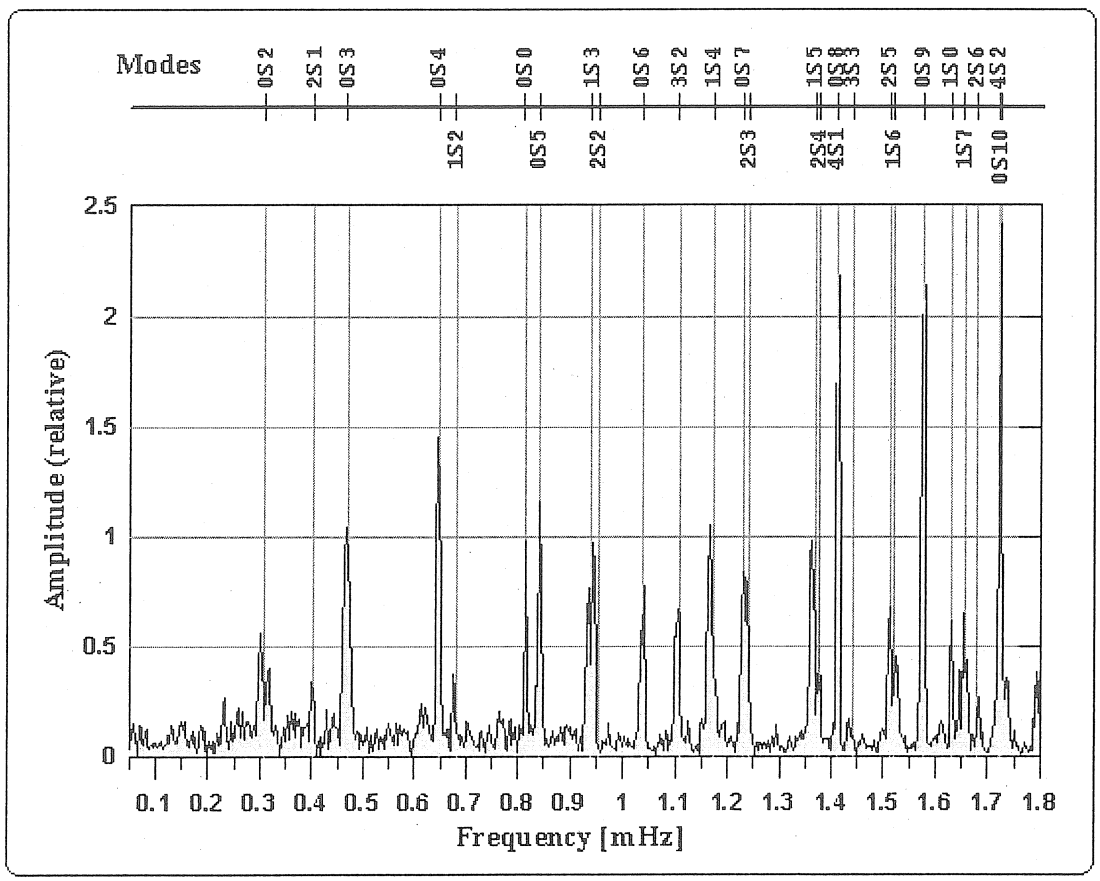

Fig 7 Spheroidal free oscillation modes after the Peru earthquake on June 23rd 2001

The data of this Earthquake have been analyzed for detection of the free oscillation modes of the Earth. For this purpose a data set of 96 hours after the Earthquake has been corrected for atmospheric pressure. After low pass filtering (corner frequency of the filter 6 mHz) of the data the mode spectrum has been calculated by using a Hanning window (Fig. 7). Above the spectrum the different spheroidal modes are listed. Their model frequencies are at the horizontal grid lines.

The spectrum shows the model modes up to the frequency of 0S10. Especially the long periodic modes 0S3, 2S1 and 0S2 are very well marked after this Earthquake and less disturbed because of the low noise site. Compared to the results of Van Camp (1999) 2S1 and 0S2 are clear detected.

7. Acknowledgment

We thank very much Jacques Hinderer, Martine Amalvict and Bernard Luck "Ecole et Observatoire des Sciences de la Terre" Strasbourg ,France for carrying out absolute gravity measurements at SAGOS with the Absolute Gravimeter FG5 in February 2001.
We thank very much Jaakko Makinen " Finnish Geodetic Institute" Masala, Finland for carrying out absolute gravity measurements at SAGOS with the Absolute Gravimeter JILAg5 in March 2001.

References

Banka, D., Crossley, D., (1999) Noise levels of superconducting gravimeters at seismic frequencies, Geophys. J. Int. 139, 87-97

Crossley, D., Hinderer, J., Casula, O., Francis, O., Hsu, H.T., Imanishi, Y., Jentzsch, G., Kääriäinen J., Merriam J., Meurers B., Neumeyer J., Richter B., Sato D., Shihuya K., van Dam T., (1999) Network of Superconducting Gravimeters Benefits a Number of Disciplines, EOS. Trans. Am. Geoph. Union, 80, 11, 125-126

Ducarme, B., Sun, H.-P., Xu, Q.X. (2002) New Investigations of Tidal Gravity Results from the GGp Network, submitted to Marees Terrestres Bulletin d'Informations, Brussels

Hinderer, J., Amalvict, M., Franzis, O., Mäkinen, J., (1998) On the calibration of superconducting gravimeters with the help of absolute gravity measurements, in Proc. 13th Int. Symp. Earth Tides,
Brussels 1997, Eds.: B. Ducarme and P. Paquet, 557-564

Hinderer, J., Florsch, N., Mäkinen, J., Legros, H., Faller, J. E., (1991) On the calibration of a superconducting gravimeter using absolute gravity measurements, Geophys. J. Int., 106, 491-497

King, R. W., and Bock Y., (1999) Documentation for the GAMIT GPS analysis software, Mass. Inst. of Technol., Cambridge Mass.

Kroner C., Jentzsch G., (1999) Comparison of different barometric pressure reductions for gravity data and resulting consequences. Phys. Earth Planet. Inter. 115, 205-218.

Neumeyer J. (1995) Frequency dependent atmospheric pressure correction on gravity variations by means of cross spectral analysis. Marees Terrestres Bulletin d'Informations, Bruxelles, 122, 9212-9220.

Neumeyer J., Barthelmes F., Wolf D. (1998) Atmospheric Pressure Correction for Gravity Data Using Different Methods. Proc. of the 13th Int. Symp. on Earth Tides, Brussels, 1997, Eds.: B. Ducarme and P. Paquet, 431-438.

Neumeyer J., Barthelmes F., Wolf D., (1999): Estimates of environmental effects in Superconducting Gravimeter data. Marees Terrestres Bulletin d'Informations, Bruxelles, 131, 10153-10159

Neumeyer, J. and Stobie B., (2000): The new Superconducting Gravimeter Site at the South African Geodynamic Observatory Sutherland (SAGOS). Cahiers du Centre Europeen de Geodynamique et de Seismologie, Volume 17, 85-96.

Neumeyer J., Brinton E., Fourie P., Dittfeld H.-J., Pflug H., Ritschel B., (2001): Installation and first data analysis of the Dual Sphere Superconducting Gravimeter at the South African Geodynamic Observatory Sutherland. Journal of the Geodetic Society of Japan Vol. 47, No.1, 316-321

Neumeyer,J., Barthelmes F., Dittfeld H.-J., (2001) Ergebnisse aus einer sechsjährigen Registrierung mit dem Supraleitgravimeter am GFZ Potsdam, Zeitschrift für Vermessungswesen, Heft 1, Jg. 126, 15-22

Sun H.-P., (1995) Static deformation and gravity changes at the Earth's surface due to the atmospheric pressure. Observatoire Royal des Belgique, Serie Geophysique Hors-Serie, Bruxelles.

Van Camp M., (1999) Measuring seismic normal modes with the GWR C021 superconducting gravimeter. Phys. Earth Planet. Inter. 116, 81-92.

Van Camp M., Wenzel H.-G., Schott P., Vauterin P., Francis O., (1999) Accurate transfer function determination for superconducting gravimeter, Geophys. Res. Lett., VOL. 27, NO. 1, 37-40.

Wenzel, H.-G., (1996) The nanogal software: Earthtide data processing package ETERNA 3.3. Marees Terrestres Bulletin d'Informations, Bruxelles, 124, 9425-9439.

Comparison of results obtained with a dual sensor superconducting gravimeter

C. Kroner, Th. Jahr and G. Jentzsch
Institute of Geosciences, Friedrich-Schiller-University Jena

Extended Abstract

In this extended abstract we sum up some new results regarding gravity observations at the Geodynamic Observatory Moxa (Germany) and refer to already published works (Kroner, 2001; Kroner et al., 2001).

Superconducting gravimeters are a sensitive tool that allows studies of variations in the earth's gravity field from long-periodic seismology to long-term changes like polar motion. Different models of these gravimeters are available, one having a dual sensor system. The original intend behind this model was to have a mean to check the gravity data for arbitrary steps, a problem that occurred in the earlier gravimeter generation. Additional side coils keep the sphere of the upper sensor unit exactly above the lower one. The distance between the sensor units is approx. 20 cm.

From analyses of 27 months of gravity data obtained with the dual sensor superconducting gravimeter at the Geodynamic Observatory Moxa informations are gained about the agreement and the discrepancies between the two data sets. The signal contents is separately compared in the free oscillation band, the tidal frequencies, and in the long-term trend.

1. Free oscillation band and tidal frequencies

In both frequency ranges the data of lower and upper sensor show an almost indistinguishable signal contents. The tidal parameters (amplitude factor δ and phase lag Δ) obtained for the diurnal to ter-diurnal tidal bands and for the long-periodic tides are identical within the error bars (Table 1). The mean power spectra of the residuals (Figure 1) between 0.1 and 50 mHz are close the 'New Low Noise Level' (NLNM; Peterson, 1993). The spectrum of the difference data between the two sensors is characterized by a uniform level between 0.4 and 15 mHz. In general the curve of the difference data is on the same level or only slightly lower

Tab.1: Tidal parameters obtained with ETERNA 3.4 (comp. Wenzel, 1996) for lower and upper sensor, 99/12/19-02/02/17.

wave group	lower sensor		upper sensor	
	δ	Δ[°]	δ	Δ[°]
O1	1.14932	0.1512	1.14932	0.1505
	0.00008	0.0039	0.00008	0.0041
K1	1.13684	0.2446	1.13685	0.2452
	0.00006	0.0030	0.00006	0.0031
M2	1.18635	1.6250	1.18635	1.6264
	0.00005	0.0023	0.00005	0.0023
S2	1.18437	0.3539	1.18461	0.3481
	0.00010	0.0049	0.00010	0.0050
m0	0.627 nm/s²		0.642 nm/s²	

wave group	lower sensor		upper sensor	
	δ	Δ[°]	δ	Δ[°]
SSA	1.14911	-4.9813	1.16137	-2.9399
	0.26270	14.3762	0.26126	14.1231
MM	1.17286	0.7983	1.16744	0.8423
	0.02183	1.0480	0.02169	1.0458
MF	1.13787	0.1540	1.13726	0.2211
	0.00630	0.3166	0.00626	0.3146
MTM	1.15111	-1.4269	1.15108	-1.5692
	0.02105	1.0557	0.02091	1.0486
m0	3.814 nm/s²		3.753 nm/s²	

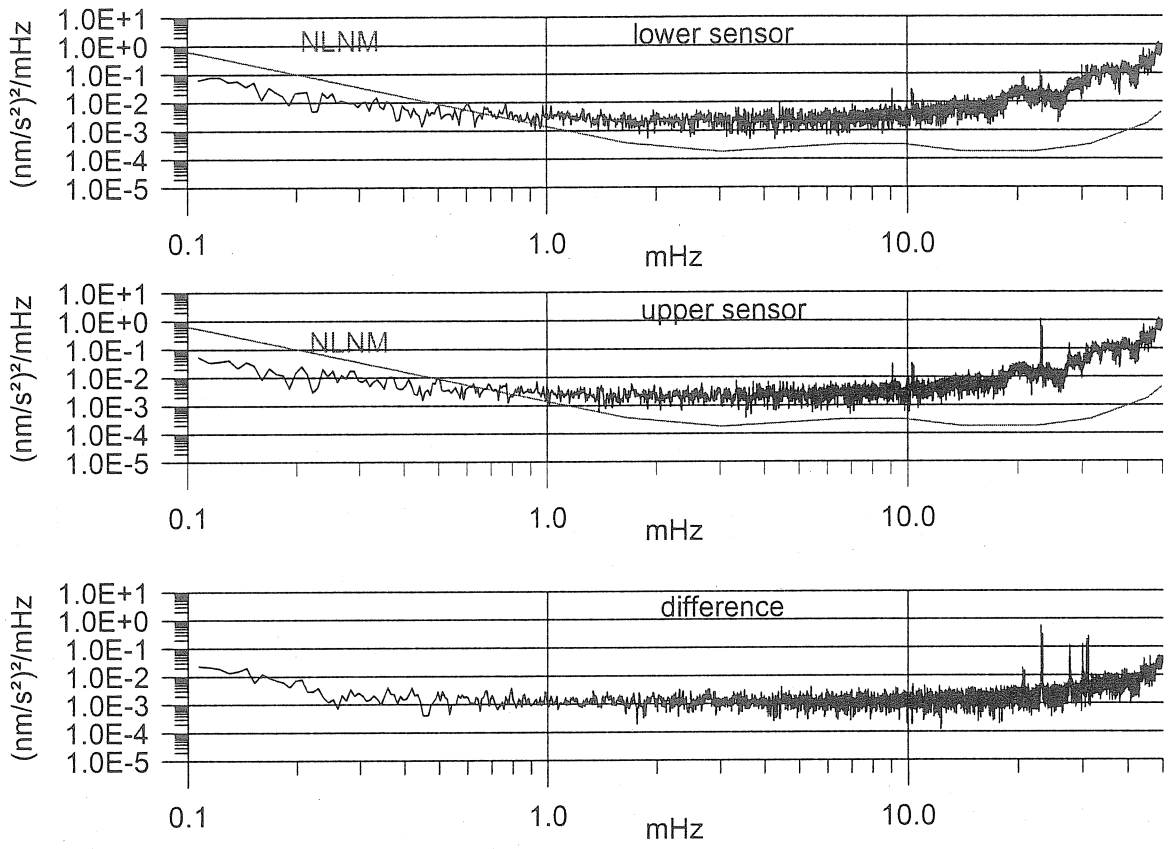

Fig. 1: Mean power spectral density of gravity residuals of lower and upper sensor and their difference for five arbitrary days. For comparison the curve of the NLNM is given (Peterson, 1993). The calculation of the spectra is carried out according to Banka et al. (1997). The peaks at frequencies above 20 mHz cannot be explained yet.

than the curves of the residuals. This indicates that in this frequency range instrumental noise dominates. The power spectral density of the data at frequencies below 0.14 mHz (= 0.5 cph) is given in Figure 2a. These spectra are no mean spectra, but were calculated from the total 27 months of data. In addition the power spectrum of the sum and the difference of the gravity data is shown (Fig. 2b). The spectra are characterized by a flat level between 0.15 cph (0.04 mHz) and 0.5 cph (0.14 mHz) and a rising level below 0.15 cph. In the semi-diurnal band energy due to tides is still left in the data. The sum and the difference spectrum show the same features, but the levels of the curves clearly differ from those of the single gravity data sets. The curve of the difference spectrum is about one order of magnitude below and the one of the sum spectrum about one order of magnitude above the level of upper and lower senor. This result indicates that to a certain extent the data of the two gravimeter sensors have an identical signal contents. The source of this energy is not clear. It could be environmental influences like hydrologically-induced effects that affect the whole spectral range of observation without having peaks at distinct frequencies. In order to clarify this result similar spectra should be calculated for other superconducting gravimeters with a dual sensor system and compared with the Moxa spectra.

Finally, for both, the free oscillation band as well as for the frequency bands of the short-periodic tides the tendency is discernable that the data of the lower sensor are slightly less noisier than the data of the upper sensor. The opposite is valid for the long-periodic tidal bands.

2. Long-term variations

When tides, modeled polar motion and barometric pressure influence are removed from the data, a linear long-term trend of both residual curves emerges. The drift rate of the lower sensor is about 44 nm/s²/a, the upper sensor shows a drift about 26 nm/s²/a. There is no explanation available yet of this different drift behaviour. The comparison between drift-free residuals and the polar motion signal shows a good agreement. An adjustment of the polar motion signal to the residuals yields an amplitude factor of 1.15±0.05 for the lower sensor and of 1.16±0.06 for the upper sensor.
The difference curve between the data of lower and upper sensor with only the different long-term trend removed has a peak-to-peak amplitude of about 20 nm/s² and contains a conspicuous long-periodic variation in the range of about one year (Fig. 3). A similar variation can be found in air temperature. Since it is known that the gravimeter acts as a gradiometer with regard to hydrological fluctuations in the observatory surroundings (Kroner, 2001), it can be assumed that the correlation with air temperature goes back to soil moisture changes which are strongly correlated to saisonal air temperature variations. Longer data sets and the calculation of the water budget for Moxa Observatory will give more information about this.

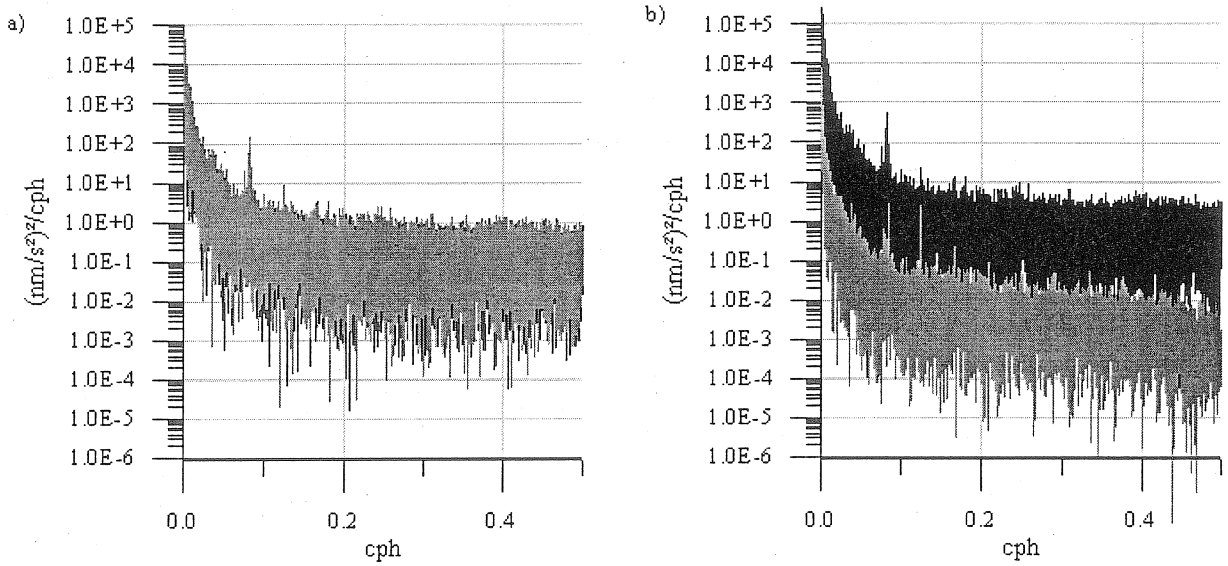

Fig.2: Power spectral density of gravity residuals: a) – lower sensor, – upper sensor, b) – sum of residuals, – difference of residuals.

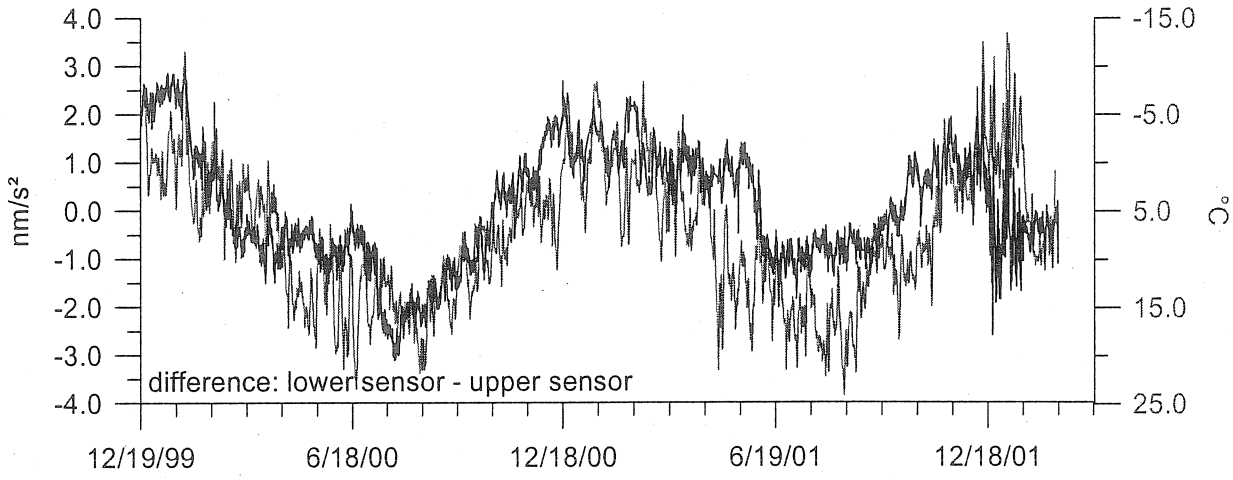

Fig. 3: Difference of gravity residuals and comparison with air temperature, 99/12/19-/02/02/17.

References

Banka, D., Crossley, D., and Jentzsch, G., 1997. The seismic noise magnitude and its application to superconducting gravimeters. Eos, Trans. Am. Geophys. Union, 78 (46, Suppl.), 462.

Kroner, C., 2001. Hydrological effects on gravity data of the Geodynamic Observatory Moxa. J. Geod. Soc. Japan, vol. 47, no. 1, 353-358.

Kroner, C., Jahr, T., and Jentzsch, G., 2001. Comparison of data sets recorded with the dual sphere superconducting gravimeter CD 034 at the Geodynamic Observatory Moxa. J. Geod. Soc. Japan, vol. 47, no. 1, 398-403.

Peterson, J., 1993. Observations and modeling of seismic background noise. *Open File Report* 93-332, U.S. Department of Interior, Geological Survey, Albuquerque, New Mexico.

Wenzel, H.-G., 1996. The nanogal software: Earth Tide data processing package ETERNA 3.30. Bull. d'Inf. Marees Terr., 124, 9425-9439.

On the use of AG data to calibrate SG instruments in the GGP network. Example of Strasbourg - J9

M. Amalvict, J. Hinderer, P. Gegout, S. Rosat and D. Crossley

EOST - I.P.G. Strasbourg (CNRS – ULP)
5 rue René Descartes 67084 Strasbourg cedex France

mamalvict@eost.u-strasbg.fr

Abstract

This paper is devoted to the presentation of several types of results related to the calibration of the Strasbourg superconducting gravimeter (SG) by the use of parallel recording with the Strasbourg absolute gravimeter (AG). First we compare the scale factors resulting of two calibration algorithms: one involves the individual drops of the AG while the second one involves the AG gravity averaged over a 'set'; we find that the results of two methods are in very good agreement when there is no perturbation (such an earthquake) during the period of measurements. Second we analyse the series of individual scale factors derived from March 1997 to June 2001; the series does not exhibit any clear behaviour (trend, periodicity, ...), in opposition to what is commonly observed with the series of mean values of gravity. Finally, we present what we name a "global calibration" which consists in a single calibration process of the whole series of data get after merging the individual experiments. The feasibility of this process is due to the small drift of the SG. The scale factor for the global calibration is - 79.40 ± 0.03 μGal/volt and is close to the mean value of the 32 individual scale factors, which is - 79.19 ± 0.35 μGal/volt.

1. Introduction

Many presentations and discussions during the third GGP workshop held in Jena in March 2002 have pointed out that the knowledge of the precise calibration factor of SGs plays a more and more crucial role. This is due to the increasing accuracy required in the processing of both absolute and relative gravity data, in order to observe geodynamical phenomena. In this work, we focus on the calibration of the SG#C026 which will be treated as a case-example for any other SG. This is the first part of a wider paper involving calibrations of SGs belonging to the GGP network (Crossley et al., 1999), performed with the FG5#206 (Amalvict et al., 2002a). The compact SG#C026 has been continuously recording, at the Gravity Observatory, J9, located close to Strasbourg, since July 1996 (following SG#T005 which was operating since 1987). Its scale factor is derived from the parallel record of gravity variations by the AG FG5#206 which (as well as the SG), belongs to the French scientific community and is operated by the team of the Gravity Observatory since its purchase in January 1997. When the two instruments are operated at the same time at the Strasbourg-J9 Observatory, they record the gravity variations in two different rooms separated by 10 meters or so.

2. Calibration algorithms

Different calibration methods are used to calibrate SGs, leading to comparable results (Francis et al., 1998). Here, we apply the procedure of superposing the records obtained with two kinds of instruments (SG/AG). The principle is to fit the two data sets using a least square adjustment according to the linear relation:

$$y=bx+a$$

where y stands for the AG data and is expressed in μGal, x for the SG feedback output and is expressed in volt, b is the scale factor expressed in μGal/volt, and a is the offset (value for which the fitting line intercepts the ordinate-axis) is expressed in μGal. As the two meters record the same signal, which means that they are submitted to the same gravity, no correction of (geo)physical phenomenon is applied to either data set.
At Strasbourg, there are two different sampling rates for the SG: 2 seconds and 1 minute. The SG data are first cleaned for spikes, large and identified offsets, gaps, if any. The principle of the FG5 is based on the free fall of an object in the vacuum. According to the operating procedure of the AG, a number of drops (e.g. 25, ..., 150) are grouped in a so-called 'set' and then a statistical value of gravity is computed for the set. We use 10 or 15 seconds between two drops and 15, 30 or 60 minutes between two sets.
We present two ways of calibrating the SG, according to these two entities: the drops and the sets and we shall first ask ourselves how much the value of the calibration factor is depending on the algorithm used for its derivation.

a. Drop by drop algorithm

In this first method, we use the individual *drop* gravity values of the AG (y in μGal) without any processing, which means that no values are *a priori* removed from the data. Nevertheless, a rejection criterion is applied later: a statistics is calculated for every set leading to a given σ, then a drop gravity value is rejected when the difference between this value and the mean gravity value of the set is greater than $n\,\sigma$ (currently n=3; this is the value used in the examples given in Table 1), where the value of n is adjustable, depending on the noise level; a study of the influence of this parameter is in progress. To these data, we superimpose the SG output for gravity values with a 2 second sampling (x in volt); each drop of the AG is then compared to the closest sample of the SG.

b. Step by step algorithm

In this second method, we use the *set* gravity values of the AG (y in μGal) resulting of the statistical processing of the drop gravity values; a rejection criterion of outlier sets (1σ) is applied in this first process of the AG data, prior to the calibration. Then, from the SG output for gravity values with a 1 minute sampling (x in volt), the calibration software derives the value of the output at the time corresponding to the time of the set. Finally we superimpose the two series of data.

c. Comparison of the results

We present in Table 1 the calibration factors obtained when using the two codes for an arbitrary selection at different periods of time. We see that under 'normal' conditions, the values of the scale factors are close, as well as the corresponding standard deviation. Nevertheless, in the case of June 2001, the greater discrepancy between the results is due to the fact that an earthquake of magnitude larger than 8, occurred in Peru during the parallel measurements. In the set by set method, outlier sets are removed during the processing of AG data, which is not the case for the drop by drop method. It is clear that a drop rejection should be done in such a noisy situation; the study exhibiting the influence of the level of the

criterion rejection is in progress. The last column of Table 1 is the ratio $(b_d - b_s)/b_s$; it is, as expected, very small except in the case of the Peru earthquake in June 2001.

	set by set scale factor b_s µGal/volt	σ (b)	drop by drop scale factor b_d µGal/volt	σ (b)	$(b_d - b_s)/b_s$ 10^{-4}	
July 1998	-79.04	0.12	-79.05	0.12	1.3	
January 2000	-78.96	0.31	-78.94	0.38	-2.5	
April 2001	-78.96	0.28	-78.90	0.39	-7.6	
May 2001	-79.25	0.09	-79.21	0.13	-5.1	
June 2001	-78.98	0.08	-79.37	0.26	49.4	Peru earthquake

Table 1. Scale factors according to different experiments and methods.

3. Four-year series of individual calibrations

In a second stage, we present the results of the different calibrations experiments performed individually. For this purpose, we analysed the data according to the set-by-set method.

a. Main features

As we already mentionned, it is very important to be sure of the accuracy of the scale factor, in order to carefully analyse the information provided by the long records of the SGs. At the Strasbourg Observatory, we are in a good situation for having several determinations of the calibration factor per year. Thus, we have derived 32 individual calibration factors from March 1997 to June 2001. The extreme values are - 80.33 (May 1997) and – 78.44 (December 2000), leading to a peak to peak discrepancy of 1.89 µGal/volt or 1.2 % maximum difference. The mean value of the 32 experiments is b = - 79.19 ± 0.35 µGal/volt. This value is in agreement with the ones previously derived (Amalvict et al;, 1998, 2001a). Taking into account the error bars on this mean value, only three determinations of the scale factor are outliers, namely May 1997, September 1999 and December 1999. Further on, no obvious trend is observed in these data.

b. Periodogram

In view of the previous paragraph, the calibration factor can be regarded as quite stable in time; nevertheless, looking for a potential periodicity of the scale factor, we present a periodogram of the data. The largest peak, still only weakly significant at a probability of 0.5, is at roughly four cycles per year, which means a period of about three months; such a possible periodicity would still have to be (geo)physically explained. A similar study on the mean gravity value at J9 during the same 5-year time span leads to a much more clear annual variation (Amalvict et al., 2002b).

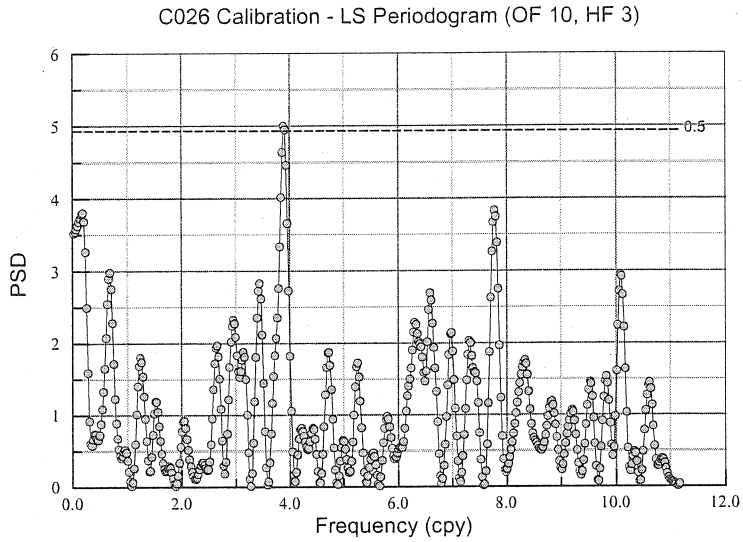

Figure 1. Periodogram of the scale factor individual determinations.

c. Discussion

Thus, we have not observed any clear variation in time of the scale factor of the SG (no trend, no periodicity). Of course, we feel quite happy with this since it would be quite difficult to explain any change in the value of the scale factor. Such a stability is observed elsewhere (Falk et al., 2001, Ogasawara, 2001); nevertheless some other series can present a trend which is certainly an artefact due to the small number of measurements (Amalvict et al., 2001b). One could think of some variations in the electronics due to temperature variations for instance. In that respect, it is worth noting that, in our data set, the extreme values of the calibration factor correspond to the extreme values of the individual determination of mean g. This could indicate poor AG measurements due to unexplained instrumental problems.

4. Global calibration

Assuming that i) the drift of the SG is small (the 'instrumental' drift is about +3.96 μGal/year) and ii) it can be well corrected for spikes, offsets, gaps, the data have been processed all together as a single experiment, in order to obtain only one calibration factor for the whole series. The software for the set by set method has been used.

a. Main features

For the absolute gravimeter data, we have concatenated the 32 individual series, which corresponds to 9 937 sets (after having previously removed noisy sets in a pre-processing) and about 450 000 drops. The SG data consist of roughly 2 300 000 values at 1 minute sampling; the offsets, due to storm, lightning, helium refilling, earthquakes, ... have been corrected for, which is the most delicate operation to be performed since it requires often subjective decisions concerning the significance and correction of offsets that appear in the data (see the discussion in Hinderer et al, this issue).

Some comments should be made concerning the determination of the SG drift. Analysing the time series of the mean values of the gravity at J9 from March 1997 to June 2001, we observe a linear trend of +1.2 μGal/year (Amalvict et al., 2002b). Our assumption is then that the total (i.e. observed) SG drift is the sum of the (purely) instrumental SG drift and of

the "geophysical" trend deduced from AG observations. The SG data being then as "clean" as possible, we process as usually to derive the calibration factor.

b. Results

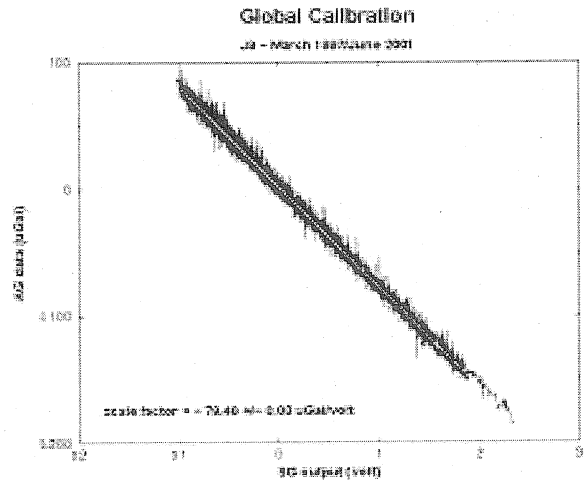

Figure 2. AG versus SG data in the global calibration experiment from March 1997 to June 2001.

We obtain a calibration factor equal to - 79.40 ± 0.03 μGal/volt, which can be compared to the mean value of the 32 individual calibrations which was -79.19 ± 0.35 μGal/volt. The (formal) standard deviation is much smaller for the global calibration, due to the huge number of processed data. We can also note that a similar derivation has been previously done for a shorter period of time (March 1997 – April 1998) leading to a value of – 79.21 ± 0.05 μGal/volt (Amalvict et al, 1999).

5. Conclusions

We have presented different results referring to the calibration of SG#C026 using AG FG5#206 at Strasbourg-J9: i) the linear adjustment by two methods using all individual drops or separate sets leads to no significant difference in the calibration factors; ii) 32 individual calibration factors have been obtained between March 1997 and June 2001, the average of which is b = - 79.19 ± 0.35 μGal/volt. The value is stable and is not related to the seasonal fluctuation observed on the gravity itself; iii) the instrumental drift of the SG (observed drift - AG trend) is very small, which allows to perform a calibration on the whole period involving parallel measurements. The calibration factor of this 'global' calibration is b = - 79.40 ± 0.03 μGal/volt, value in agreement with the mean of the individual calibrations. The actual precision on the calibration factor lies somewhere between the two values (0.35 and 0.03), the first one does not take into account the number of measurements and the second one does not take into account the 'fact that the determination of the factor is not continuous. The corresponding relative errors are respectively 4 ‰ and 0.4 ‰.
The stability of the scale factor of SG#CO26 over more than four years, whatever the period of time, is of great importance in view of geodynamical applications of SG records. It seems

that the relative error is approaching the limit value of 1 ‰ which is necessary for geodynamical goals.

6. References

Amalvict M., Hinderer J., Francis O., & Mäkinen J., 1998, Comparison between absolute (AG) and superconducting (SG) gravimeters, in Forsberg R., Feissel M. and Dietrich R. (eds) 'Geodesy on the Move'. Gravity, Geoid, Geodynamics and Antarctica, IAG Symposia **119**, 24-29.

Amalvict M., Hinderer and Boy J.P., 1999, A comparative analysis between an absolute gravimeter (FG5-206) and a superconducting gravimeter (GWR C026) in Strasbourg: news results on calibration and long term gravity changes; Bolletino di Geofisica, 40, n°2-3.

Amalvict M., Hinderer J., Boy J.P. and Gegout P., 2001a, A 3 year comparison between a superconducting gravimeter (GWRC026) and an absolute gravimeter (FG5#206) in Strasbourg (France) , Journal of Geodetic Society of Japan, **47**, 334-340.

Amalvict M., McQueen H. & Govind R. 2001b, Absolute Gravity Measurements and Calibration of SG CT #31 at Canberra, 1999-2000, Journal of Geodetic Society of Japan, **47**, 410-416.

Amalvict et al., 2002a, On the use of AG data to calibrate SG instruments in the GGP network, in preparation.

Amalvict et al.,2002b, Long term stability of the gravity at Strasbourg J9, in preparation.

Crossley D., Hinderer J., Casula G., Francis O., Hsu H.-T., Imanishi Y., Jentzsch G., Kääriänen J., Merriam J., Meurers B., Neumeyer J., Richter B., Shibuya K., Sato T. and van Dam T., 1999, Network of superconducting gravimeter benefits a number of disciplines, Eos, 80, N°11, 121,125-126.

Falk R., Harnish M., Harnish G., Nowak I., Richter B. and Wolf P., 2001, Calibration of the superconducting gravimeters SG103, C023, CD029 and CD030, Journal of Geodetic Society of Japan, **47**, 22-27.

Francis O., Nibauer T.M., Sasagawa G., Klopping F. and Gschwind J., 1998, Calibration of a superconducting gravimeter by comparison with an absolute gravimeter FG5 in Boulder, Geophysical Research Letters, **25**, n°7, 1075-1078.

Hinderer J., Rosat S., Crossley D., Amalvict M., Boy J.-P. and Gegout P., 2002, Influence of different processing methods on the retrieval of gravity signals from GGP data, B.I.M., this issue.

Ogasawara S., Higashi T., Fukuda Y. and Takemeto S., 2001, Calibration of a superconducting gravimeter with an absolute gravimeter FG5 in Kyoto, Journal of Geodetic Society of Japan, **47**, 404-409.

Acknowledgments – This is EOST contribution N° 2002-13-UMR7516.

Improved Scale Factors of the BKG Superconducting Gravimeters, Derived from Comparisons with Absolute Gravity Measurements.

Martina Harnisch *, Günter Harnisch *, Reinhard Falk **
* formerly Bundesamt für Kartographie und Geodäsie (BKG)
** Bundesamt für Kartographie und Geodäsie (BKG)
Richard-Strauss-Allee 11, D-60598 Frankfurt am Main

1. History

Calibration results of several superconducting gravimeters (SG) owned by BKG were presented at the Earth Tides Symposium 2000 at Mizusawa [1]. The calibrations were based mainly on comparisons with absolute gravimeters (AG). As far as possible, the scale factors were compared with results from the Frankfurt Calibration System (FCS), which uses an artificial calibration signal, generated by sinusoidal vertical movement of the SG. The scale factor of the CD030 at Bad Homburg derived from comparisons with AG is very reliable (9 campaigns with the absolute gravimeter FG5-101, error of the weighted mean ±0.88 nm s^{-2}/V for the lower and ±0.84 nm s^{-2}/V for the upper system). However, the correspondent FCS results deviate by 2.81 nm s^{-2}/Volt (lower system), or, 2.96 nm s^{-2}/Volt (upper system), respectively. Commonly the differences between the two independent calibration methods are near the significance level. It is striking that without exception the FCS results deviate in the same direction from those of the AG comparisons.

To find an explanation for these discrepancies, the evaluation procedures of both calibration methods were examined and new calibration experiments were performed. In the following, some critical points of the AG comparison method are considered. All of the data of AG comparisons concerning the CD030 were reprocessed under the new aspects. Finally, both calibration methods were reexamined again with respect to possible systematic deviations between the results of both methods. Detailed investigations of the FCS method shall be published in a separate contribution [2].

2. Basic principle of the calibration by comparisons with absolute gravity measurements

At the same site, SG and AG should measure the same gravity variations, e.g. the tidal signal. While the AG values are measured directly in cgs units, the output of the SG is given in Volt. Comparing the output of both instruments, a scale factor may be derived, which converts the data recorded by the SG into cgs units (µGal/V, better nm s^{-2}/V). Any environmental influences (e.g. air-pressure variations, hydrological influences, polar motion etc.) do not disturb because they affect both instruments in the same way. On the other hand, all disturbing influences acting on any one of the instruments alone, must be eliminated very carefully. This is valid e.g. for the instrumental drift of the SG.

A great advantage of the comparisons with AG is that they are made "in situ", i.e. the calibration measurements do not influence the normal operation of the SG. This also implies that the whole recording system and its specific transfer characteristic (amplifier, digital voltmeter etc.) are the same during the calibrations as during the normal operation of the SG.

The very different accuracies of the of AG and SG are problematic. The result of gravity measurements with the AG is derived from a large number of individual fall experiments of a test mass ("drops"). In contrast, for calibration purposes the gravity values derived from each drop are used as basic data. These single values are much less accurate than the final result of the absolute measurements as well as also the gravity recorded by the SG.

The calibration of SG by comparison with synchronous measured absolute values works at the error limit of the modern AG. Commonly a calibration accuracy in the order of $1 \cdot 10^{-3}$ or better is expected. In consideration of the maximum tidal signal of about 3000 nm s^{-2}, it follows, that the error of the absolute measurements must not exceed 3 nm s^{-2}. It is clear, that such an accuracy may be reached only statistically by averaging over a large number of single free fall experiments (drops). The error of one drop from the fit to a parabolic trajectory is presently for FG5-101 in the range of 5 ... 10 nm s^{-2}.

For the comparison the data of AG and SG must be synchronized. For each drop-value the correspondent SG value is estimated by interpolation of the more accurate SG data, which nowadays are sampled at shorter time intervals than the AG data. It has been ensured, that no significant errors arise during this step of the data processing.

The modern AG are equipped with computers, which control the whole measuring process including the application of corrections for the different disturbing influences, data statistics and estimation of the final result. As a consequence, all data, especially the g-values of the single drops are corrected ones. However, in addition, the drop results as well as also the corresponding corrections can be read from the gravimeter, and, as a first step of the comparison procedure, the "original" drop values have to be reconstructed by undoing the corrections, which are not connected with the measuring process itself (tides, air pressure, polar motion).

The correlogram of the synchronized AG and SG data has the shape of an elongated cloud of points. Its slope is the scale factor of the SG, which can be estimated by linear adjustment.

At the stations equipped with SG owned by the BKG many absolute measurements took place, which commonly not were planned from the aspect of SG calibration. Nevertheless, all absolute measurements carried out in parallel with SG are used for calibration purposes. Therefore, the AG data are not always optimal from the viewpoint of calibration (small amplitudes of the tidal signal, short data series, data series broken into different subsets). But small errors of the scale factor may also be reached under unfavorable conditions as may be seen from fig. 7 (symbols with open circles, which mark measurements at low tidal signal).

To reach optimal accuracy for the scale factor it is necessary to check all steps of the calibration procedure and to exclude different error sources especially in the absolute measurements.

3. Tidal corrections

The basis for the estimation of the scale factor by linear regression are the original drop values, uncorrected for tides and other influences. Tidal corrections are only needed in an intermediate step when the AG data are prepared for the elimination of outliers. For that purpose however, the tidal correction must be very precise, above all in the short periodic range. Especially in older versions of the gravimeter software the accuracy of the tidal corrections was not sufficient. It is, however, no problem, to use any tidal corrections based on a series expansion of the tidal potential together with a set of tidal parameters valid for the station in consideration. These tidal corrections are without direct influence on the further evaluation process.

If the absolute measurements are extended over a large period, incompletely eliminated constituents of the tides or of the air pressure influence may feign a drift of the drop values. For the detection of outliers this "drift" has to be corrected by fitting a linear model. After the outliers have been eliminated the drift correction has to be cancelled again as it is done with other corrections. For example an apparent driftrate of about 0.128 nm s^{-2}/h was derived from the AG data of the campaign 7.-12.12.1999. After the drift correction has been applied the scale factor changed from (-735.26 ± 1.36) nm s^{-2}/V to (-735.79 ± 0.99) nm s^{-2}/V (moving window, asymptotic fit and extrapolation to zero size).

4. Instrumental drift

Commonly the instrumental drift of SG is very low. Therefore, and due to the short duration of the absolute measurements, in most cases the influence of the drift on the calibration results may be neglected. Only in few cases the drift is so large, that drift corrections must be applied. Especially in the period after initialization or re-initialization of the SG, anomalous drift behavior with non-linear constituents ("exponential drift") may occur. However, in such cases, the drift during the period of the absolute measurements may be approximated by a straight line.

5. Offsets between data sets of the absolute measurements

Offsets are not characteristic for absolute gravity measurements. However, to avoid systematic errors caused by an incorrect adjustment of the apparatus, sometimes the adjustment is repeated after a certain time. In such cases the data set of the AG commonly is broken into different subsets. The same is valid if the gravimeter on the surface of the pillar is moved from one place to another.

There are several ways to determine the offsets between the subsequent subsets. In the simplest case the offsets are derived from the arithmetic mean values of the subsets. Another method is the use of a step algorithm as it is done during the preprocessing of tidal recordings. The best way is a third. It consists in a trial and error procedure, which minimizes the standard deviation m_0 and the error m_{SF} of the scale factor in dependence of different values of the offset. The left frame of fig. 1 shows, that the scale factor nearly linearly depends on the offset, which is applied to correct the data. This makes evident, that incorrectly estimated offsets necessarily must lead to falsified calibration results. On the other hand, the right frame shows that m_0 and m_{SF} go through a clear minimum. The optimum offset is that, at which the minimum of m_0 or m_{SF} is reached.

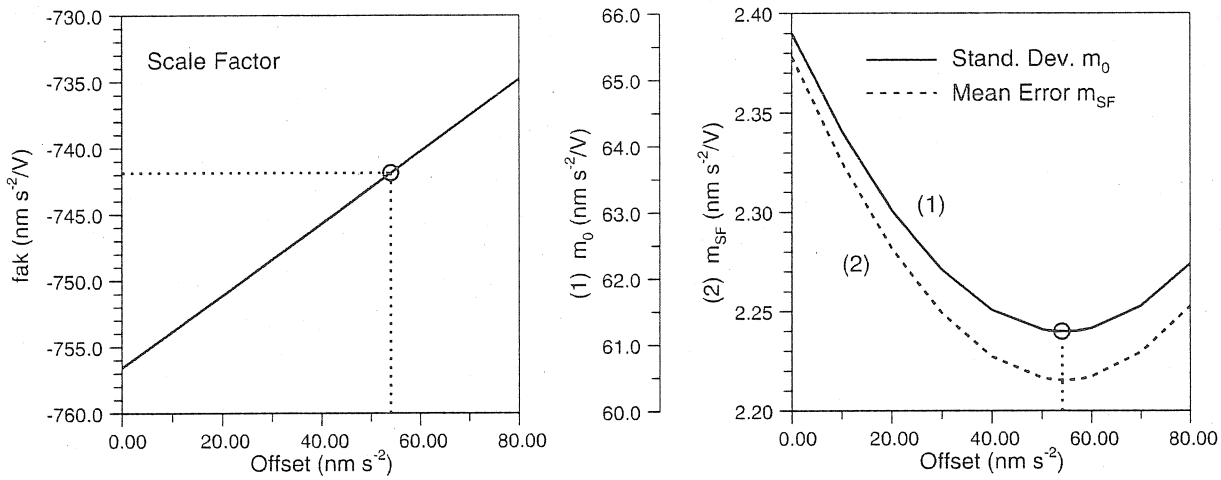

Fig. 1: Dependence of the scale factor of the SG and of its mean error on the offset, which is applied to correct the AG data (Example of the CD030, Bad Homburg, 13.-15.7.2001)

Fig. 2 gives an example of a data set, which is influenced by two offsets. If the offsets were not corrected, a scale factor of (-711.199 ± 2.401) nm s^{-2}/V would result (upper frame). Offset corrections change the result to (-739.446 ± 1.880) nm s^{-2}/V if they are derived from the difference of the mean values of neighbored sections of the data set and to (-737.787 ± 1.883) nm s^{-2}/V if they are derived by the m_0-criterion (lower frame). The influence of the step corrections is considerable. Leaving the uncorrected value out of consideration, the two other results with offset corrections derived in different ways also deviate from each other by 1.66 nm s^{-2}/V, i.e. by about 0.2 percent.

Fig. 2 also gives an impression of the different accuracies of the AG and the SG data. The drop values of the AG form an extended band-like cloud of data points with a vertical stripe pattern. The width of the band corresponds to the large scattering range of the absolute measurements. Although the most deviating values are deleted, a more or less large number of remaining outliers can be clearly recognized. The stripe pattern is caused by the succession of measurements ("sets") and breaks. The breaks between the sets are used to check the instrument. Due to the considerable less scattering of the SG data the correspondent cloud of data points looks like a smooth broken line, no deviating points are to be seen.

Offset correction and number of the deleted outliers are dependent from each other. The estimation of offsets needs a data set, which is freed from outliers. To this end in a first approximation the weak $2s_0$-criterion was used. This is valid for all examples summarized in table 1. In order to check the influence of outliers on the estimation of the offset, the data of calibration no. 8 were used. In a second step the skew criterion was applied with different threshold values. For each threshold the estimation of the offset was repeated. While the number of detected outliers clearly roses, the estimated offsets vary in a range of about ±1 nm s^{-2}. However, at high values of the threshold deviations from this general behavior are possible.

6. Elimination of outliers

Commonly in the data of absolute measurements several values occur, which deviate more or less from the majority of the others. Such outliers indicate that the individual drop is disturbed in any way. The reason of outliers can be mechanical perturbations of the drop sample. Single drop results can

also be affected by a laser standard "out of lock" or a short disturbance of the rubidium frequency. The right selection of the outliers to be eliminated is the most crucial point in the calibration of SG by comparison with AG. - The error estimates of the parabolic fit of the single drops have not been used for the identification of outliers in this study.

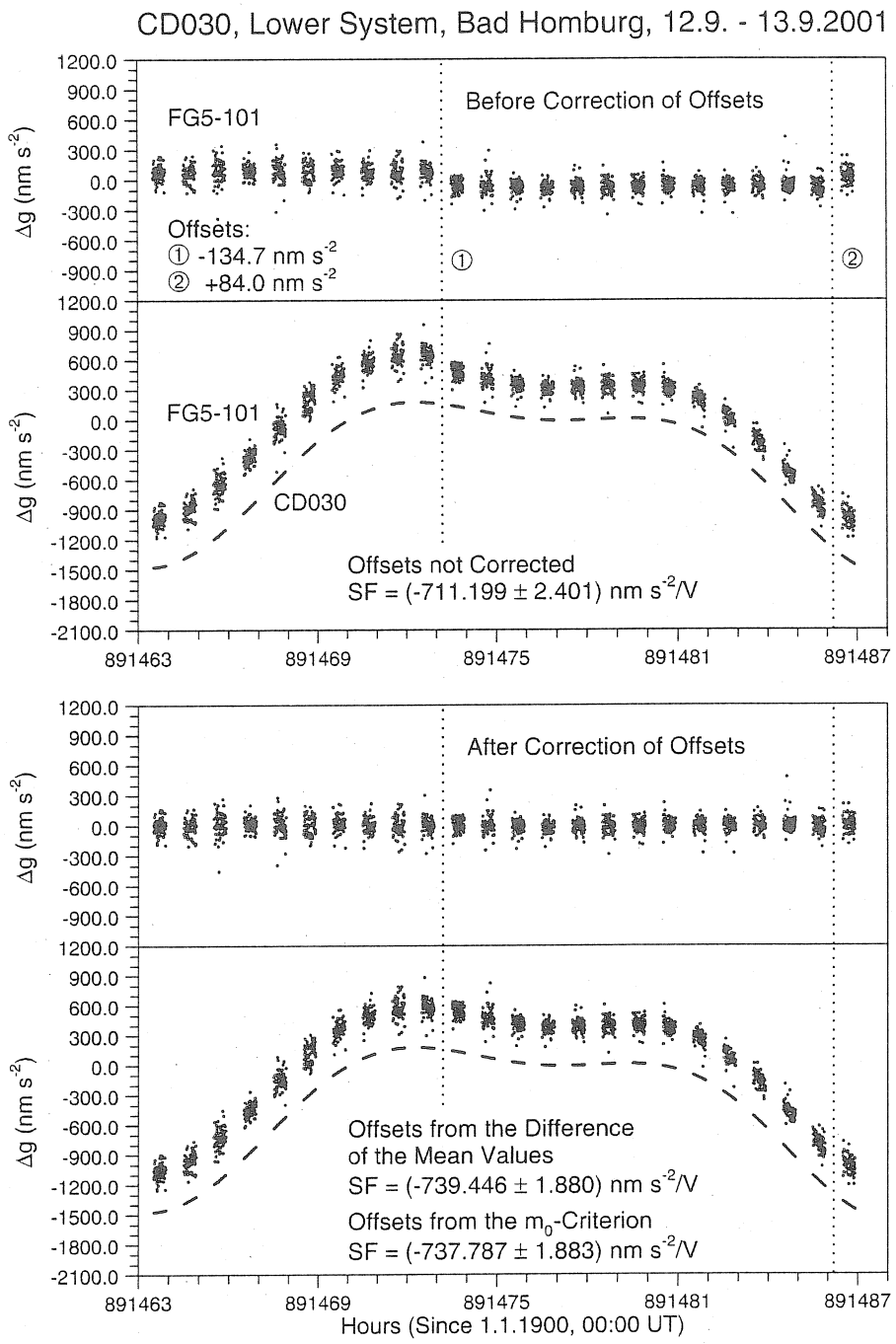

Fig. 2: Tidal signals measured by AG and SG. AG data influenced by offsets (Example of the CD030, Bad Homburg, 12.-13.9.2001)

To minimize the computational problems the absolute measurements should be arranged in such a way that generally from the start outliers are avoided as far as possible. From the viewpoint of the calibrations low repetition rates of the drops are to be preferred. Obviously the number of outliers reduces, if the drops follow at greater time intervals, e.g. every 20 s instead of 10 s as it is common use. However, up to now not enough data are available for a systematic investigation of this problem.

On the other hand, if the assumption is correct, the absolute measurements themselves could benefit from a reduction of the repetition rates.

From the viewpoint of the accuracy the tidal variation during the calibration experiment should be as large as possible. Above all this depends from the right choice of the measuring period. Always, the data set of each measuring campaign has to be handled as a whole. This is especially valid for the elimination of outliers.

Statistical methods have to be used for the detection and elimination of outliers. It is clear that the rules for the application of the different statistical tests have correctly to be fulfilled. First of all the data must be homogeneous. Therefore they have to be corrected with respect to several disturbing influences (e.g. offsets due to different installations or readjustment of the absolute gravimeter, earth tides, gravity effect of air pressure, polar motion). After the outliers have been eliminated, the original data are again used. The corrections are without influence on the further steps of the calibration procedure.

Due to the more or less large number of outliers, at least the raw data are not normally distributed. Therefore only such tests are allowed, which are not based on the assumption of a normal distribution. The tests are cyclically applied. If the test value points out that deviations from the normal distribution exist, the most distant value (with respect to the median value of the remaining data set) is deleted and the next test cycle starts. The procedure stops if the test value remains below a fixed threshold.

The following tests were tried.

- **Comparison of two variances ("$2s_0$-criterion", modified F-test)**

The variance of the sample is computed twice. The first estimate s is derived in the common way as if the data would be normally distributed. The second estimate s_0 is derived from the quartiles q_{25} and q_{75} of the sample, taking into consideration that for a normally distributed sample the relation $s_0 = (q_{75} - q_{25})/1.349$ is valid. If s exceeds 2 s_0 than deviations from the normal distribution have to be assumed. More correctly speaking the ratio s^2/s_0^2 is tested and the factor 2 stands in a simplified manner for the theoretical threshold defined by the F-distribution.

- **Deviation of the variance from a hypothetical value (χ^2-test)**

Using the same two estimates s and s_0 of the variance a test value $\chi^2 = s^2 (N-1)/s_0^2$ is derived. If χ^2 exceeds a certain tabulated value, deviations from the normal distribution and therefore the existence of outliers are to be assumed.

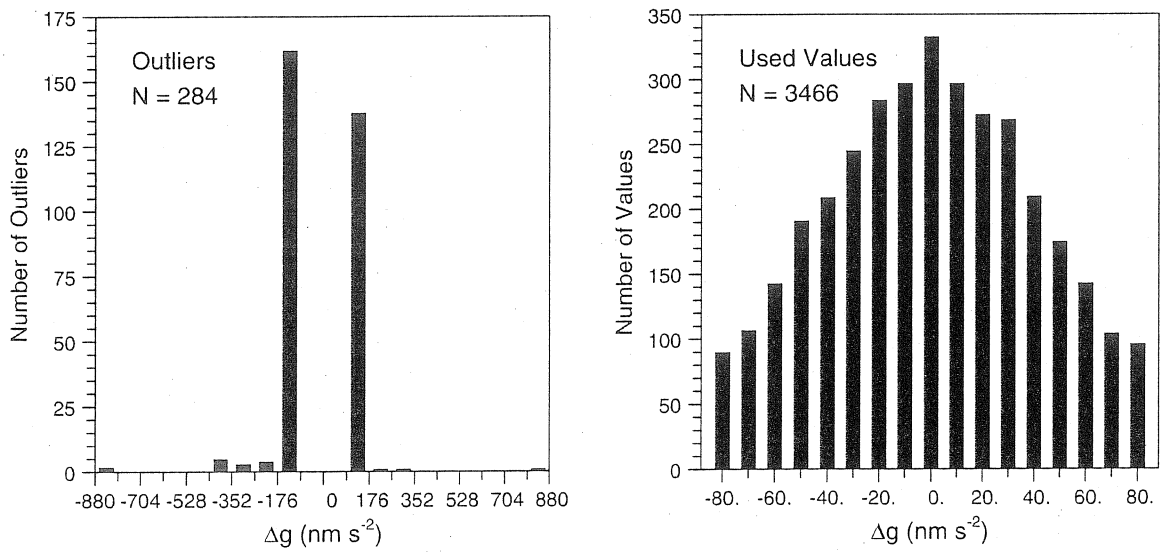

Fig. 3: Frequency distribution of the single drop values during a measuring campaign with the AG (Example FG5-103, Bad Homburg, 2.-3.12.2000). On the right: central part of the histogram. On the left: tails on both sides of the histogram, showing the skew of the frequency distribution

- **Deviation of the mean from a hypothetical value (u-test)**

The mean value of the data set, which is identical with the moment of first order m_1, is compared with the median. If the test value $u = |m_1 - med|\ SQRT(N)/s_0$ exceeds a certain tabulated threshold of the normal distribution (e.g. u = 1.960 for a error probability of 0.05), the mean value deviates significantly from the median, i.e. in this case a non-normal distribution and the existence of outliers have to be assumed.

- **Skew of the total data set (threshold criterion)**

A fundamental feature of the normal distribution is its symmetry. On the other hand, a skew unequal zero points out, that the distribution is non-normal. For instance fig. 3 shows the histograms of the outliers (left side) and of the remaining absolute values after the skew test (right side). The skew Sk depends on the statistic moment of third order m_3. It is defined by $Sk = m_3/s^3$, where $s^2 = [vv]/(N-1)$ and $m_3 = [vvv]/N$. The problem is, to find a suited threshold for the decision whether a sample is normally distributed or not. To this end the following variants were tested.

In the simplest case a single fixed threshold was used, e.g. 0.2. The greater the threshold the lower the number of detected outliers.

Normally the skew starts with large values (some tenth or more). After a sufficient number of outliers was deleted, the skew reaches the neighborhood of zero and the distribution of the remaining absolute values becomes nearly a normal one. In the following cycles if more and more outliers are deleted, the skew may move around the zero level. For some time an increase of the skew is also possible. Therefore the elimination process is stopped only when the skew remains at least for 5 cycles below the threshold.

More commonly it was tried, to vary the threshold from values of about 0.2 down to very low values when the number of outliers exceeds 2000 or about the half of the total number of data. The number of detected outliers rapidly rises with the diminution of the threshold. A clear tendency of the resulting scale factors is not to be seen. The variation of the scale factor of each calibration experiment follows an individual curve. Two examples are shown in fig. 4. The scattering range of all curves valid for the different calibration experiments is very large. The single results may be summarized, if an optimum scale factor is derived, which minimizes the differences to the minimally deviating result of each calibration experiment.

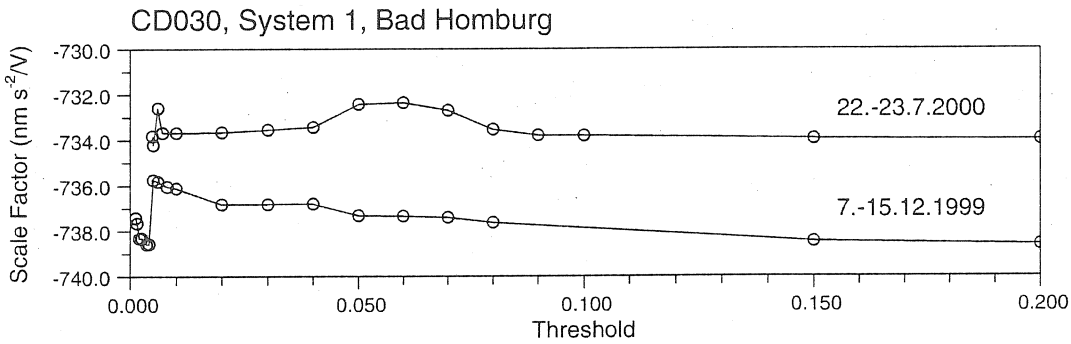

Fig. 4: Dependence of the scale factor on the applied threshold of the skew test. The threshold is lowered until the number of detected outliers exceeds about the half of the original number of AG data

- **Minimum of the skew of different subsets (moving window)**

No particular threshold is used. Instead of them the skew is estimated for consecutive subsets of given size (described by a certain percentage of the total data set), which are moved step by step over the sorted set of AG data. In a certain position of each of these windows the skew reaches a minimum. The correspondent data set is used for the estimation of the scale factor while the data outside the window automatically are rejected as outliers. The procedure is repeated with windows of different size. In this way for each calibration experiment a series of scale factors results, each of them valid for a certain size of the data window. Two of such curves with clear different behavior are given in fig. 5. Additionally for each calibration experiment an asymptotic value may be derived by

fitting a polynomial of third degree with a horizontal tangent in the inflection point ("extrapolation to zero size").

The influence of the number of eliminated outliers on the difference between mean value and median is shown in fig. 6. It may be seen, that there is no asymptotic approach to the zero level. Due to the outliers, which are included in the data set, the difference starts with large values. If more and more outliers are eliminated the difference decreases, passes the zero level, rises again and finally it varies in a narrow stripe around zero. This behavior is similar to that of the skew as it was discussed above. If the elimination of outliers is stopped too early, the remaining asymmetry of the data set may falsify the estimation of the scale factors.

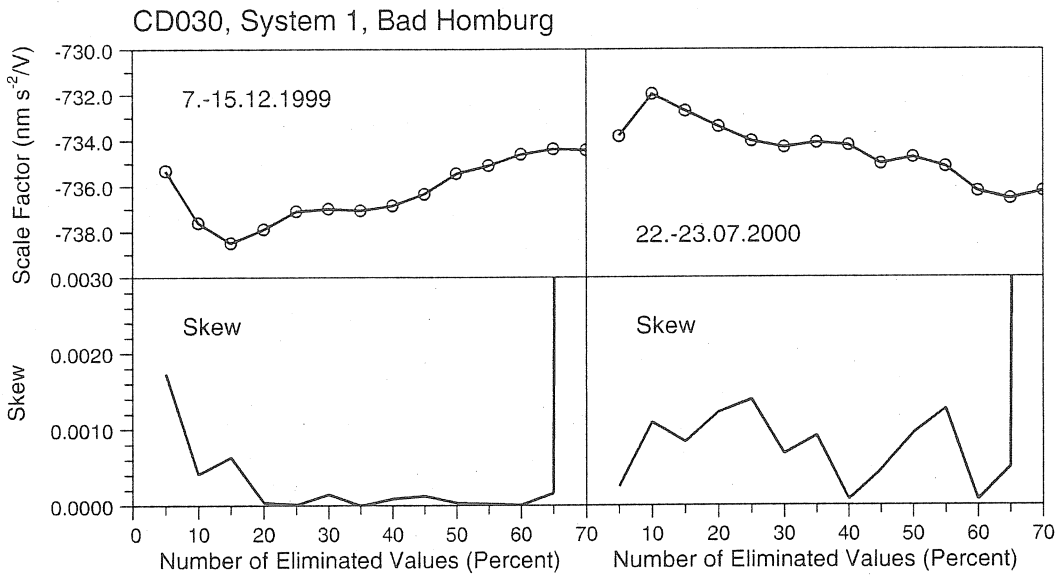

Fig. 5: Influence of the size of the moving window on the estimated scale factor. The size of the window is diminished step by step until the skew increases abruptly.

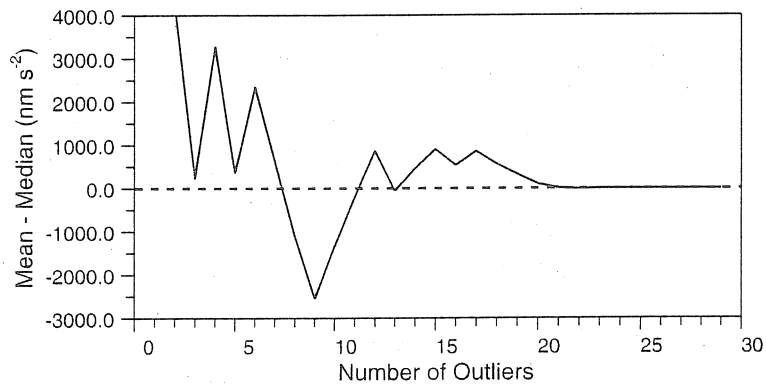

Fig. 6: Influence of the number of eliminated outliers on the difference between mean value and median of the AG data set (Example FG5-101, Bad Homburg, 12.-13.9.2001)

7. Results from the Dual Sphere Gravimeter CD030 at Bad Homburg

All earlier calibrations of the CD030 based on comparisons with AG were reprocessed with regard to the new viewpoints described above (m_0-criterion for the estimation of offsets, skew-criterion for the detection of outliers). In doing this, not all calibration results changed. Several AG comparisons remained unchanged because there neither were offsets nor was the frequency distribution significantly

asymmetric. If the skew is near zero, the $2s_0$- criterion is sharp enough for the elimination of outliers. - Additionally the results of some new calibration experiments were included (nos. 10 - 20).

In all cases where the AG data are split into different subsets, the minimum-criterion of m_0 was used for a new estimation of the offsets (calibrations nos. 1, 2, 3, 4, 8, 15, 16, 18, 19). The values of the revised offsets deviate more or less from the previous results (tab. 1, columns 2 and 5). In all examples the mean square errors of the scale factors decrease (columns 4 and 6).

Due to the more stringent skew criterion a greater number of outliers is detected than with the $2s_0$-criterion used before (columns 3 and 7). In some cases the number of values to be deleted changes only slightly and therefore the influence on the scale factor is low. In the other cases the number of outliers grows stronger and as a consequence the scale factor and its mean square error are influenced considerably (columns 4 and 8). However, the results change upward as well as downward as may be seen from the up- and down-arrows in column 9. Though the majority of the results tends to lower values the weighted overall mean increases by about 0.6 nm s^{-2}/V [1].

Tab. 1: Change of the calibration results of the lower system of CD030 due to the new estimation of offsets (minimum of m_0) and the stronger test for outliers (test for the skew of the frequency distribution). V1 = $2s_0$-criterion, V4 = skew-criterion). Calibration no. 19 was not included in the mean values given in the last line

	Period	Offset old	Outliers old	Scale Factor old	Offset new	Scale Factor new, V1	Outliers new	Scale Factor new, V4	D.
		nm s^{-2}		nm s^{-2}/V	nm s^{-2}	nm s^{-2}/V		nm s^{-2}/V	
	(1)	(2)	(3)	(4)	(5)	(6)	(7)	(8)	(9)
1	7.-15.12.1999	- 51 +372 - 6 -365	82	-735.86 ± 1.79	- 58 +366 - 12 -370	-738.51 ± 1.78	83	-738.66 ± 1.77	
2	23.-24.1.2000	+ 5 -16	4	-734.30 ± 2.29	0 - 9	-732.17 ± 2.29	16	-734.20 ± 1.47	
3	7.-9.3.2000	+11 +21	5	-742.01 ± 2.90	+ 9 + 9	-741.98 ± 2.88	13	-739.76 ± 2.10	
4	28.-29.3.2000	- 3 +19	4	-739.00 ± 5.00	+ 2 +16	-741.08 ± 5.00	14	-738.68 ± 3.26	
5	17.-18.4.2000	–	13	-744.42 ± 8.20	–		22	-741.51 ± 7.59	
6	20.-22.5.2000	–	32	-740.74 ± 2.69	–		44	-738.84 ± 1.81	
7	8.-9.6.2000	–	26	-734.50 ± 4.05	–		111	-743.23 ± 2.54	
8	29.-30.6.2000	+ 4	2	-737.02 ± 1.44	+13	-740.38 ± 1.44	10	-740.40 ± 0.78	
9	22.-23.7.2000	–	3	-734.09 ± 2.48	–		10	-733.98 ± 2.44	
10	24.-25.8.2000	–	6	-738.35 ± 2.12	–		54	-736.75 ± 1.18	
11	28.-29.9.2000	–	5	-739.45 ± 2.58	–		11	-738.38 ± 1.86	
12	31.10.-1.11.00	–	1	-739.76 ± 2.57	–		8	-738.36 ± 1.49	
13	2.-3.12.2000	–	1	-737.81 ± 1.99	–		40	-739.45 ± 1.44	
14	17.-18.5.2001	–	15	-736.67 ± 4.33	–		20	-737.08 ± 3.50	
15	13.-15.7.2001		7		+54	-741.84 ± 2.22	17	-742.59 ± 1.43	
16	12.-13.9.2001	-142.8 + 89.6	23		-134.7 + 84.0	-737.79 ± 1.88	29	-737.63 ± 1.62	
17	20.-21.9.2001	–	18	-741.39 ± 2.88	–		300	-738.15 ± 1.38	
18	13.-14.1.2002		3		- 9.6	-736.00 ± 2.10	14	-736.32 ± 1.28	
[19]	12.-13.2.2002		0		- 5.8	-730.52 ± 2.36	19	-729.58 ± 1.48	
20	26.-29.3.2002		6		-23.0 +3.5 +19.6	-742.57 ± 3.25	97	-736.82 ± 1.59	
Mean				-737.95 ± 0.58 19 Measurem.				-738.51 ± 0.52 19 Measurem.	

Correspondent conclusions with concern to the reprocessing of the comparisons with absolute measurements are valid also for the gravimeters C023 at Medicina and CD029 at Wettzell.

[1] If scale factors are compared, in the following text always the absolute values are considered.

Considering the fact, that deviations from the normal distribution have a great influence on the estimated scale factors, some additional experiments have been made with different strategies for the detection and elimination of outliers. This corresponds to the processing of the absolute measurements themselves, where commonly a greater number of outliers is eliminated.

At first the skew criterion was applied with different thresholds. Two examples of the influence on the estimated scale factors are given in fig. 4. The curves of the different calibration experiments scatter over a range of more than 10 nm s^{-2}/V. As a common tendency for each calibration experiment the estimated scale factors decrease with decreasing threshold. However, in detail there are many deviations. If the scale factors, resulting for a certain threshold are averaged over all the experiments, the same tendency results. If the threshold 0.2 is used, between 8 and 111 outliers are deleted and a scale factor of (-737.93 ± 0.67) nm s^{-2}/V results. On the other hand, if the threshold is lowered to 0.05 between 20 and 1561 outliers are deleted and the scale factor changes to (-737.72 ± 0.53) nm s^{-2}/V. In a similar way from the first minimum of the skew the value (-736.93 ± 0.42) nm s^{-2}/V results, while the smallest useful threshold leads to (-736.54 ± 0.52) nm s^{-2}/V. The optimum scale factor, which summarizes the results of all the different calibration experiments results to -737.17 nm s^{-2}/V.

Finally the moving window technique was applied with window sizes between 30% and 95%, i.e. between 5% and 70% of the data were excluded (fig. 5). If windows of 60% and 95% are used, scale factors (-737.10 ± 0.50) nm s^{-2}/V and (-737.67± 0.61) nm s^{-2}/V result. This confirms again that the greater the window, i.e. the smaller the number of values, which are not considered ("outliers"), the greater the resulting scale factor. If the asymptotic values of the single calibration experiments are averaged (extrapolation to windows with zero size), a value of (-736.72 ± 0.50) nm s^{-2}/V results, which corresponds to the optimum value given above.

Compared with the FG5-101 (BKG, Frankfurt a.M., Germany) the data of FG5-103 (POL, Bidston, U.K., calibration no. 13) show a deviating behavior. At low numbers of outliers both instruments agree well. If the number of eliminated outliers rises, the scale factor derived from the data of FG5-103 tends to significantly greater values (about –744 nm s^{-2}/V), i.e. the difference between the results of both AG increases. However, this statement is only based on one calibration experiment and it is dangerous to rush to conclusions.

Tab. 2: Calibration of the dual sphere gravimeter CD030 by comparisons with absolute gravimeters and by the Frankfurt Calibration System (FCS)

CD030, Bad Homburg	Lower System			Upper System		
	Scale Factor nm s^{-2}/V	Phase L. s	N [4])	Scale Factor nm s^{-2}/V	Phase L. s	N [4])
Comparison with Absolute Gravimeters						
Dec. 1999 - July 2000 [1]) Dec. 1999 - Mar. 2002 [2])	-736.90 ± 0.88 -738.51 ± 0.52		9 19	-676.26 ± 0.84 -677.91 ± 0.60		9 16
Frankfurt Calibration System (FCS)						
February 2000 February 2000 [3])	-739.71 ± 0.23 -739.75 ± 0.25	40.18 40.18		-679.22 ± 0.41 -678.68 ± 0.72	41.58 41.60	
December 2000	-739.58 ± 0.19	40.37	2/12			2/15
Mean [3])	-739.66 ± 0.16	40.28		-678.68 ± 0.72	41.60	
Difference FCS – Absolute Comparison						
August 2000 [1]) April 2002 [2])	2.81 1.15			2.96 0.77		

[1]) State August 2000 (ETS2000, Mizusawa [1])
[2]) State April 2002
[3]) Revised result, March 2002
[4]) N means
- number of absolute measuring campaigns for the comparison method
- number of calibration sequences during one calibration experiment for the FCS method. The number of different periods during each calibration sequence follows the slash.

From the different experiments with more stringent criteria for the elimination of outliers scale factors in the range between about -736.5 and -737.0 nm s^{-2}/V were derived. This moment the single results

shall not be discussed in detail. Generally, it may be stated that with increasing number of outliers the scale factors tend to smaller values. At the same time the results seem to be stabilized. Obviously the results are influenced by systematic errors, depending on the number of outliers. Therefore only groups of scale factors may be averaged, which are derived with similar criteria for the elimination of outliers. It has to be assumed that the asymmetry in the frequency distribution is fundamentally (at least to a certain, very low extent) and not only caused by a more or less large number of single outliers. A decision, which are the most reliable results would be made easier if the results could be compared with reliable results from the Frankfurt Calibration System (FCS), which is based on a fundamentally different principle. At present it must be stated, that all scale factors derived from comparisons with AG are less than the results of the FCS, which are available up to now. The smallest deviations occur, if the skew test with a threshold of 0.2 is applied. All attempts to get a better agreement by more stringent criteria for the elimination of outliers result in smaller scale factors, i.e. in an increasing difference between both calibration methods. Therefore the following considerations exclusively refer to the skew test with threshold 0.2.

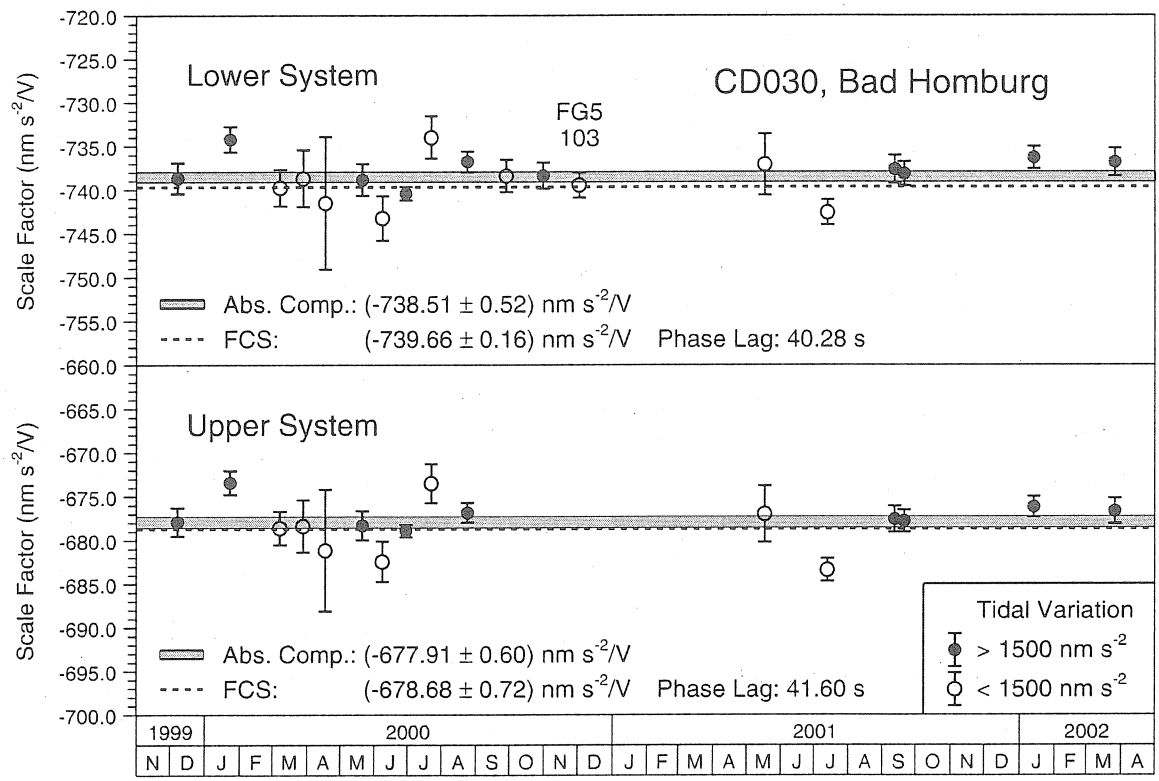

Fig. 7: Scale factors of the CD030, derived by comparisons with AG. Grey stripe: ±1σ-range of the weighted mean of the 19 single values (The strongly deviating result of calibration no. 19 was not included). Broken lines: results of the Frankfurt Calibration System (FCS), state of March 2002

8. Comparison with older results and with the FCS

A summary of the results of different calibrations of the dual sphere gravimeter CD030 is given in tab. 2 and fig. 7. In the upper frame of fig. 7 the values of the lower system are compared with the FCS result. The results of the AG comparisons are given in detail in table 1, column 8. The lower frame demonstrates the correspondent results concerning the upper system.

Generally since the ETS2000 the discrepancy between the comparisons with absolute measurements and the FCS results diminished. Both calibration methods contribute to this improvement.

The comparisons with AG were reprocessed with respect to the improved estimation of offsets and more stringent criteria for the elimination of outliers. Moreover 11 new absolute measurements at Bad

Homburg could be additionally taken into the considerations. In this way, the scale factor of the lower system changed from (-736.902 ± 0.882) to (-738.512 ± 0.515) nm s^{-2}/V and that of the upper system from (-676.263 ± 0.839) to (-677.914 ± 0.604) nm s^{-2}/V. As a general tendency the revised results lower the discrepancy between the FCS and the comparisons with AG.

The calibration results on the basis of the FCS were also revised and the results of a new FCS experiment could be included. Very encouraging was a separate experimental determination of the frequency transfer function of the FCS. A detailed description of some new aspects of the FCS method shall be given in a separate contribution [2].

As may be seen from tab. 2 for the lower system two FCS calibrations are available (February and December 2000). The second calibration deviates by only 0.171 nm s^{-2}/V from the revised result of the first one. Roughly speaking the scale factor remains nearly unchanged with respect to the state of August 2000 [1] (with a very slight tendency to decrease the discrepancy between the both calibration methods). During the FCS calibration in December 2000 the upper system of the CD030 was out of order. Therefore, only results from the calibration in February 2000 are available for the upper system. In contrast to the lower system the revised result changed by 0.547 nm s^{-2}/V with a clear tendency to reduction in the discrepancy with respect to the results of comparisons with absolute measurements.

Altogether, the discrepancy between the FCS method and the comparisons with AG reduces from 2.810 nm s^{-2}/V (state August 2000) to 1.062 nm s^{-2}/V (state March 2002) for the lower system or from 2.962 nm s^{-2}/V to 0.684 nm s^{-2}/V for the upper system, respectively. Also, if the remaining discrepancy is not significant in the strong sense of statistics, it needs to be explained. It is striking, that without any exception the absolute value of the FCS calibration is always greater than the mean value of the scale factor derived from comparisons with absolute gravity measurements.

9. Conclusions

From the critical revision of the evaluation procedures, the results of different comparisons with absolute gravimeters and some applications of the Frankfurt Calibration System (FCS) the following conclusions may be drawn.

1. The example of the dual sphere gravimeter CD030 encourages use of comparisons with absolute gravimeters as a reliable method for the calibration of superconducting gravimeters. While the accuracy derived from a single measuring campaign may reach the order of 1.5 nm s^{-2}/V, the mean of several comparisons, spread over a longer period, gives stable results with an accuracy of better than $1 \cdot 10^{-3}$.

2. Great care has to be taken in the elimination of outliers and the estimation of offsets. The absolute gravity data taken in this analysis could not be seen as a priori normally distributed. Therefore, common criteria based on the variance of the normal distribution are not suitable. For the elimination of outliers the skew of the data distribution has proved to be a reliable test value. Offsets may be estimated by a trial and error procedure, which searches for a minimum of the mean error of the calibration result.

3. The calibration of SG by comparison with AG has the great advantage, that the normal operation of the SG is not disturbed. Especially the entire recording electronics need not be changed. This implies, that the transfer characteristic (frequency dependence) remains unchanged and the scale factor cannot be influenced by the calibration procedure.

4. Calibrations using the Frankfurt Calibration System (FCS) are more accurate by at least one order of magnitude in comparison with calibrations on the basis of absolute measurements. The high accuracy of the FCS may be reached during a single calibration experiment, which however needs a large expenditure of work and a time of several days. As a consequence the operation of the SG is interrupted during the period of the calibration experiment.

5. The experiments with different skew thresholds for the detection of outliers show, that the calibration results systematically depend on the number of eliminated outliers. Though no objective criterion for a certain value of the threshold may be given, the results related to the threshold 0.2 are preferred.

6. Since ETS2000 [1] the discrepancy of about 3 nm s^{-2}/V between AG comparisons and FCS partly could be cleared up. About two parts of the reduced discrepancy are due to a reprocessing of the comparisons with absolute gravimeters and about one part is contributed by a revision of the FCS calibrations. In both cases new calibration experiments could also be included in the investigations.

However, the remaining discrepancy in the order of 1 nm s^{-2}/V (not significant in the strong sense of statistics) also requires further explanation. It is remarkable that the absolute value of the scale factor based on the FCS is always greater than the mean derived from the comparisons with absolute measurements.

References

1. Falk, R., Harnisch, M., Harnisch, G., Nowak, I., Richter, B., Wolf, P.
   Calibration of the Superconducting Gravimeters SG103, C023, CD029 and CD030
   J. Geod. Soc. Jap., Japan 47(2001)1, pp. 22 – 27.
2. Richter, B., Harnisch, G., Nowak, I.:
   Experimental and Computational Contributions to Estimate the Accuracy and Reliability of the Frankfurt Calibration System (FCS).
   Proc. Third Workshop of GGP, Jena, March 2002. In Preparation.

On the Calibration of a Superconducting Gravimeter GWR–C032 with an Absolute Gravimeter FG-5 in Wuhan*

He-Ping Sun, Hou-Tze Hsu, Yong Wang

(Institute of Geodesy and Geophysics, Chinese Academy of Sciences, Wuhan 430077, China,
Tel/Fax: 0086-27-86783962, email: heping@asch.whigg.ac.cn)

Abstract

By performing the FG-5 absolute gravimeter (AG) measurements at station Wuhan/China for two campaigns in 1999 and 2000 (each for 3 days), the calibration factor of the GWR-C032 superconducting gravimeter (SG) as of -84.6242 μgal/V with precision of 0.2% is determined accurately.

1 Introduction

The Superconducting gravimeters (SGs) are widely used to observe the change in temporal and spatial gravity field, considering their characteristics as of the high-precision, good continuity and stability (Warbuton, 1985). However, it is necessary to calibrate the direct output (change in voltage) of a gravimeter by using scale value (calibration factor) before getting the change in real gravity. Studies show that the accurate calibration factor benefits to late explanation in the results of the tidal analysis and in the geodynamics (Francis, 1997, Hinderer et al 1998, Amalvict 2001). The un-accurate calibration factor will biase observed tidal parameters to tidal models. Therefore, to acquire high precise scale value is one of the important fundamental study works (Sun et al, 2001a, Ducarme et al 2001, Ogasawara et al, 2001).

With wide use of the high-precision absolute gravimeters (AGs) in recent yeas, it is possible to record precisely the tidal gravity change. Therefore, if we increase the free fall numbers and extend observational interval for the AG measurements, the SG calibration factor can then be determined (Sun et al, 2001a). The Wuhan SG measurements started in August 1985, the instrument takes up currently important observation duties for the Global Geodynamics Projects (GGP). The first calibration factor as of –28.575 μgal/V was determined using a weighted sum technique to main wave amplitude factors recorded with Lacoste-Romberg (LCR) tidal gravity instruments (ET15 and ET 21) during the cooperation between China and Great British between 1985 and 1987 (Hsu et al, 1989). The SG was upgraded in 1996 due to the aging of unit sensing elements, also in accordance with GGP regulations. As the background noise of the original station is relatively large, it was re-installed at new site (114.49°E, 30.52°N, 80.0 m) away from old station about 25 km (Sun et al, 2001b). Therefore the new calibration factor is necessary to be re-determined precisely by using some reasonable techniques.

2 AG and SG Observations

2.1 The first campaign in January, 1999

In order to obtain the calibration factor with high precision and strong reliability, the period in large tides is selected for the AG and SG measurements, from at 04:00:00, January 29, 1999 to at 06:26:20, February 1, 1999 (Greenwich time). The AG was installed in the room parallel to the SG

* Supported jointly by Nature Science Foundation of China (49925411 and 40074018) and Chinese Academy of Sciences (KZCS2-106)

with distance about 10 m, the laser speed and the valid height of the instrument are only necessary to be corrected considering that the changes in gravity at two points are identical.

Figure 1 represents the temporal change of original measurements, the thick line figured by the symbol + refers to AG observing values with unit in μgal shown as right axis, each + symbol for one fall. The thin line refers to the SG observations with unit in mV (milli-volt) shown as left axis. It is found that the SG measurements are quite stable, the curve is smooth and no gaps at all, but there are many scattered values for the AG observations, it is due to the un-matching synchronously between the distance measured by the laser interfering and the sampling of the pulse number related to the time interval. The discrete values should be removed before the SG scale value to be determined.

The observing procedure of the AG is set in advance and accomplished automatically by a PC computer. The basic rule of the fall setting is arranged for each fall interval to be 20 s, stopping 3 m each hour, the time length of the AG measurements is totally 74 h and 26 m and 20 s. Therefore there will have predictable 12733 observed AG measurements. But there are in total 13 gaps with 2465 falls missing with interruption rate as of 19%, it is due to the data recording system failure caused by large electric pulse.

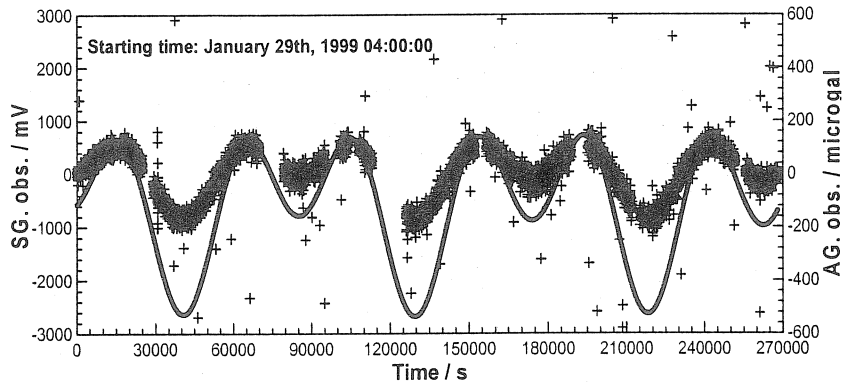

Fig 1 Original measurement of AG and SG in 1999 campaign

2.2 The second campaign in August 2000

Considering the shortcomings of the AG measurements in 1999, especially large interruption rate, we redesign a scheme of the AG measurements. As in first campaign, the period having large tides is selected, from at 04:30:00, August 13, 2000 to at 04:39:40, August 16, 2000 with total length of 72 h and 30 m. Figure 2 shows the original AG and SG measurements with same symbols as given in figure 1. Comparing to the first campaign, there exists a large gap in the SG measurements from at 23:35:50, August 15, to at 03:36:10, August 16, with interruption length as of 4 hours and 20 seconds, it is due to the failure of the SG data acquisition system.

The dispersion of the AG measurements is less than that in first campaign, this is due the FG5 to be in much better status and steadier station meteorological condition than that in 1999. Similar to the prior campaign, the procedure of the AG measurements is also set before hand. The difference is that the time interval of each fall is set to 10 s, and stop for 20 m after 10 m. After eliminating gaps and anomaly data, the fall numbers used in calibration work is 7331.

Figures 3 shows comparison between gravity and voltage. The change in voltage measured with the SG is shown in X axis, and the change in gravity recorded with the AG is shown in Y axis. It is found that there exists a good linear correlation which indicates a single calibration factor can be used to describe the relation between observing gravity and change in voltage.

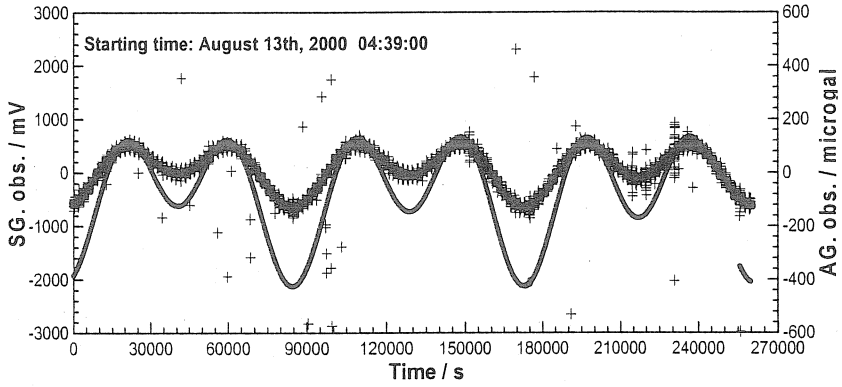

Fig 2 Original measurements of the AG and SG in 2000 campaign

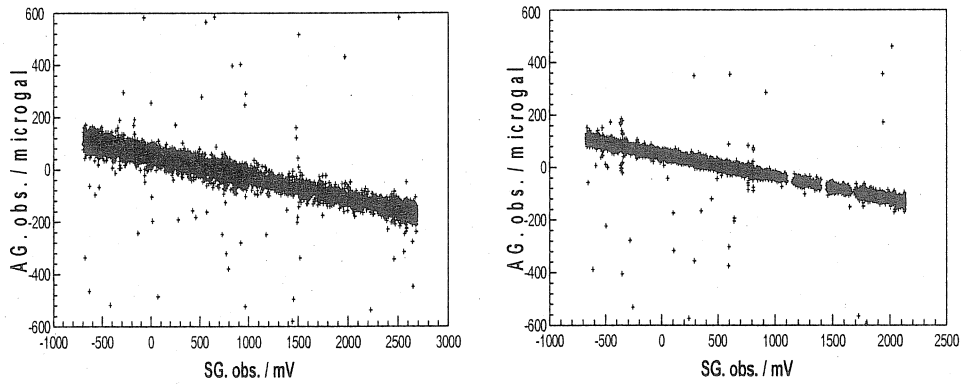

Fig 3 Relation between gravity and change in voltage in 1999 (left) and 2000 (right)
(AG: absolute gravimeter, obs: observation)

3 Results of the calibration factors and discussions

The first thing to be settled down is to remove anomaly data, the calibration factor can then be determined by using a least square polynomial linear fit. According to the statistics theory, the error data are removed by using so-called "3σ criterion". The long period drift of the observation is fitted using a Chebyshev polynomial (Sun et al, 2001a). The numerical results show the global calibration factors to be –84.3637 μgal/V with precision of 0.34% in 1999 campaign and –84.6242 μgal/V with precision of 0.20% in 2000 campaign, the disparity between them is about 0.31%. The late analysis demonstrates the first calibration factor to be too smaller that enlarges the deviation between observed and theoretical values.

The relation between observing error limit and calibration factor is studied based on the observations in 2000 campaign (figure 4). The observing error limit in μgal is given in horizontal axis, the solid line refers to calibration factor in μgal/V, and the dashed line is the global fit. Analysis shows that the change range of the calibration factor is in the order of 0.3% when tacking observing error limit between 20 and 35 μgal, the error of the calibration factor is also given. Figure 5 shows the relation between calibration factor and fall numbers, it is found that when taking fall number over 5000, the calibration factor trends stable. So we believe that the fall number of 5000 in the determination of calibration factor is enough. Therefore if designing 10 s for each fall, stop 20 m after 10 m, and if all recordings are valid, then the whole interval used in the calibration process is at least 50 hours. Taking usual anomaly data and gaps into account, selecting a period of 3 days can meet with the present precision of the calibration factor.

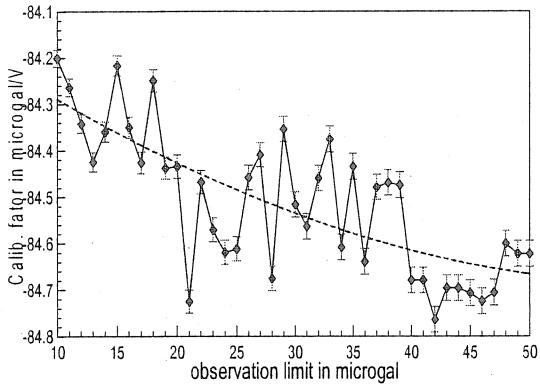

Fig 4 Relation between calibration factor and observing error limit

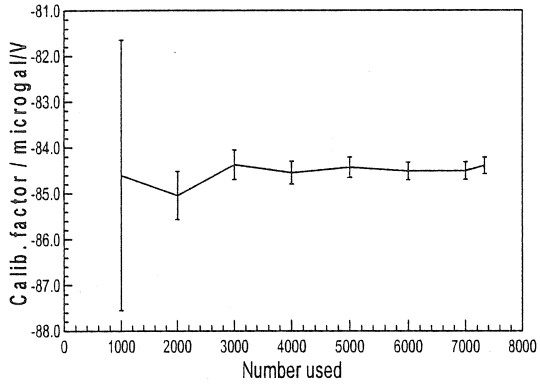

Fig 5 Relation between the calibration factor and the fall number in 2000 campaign

4 Conclusions

Summarizing the results and discussions mentioned above, we conclude that an AG under good condition can record precisely the change in tidal gravity, by performing a least square polynomial linear fit, the calibration factor can then be determined. Considering the lower calibration value and lower precision determined in 1999 campaign, the only one determine in 2000 campaign is adopted -84.6242 μgal/V with precision 0.20%. This precision is close to the one of 0.15% determined by Hinderer (1998), and the one of 0.1% obtained by Francis (1997).

Acknowledgements

Zhang Wei-Min, Hao Xing-Hua, Zhou Ba-li and Hao Xiao-Guang are acknowledged for taking part in the field AG and SG measurements. Bernard Ducarme, Royal Observatory of Belgium, is grateful for reading the manuscript and provides us with the constructive comments and corrections.

Reference

[1] Amalvict M, McQueen H and Govind R, Absolute gravity measurements and calibration of SG-CT031 at Canberra, 1999-2000, J. Geodetic Society Japan, 2001, 47(1): 410–416.

[2] Crossley D, Hinderer J and Amalvict M, A spectral comparison of absolute and superconducting gravimeter data, J. Geodetic Society Japan, 2001, 47(1): 373–379.

[3] Ducarme B, Sun HP, Tidal gravity results from GGP network in connection with tidal loading and Earth response, J. Geodetic Socity Japan, 2001, 47(1), 308–315.

[4] Francis O, Calibration of the C021 Superconducting gravimeter in Membach (Belgium) using 47 days of absolute gravity measurements. In: Segawa et al (eds). Proc International Association of Geodesy Symposia, Gravity, Geoid and Marine Geodesy, 1997, 117: 212–219.

[5] Hinderer J, Amalvict M, Florsch N, Francis O, Makinen J, On the calibration of Superconducting gravimeters with the help of absolute gravity measurements. In: Paquet P and Ducarme eds. Proc 13th Int Symp Earth tides, Brussels. Geophysical Series, Royal Observatory of Belgium, 1998, 557–564

[6] Hsu HT, Becker M, Groten E. Comparison of Gravity Tide Observations by ET16 and ET21 at Wuhan Station of China. Bull Inf Marees Terrestres, 1989, 104: 7379–7394

[7] Ogasawara S, Higashi T, Fukuda Y and Takemoto S, Calibration of a superconducting gravimeter with an absolute gravimeter FG-5 in Kyoto, J. Geodetic Society Japan, 2001, 47(1): 404–409.

[8] Sun H.P, Chen X.D, Hsu H.Z, Wang Y, Accurate determination of calibration factor for tidal gravity observation of a GWR-superconducting gravimeter, ACTA Seisologica Sinica, 2001a, 14(6): 692–700.

[9] Sun HP, Takemoto S, Hsu HT, Higashi and Mukai, Precise Tidal Gravity Recorded with Superconducting Gravimeters at Stations Wuhan/China and Kyoto/Japan. Journal of Geodesy, 2001b, 74: 711–719

[10] Warbuton RJ. GWR instruments cryogenic refrigerating manual, San Diego CA921221, USA, 1985, 1–105

Aspects of gravimeter calibration by time domain comparison of gravity records

Bruno Meurers[1]
Institute for Meteorology and Geophysics
University of Vienna

Abstract

This paper addresses the accuracy problem of gravimeter calibration performed by time domain comparison of different gravity sensors. Un-modelled instrumental drift and the noise of the data are main sources of systematic error components. Several synthetic and real case studies are discussed to estimate accuracy limits. A simple drift elimination method is proposed that is well suited to be applied also for spring gravimeters with irregular drift. At least strong drift components have to be removed otherwise both calibration factor and time lag do not necessarily converge towards the figures within the required 0.1% accuracy limit.

Introduction

High calibration accuracy is still an important issue for getting reliable results in tidal research, gravity monitoring and microgravimetry. Gravimeter calibration can be done either in time or in frequency domain by comparing the instrumental response of two sensors on common signals (e.g. earth tides, artificial gravitational or inertial effects). The most important requirement is that signals of same physical origin are compared only and that the sensor transfer functions are considered. Time domain calibration methods like regression analysis can be applied successfully even on short data sets (< 200 h). Contrary, the frequency domain calibration method requires long observation periods (≥ 720 h) in order to separate the main tidal constituents properly. Therefore it detects calibration factor variations in much lower temporal resolution than regression analysis, while drift determination, noise and different air pressure response of the sensors are less critical.

A severe problem is that the signal composition of both sensors differs due to following reasons:

- instrumental noise and response on micro-seismic noise
- instrumental drift
- transfer function introducing different time lags
- response on air pressure variations (e.g. non-compensated Archimedian forces in LCR gravimeters)

Absolute gravimeters (AG) are commonly used as reference sensors to calibrate superconducting gravimeters (SG). Experience has shown that long data series of up to 7 days' interval are necessary to get stable results with accuracy better than 0.1% (e.g. Francis 1997, Francis et al. 1998). SGs exhibit an extremely small and almost linear instrumental drift of less than a few μGal per year. Anti-alias filters and 1 Hz sampling permit additional numerical filtering of the SG output channel to obtain low noise data. Contrary, AG data is acquired with a much longer sampling interval (15 – 30 s) and generally shows a much larger scatter. Due to instrumental effects the existence of small drift components can be excluded neither in SG nor in AG records which could influence the calibration result systematically. Fig. 1 compares the

[1] E-mail: bruno.meurers@univie.ac.at

data of a calibration experiment performed in Vienna on 19990925. It demonstrates the different noise level of the data sets used, but also clear systematic effects in the AG data. This paper tries to address the influence of systematic effects on the calibration result if they remain un-modelled prior to regression analysis. This is done in a more general aspect in order to get accuracy limits not only for AG-SG intercomparisons, but also for other gravity sensor combinations including spring type gravimeters (e.g. LCR, Scintrex). In this case the strong and irregular drift of spring gravimeters is expected to introduce systematic calibration errors. In addition, LCR gravimeters are known to give an abnormal response on air pressure variations (e.g. Arnoso et al. 2001).

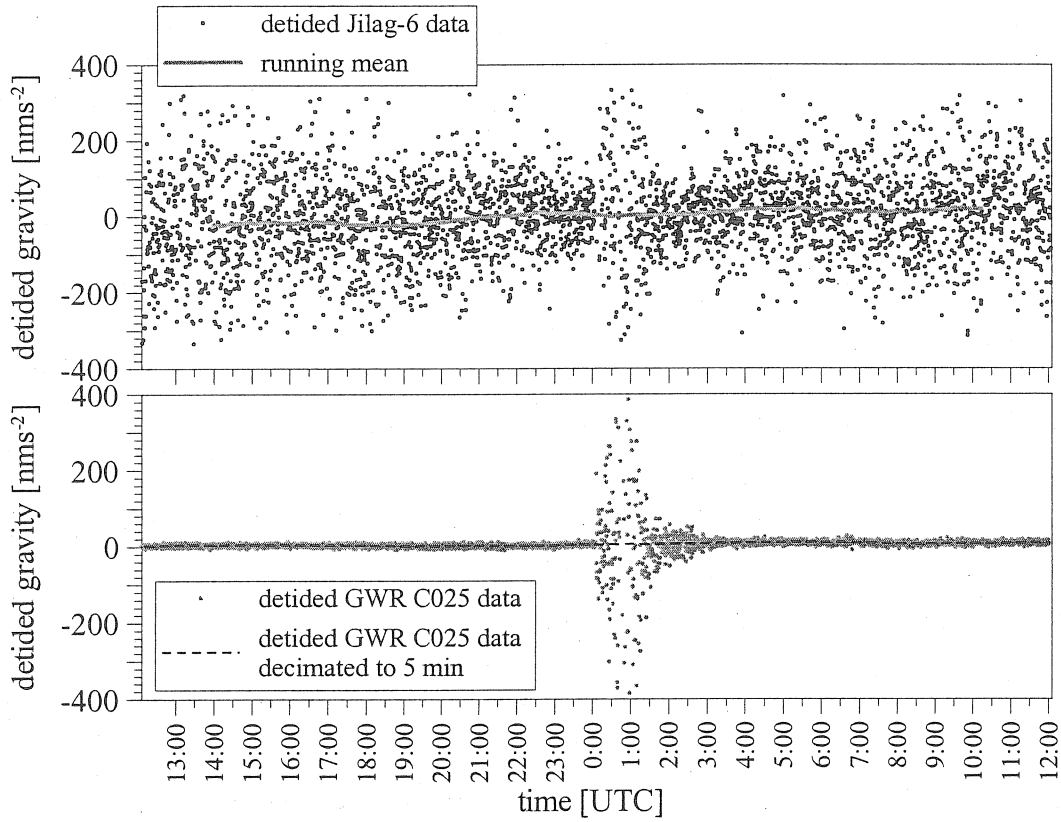

Fig. 1: Comparison of detided SG (bottom: GWR C025, 1s samples) and AG (top: Jilag-6, 25s samples) data (Vienna, 19990925)

Synthetic studies

Several test calculations have been performed to investigate the effect of

- random noise and time lag
- instrumental drift and different air pressure response

using a data set based on predicted model tides with 20s sampling. This sampling rate is typical for AG data. Both calibration factor and time lag were determined by LSQ-adjustment.

Random noise and time lag

The model tides were compared with two different data sets:

1. model tides with time lag of 20s
2. model tides with time lag of 20s and normally distributed noise with a standard deviation of 50 nms^{-2})

Several different noise models have been used. As long as the standard deviation is not larger than 50 nms^{-2}, in each case the adjusted calibration factor fulfils the 0.1% accuracy requirement. However, convergence is very slow or even does not result exactly to the expected figure. This highly depends on the noise structure. The same is valid for the adjusted time lag. In addition, time lag adjustment does not essentially improve the result of the calibration factor adjustment. Obviously small un-modelled time lags do not influence the result strongly in spite of the fact, that neglecting different sensor time lags is equivalent to an additional signal consisting of diurnal, semidiurnal and long-periodic components. If there is no noise present in the data, the adjusted calibration factor is identical almost exactly with the expected one even when the time lag is not adjusted. Adjusted time lags correspond exactly to the expected ones. Fig. 2 is shown as an example.

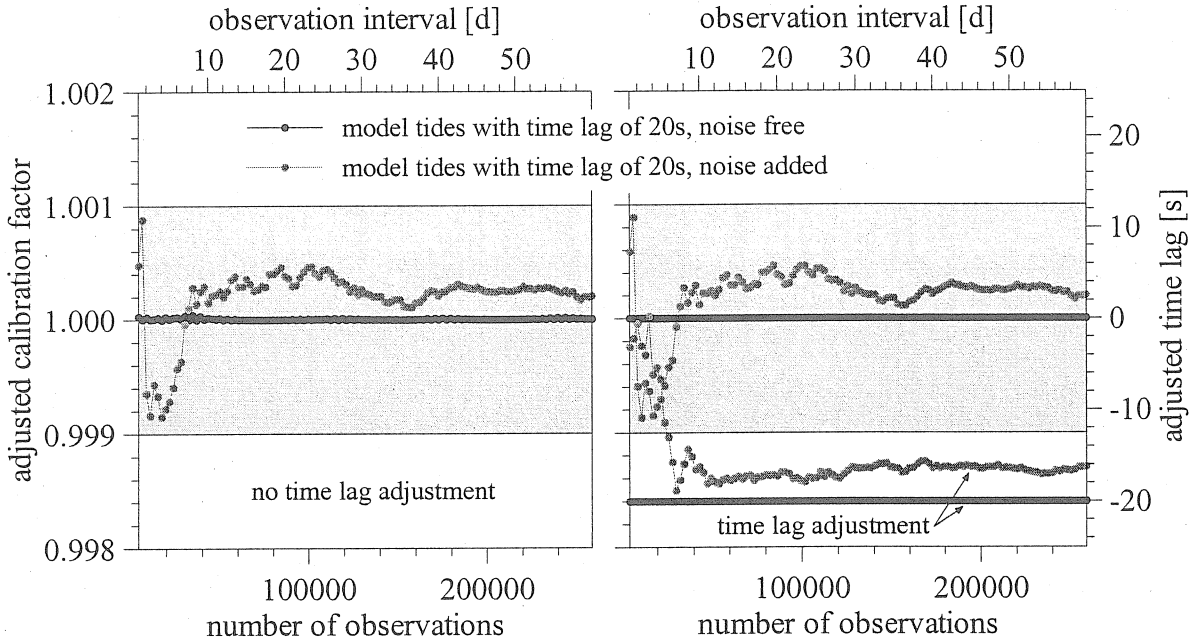

Fig. 2: Influence of phase shift and noise on the adjusted calibration factor. Adjustment results are shown in dependence upon the number of samples used. Both sensors' data consist of model tides (20s samples); those of the 2nd sensor have a time shift of 20s. Grey dots indicate the results obtained when random noise is superimposed to the data of the second sensor.

Instrumental drift and different air pressure response

A major problem is the presence of instrumental drift in the compared data sets, because drift separation in the time domain is a difficult task. Francis and Hendrickx (2001) applied a simultaneous adjustment of the calibration factor and a third degree drift polynomial when calibrating a LCR gravimeter by collocated SG observations. They achieved temporarily stable accuracy of about 0.1% by analysing 15 days' intervals. However, the drift behaviour of some spring gravimeters does not permit low degree polynomial adjustment. For those cases another method is proposed here. It is based on the approach by Lassovsky (1956) who used the zeros of model tides as supporting points of the drift function. In this study a similar procedure has been applied. After subtracting the air pressure effect by using a single admittance model, gravity readings at moments when the model tides are zero yield the drift supporting points. Finally a continuous drift function is constructed by cubic spline interpolation.

In order to investigate both the efficiency of this method and the effect of un-modelled drift components, several test calculations have been performed by comparing model tides (20s

samples) to those with different drift models superimposed. The drift models consist of both a linear and a random component:

1. systematic component: 5 nms^{-2}/14 days,
   random component: 10 supporting points/14 days, standard deviation 5 nms^{-2}
2. systematic component: 5 nms^{-2}/14 days,
   random component: 30 supporting points/14 days, standard deviation 5 nms^{-2}
3. systematic component: 30 nms^{-2}/14 days,
   random component: 10 supporting points/14 days, standard deviation 5 nms^{-2}

where the number of supporting points controls the frequency content of the drift model. The selected drift parameter enables to study the effect of even very irregular instrumental drift like that of LCR gravimeters.

The examples shown in Fig. 3 prove the drift elimination method to work properly even when high frequency drift components are present. If the drift is eliminated before adjusting the calibration factor, the latter converges very quickly towards the expected figure. High frequency drift components make convergence worse. In this case a time interval of about 6-8 days is required to get accurate results. If the drift is not subtracted, the error of the adjusted calibration factor remains below the 0.1% accuracy level after one week observation period except when high systematic drift components are present.

The dependence of the calibration result on the pre-processing method is tested finally by using real gravity data from GWR C025. Model tides derived by tidal analysis of a 6.5 years' recording of this SG in Vienna served as reference signal. As second sensor, SG data sets covering a 14 days' interval each were applied after different kind of pre-processing:

1. no corrections
2. air pressure correction (single admittance model), but no drift elimination
3. no air pressure correction prior to drift elimination
4. air pressure correction prior to drift elimination

All data sets were decimated to 20s samples. Fig. 4 (top) shows the residuals after subtracting the drift for the case studies 4 (black) and 3 (grey) respectively. It proves that considering the air pressure effect is a necessary step to get more reliable drift functions. If this effect is not corrected, it remains as high frequency drift signal in the data and therefore sometimes cannot be fully eliminated by the proposed method. This aspect is important, if the two sensors are expected to respond on air pressure differently (e.g. LCR gravimeters). The results of the calibration factor adjustment are displayed in Fig. 4 (bottom). If no correction is performed at all, both the calibration factor and time lag converge after an about 7 days' observation interval, but to wrong figures. Fast and stable convergence occurs only after removing the air pressure effect and instrumental drift. Reliable time lags are obtained only if the air pressure effect is subtracted and if drift remains untouched. Drift elimination corrupts the time lag information of the data. As mentioned before, time shifted data can be composed of the original one and of a systematic drift consisting of semidiurnal, diurnal and long period components that are removed at least partially by drift elimination.

The time domain calibration method is well suited to determine calibration factor variations in high temporal resolution. This is demonstrated by the last case study. During a more than 1-year period started in June 2000, the LCR D-9 gravimeter equipped with a SRW-D type feedback system (Schnüll et al. 1984) was monitoring parallel to the GWR C025 in Vienna. Tidal analyses of successive, non-overlapping periods prove that the calibration factor of GWR C025 is very constant (Meurers 2001). The amplitude factors for the main tidal waves vary by

less than 0.1% even when intervals as short as 1 month are analysed (Fig. 6, open squares). Therefore the SG can be used as stable reference to calibrate the feedback.

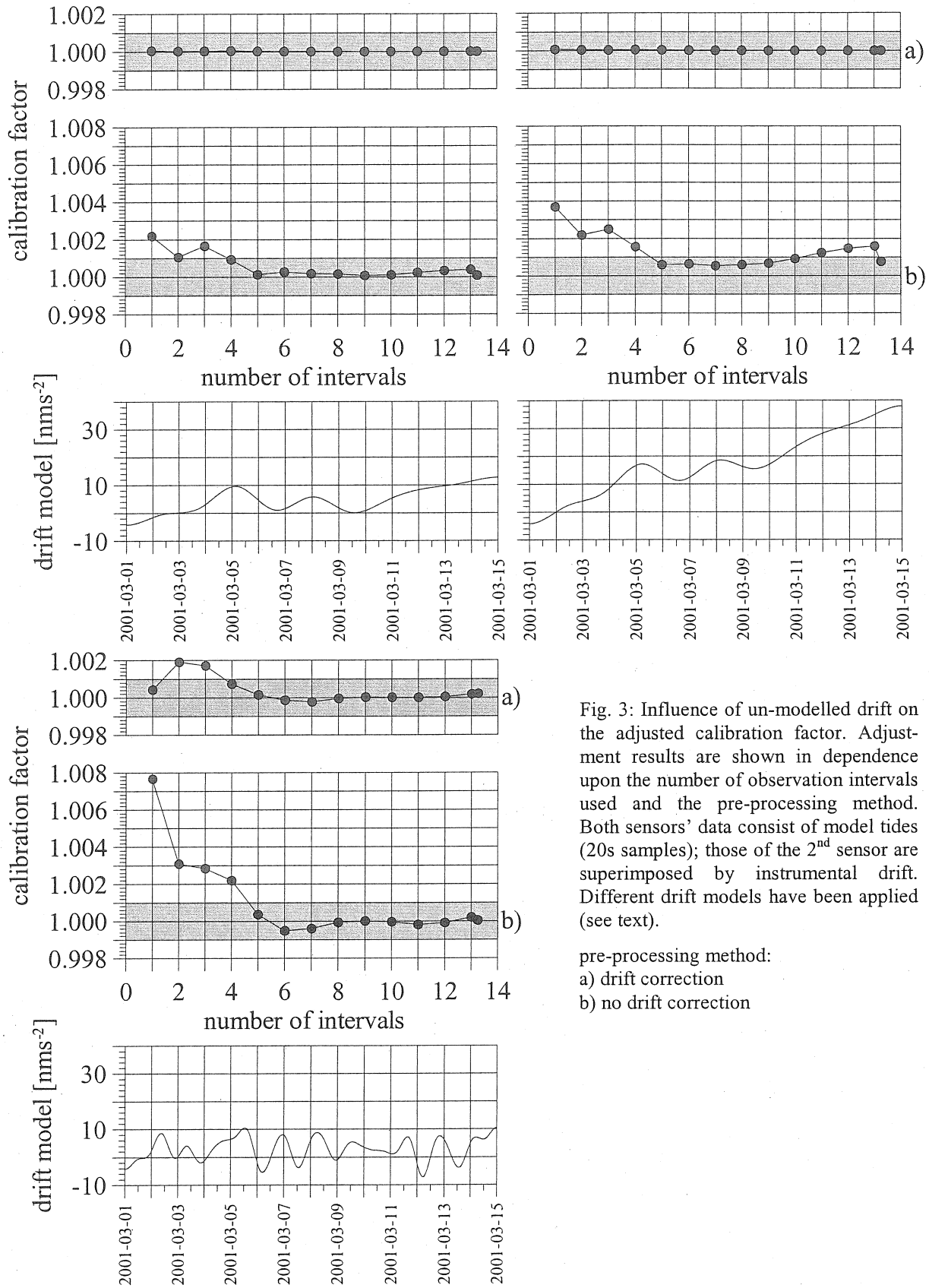

Fig. 3: Influence of un-modelled drift on the adjusted calibration factor. Adjustment results are shown in dependence upon the number of observation intervals used and the pre-processing method. Both sensors' data consist of model tides (20s samples); those of the 2nd sensor are superimposed by instrumental drift. Different drift models have been applied (see text).

pre-processing method:
a) drift correction
b) no drift correction

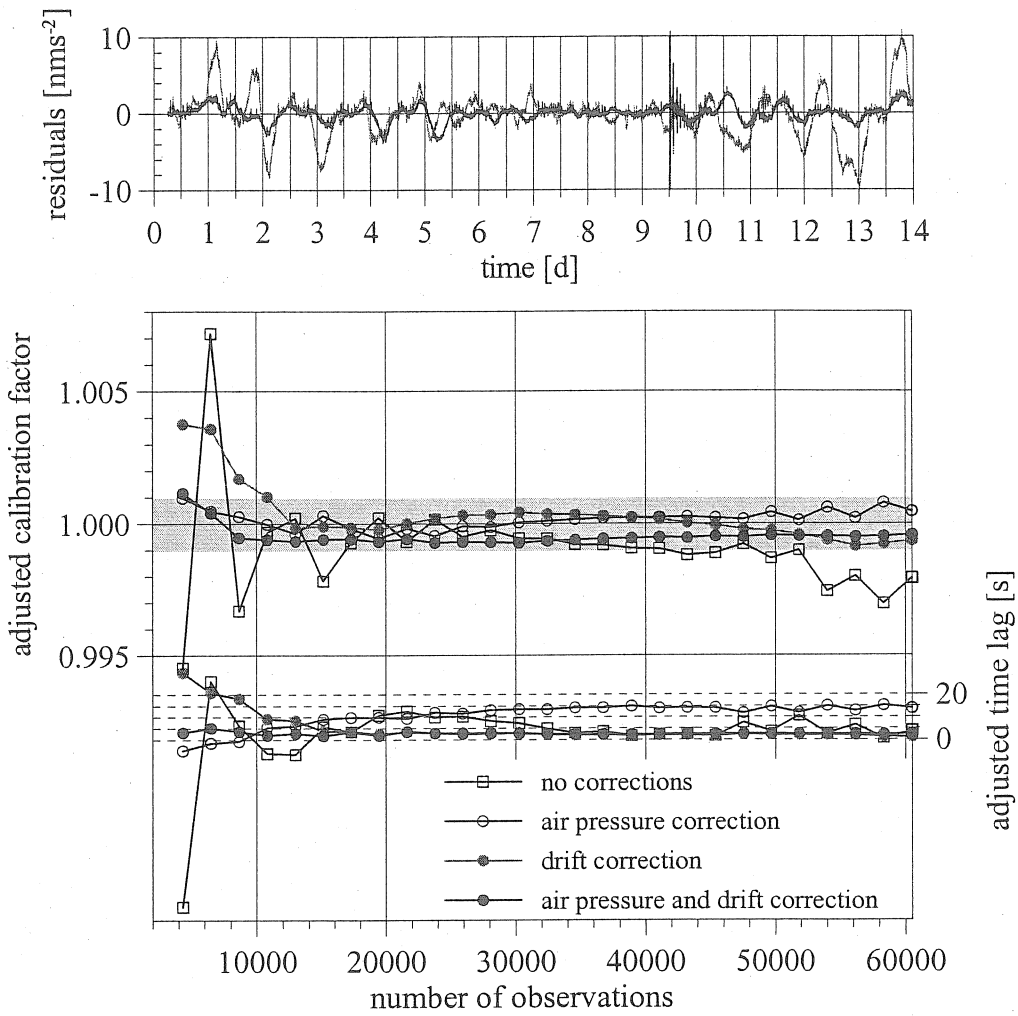

Fig. 4: Influence of different pre-processing steps on the calibration factor adjustment.
Bottom: Adjustment results are shown in dependence upon the number of observations used and the pre-processing method. 1st sensor: model tides derived by tidal analysis of a 6.5 years' recording of GWR C025. 2nd sensor: GWR C025 data (19970302 – 19970316), decimated to 20s samples.
Top: gravity residuals calculated by subtracting the drift. Air pressure has been (black) or has not been considered prior to drift elimination (single admittance model).

The feedback calibration factor turned out to be extremely unstable in time probably due to a still unknown malfunction of its electronics. The LCR D-9 as a spring-type gravimeter exhibits strong and irregular instrumental drift. In addition, its response on air pressure variations differs significantly from that of the SG. The admittance factor results to -5 nms^{-2}/hPa instead of -3.5 nms^{-2}/hPa. Therefore the drift of both sensors has been eliminated after air pressure correction applying the respective admittance factors. Prior to this step both data sets were decimated to 5 min samples. Successive overlapping intervals covering 2000 samples each (approximately 7 days) have been analysed. Fig. 5 shows the temporal variations of the feedback calibration factor resulting from the single adjustments.

The long-term behaviour of this variation can be recognized also in Fig. 6 (grey dots), where the amplitude factors of M_2 and O_1 are plotted versus time. The latter were calculated by performing tidal analyses of successive 1-month intervals evaluated by using a constant feedback calibration factor. Common features indicate sensitivity variations to be the reason. When taking the temporal sensitivity variation according to Fig. 5 into account, the amplitude factors get much more stable, especially in case of M_2, and common features disappear (Fig. 6, black dots).

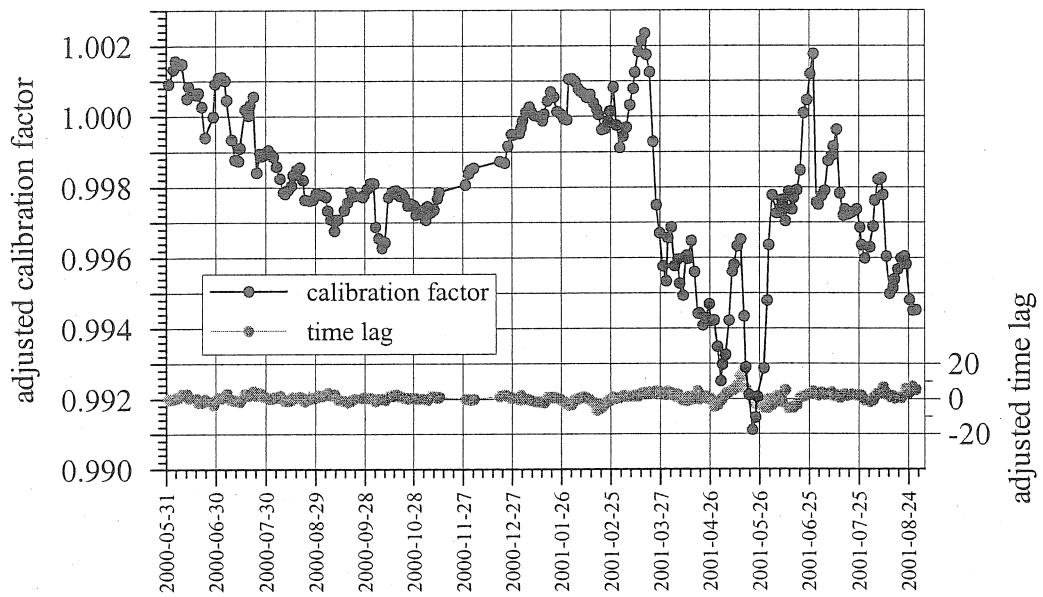

Fig. 5: Calibration factor of LCR D-9/SRW-D resulting from adjustments of successive intervals of 7 days (2000 samples, 5 min sampling) using GWR C025 data as reference.

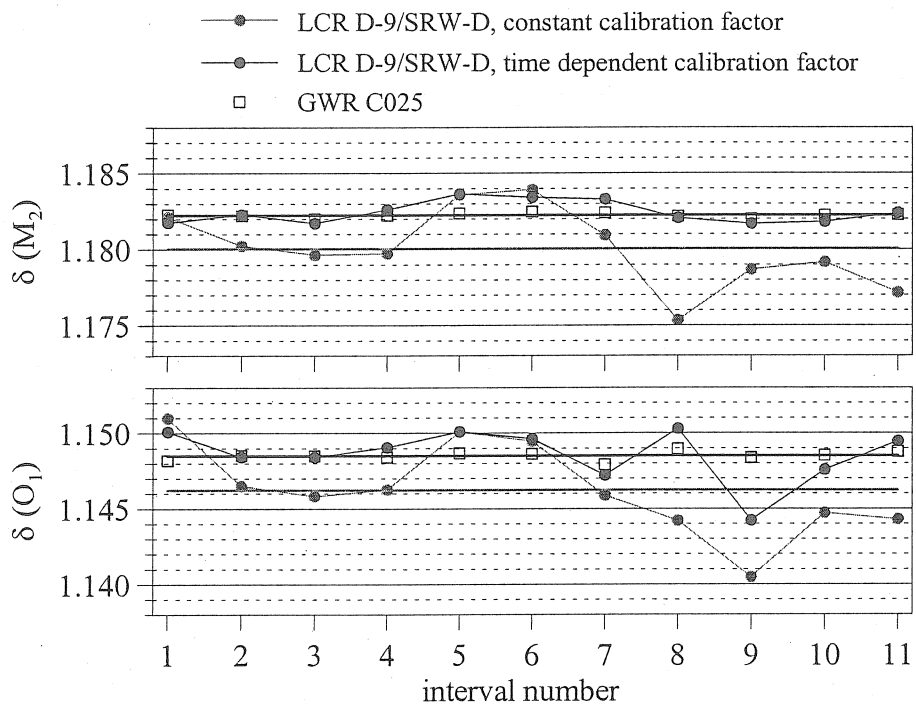

Fig. 6: Amplitude factors resulting from tidal analyses of successive intervals (1 month) recorded by LCR D-9/SRW-D and GWR C025.

Conclusions

The time domain calibration method has limited accuracy. The main sources of systematic error components are the noise of the data and un-modelled instrumental drift. For noisy data the calibration factor converges very slowly with increasing number of observations involved, but does not necessarily result exactly to the correct figure, depending on the noise structure. However, the adjusted calibration factor fulfils the 0.1% accuracy requirement. The same is

valid for the time lag adjustment that does not essentially improve the result of the calibration factor.

If strong drift components are not removed both calibration factor and time lag do not converge towards the correct figures even after observation periods longer than 7 days. On the other hand, drift elimination does no longer permit a time lag adjustment because it corrupts the phase information of the data.

If the compared sensors exhibit low and regular drift like SGs, accuracy better than 0.1% can be obtained from data covering an interval of 6-8 days. Although AG data sometimes show a small apparent drift caused by time dependent systematic effects, drift elimination is not recommended when calibrating a SG by comparing with AG data, as it removes physical signal components (e.g. air pressure effect) at least partially and perhaps differently for both instruments.

The situation is quite different when calibrating a spring-type gravimeter by comparison with SG data. Spring gravimeters often show strong and irregular instrumental drift and different response to air pressure variations. In this case the drift has to be eliminated before the regression analysis, and the air pressure effect has to be subtracted for both sensors before drift determination.

References

Arnoso, J., Vieira, R., Velez, E.J., Van Ruymbeke, M. and Venedikov, A.P., 2001: Studies of tides and instrumental performance of three gravimeters at Cueva de los Verdes (Lanzarote, Spain). Jour. Geod. Soc. Japan, **47**, 1, 70-75.

Francis, O., 1997: Calibration of the C021 Superconducting Gravimeter in Membach (Belgium) using 47 days of absolute gravity measurements. IAG Symposia, 117, 212-219.

Francis, O., Niebauer, T.M., Sasagawa, G., Klopping, F. and Gschwind, J., 1998: Calibration of a superconducting gravimeter by comparison with an absolute gravimeter FG5 in Boulder, Geophys. Res. Lett., **25**, 1075-1078.

Francis, O. and Hendrickx, M., 2001: Calibration of the LaCoste-Romberg 906 by Comparison with the Superconducting Gravimeter C021 in Membach (Belgium), Jour. Geod. Soc. Japan, **47**, 1, 16-21.

Lassovsky, K., 1956: A Fold deformacios egyutthatojanak meghatarozasa gravimetereszlelesekbol. Geofisikai Kozlemenyek, **2**, 18-26.

Meurers, B., 2001: Tidal and Non-tidal Gravity Variations in Vienna - a Five Years' SG Record, Jour. Geod. Soc. Japan, 47, 1, 392-397.

Schnüll, M., Röder, R.H. and Wenzel, H.G., 1984: An improved electronic feedback system for LaCoste&Romberg gravity meters. BGI, Bulletin d'Information, **55**, 27-36.

VAV: A PROGRAM FOR TIDAL DATA PROCESSING

A.P. Venedikov[1], J. Arnoso[2] and R. Vieira[2]

[1] Geophysical Institute, Bulgarian Academy of Sciences, Acad. Bonchev street block 3, Sofia 1113, vened@geophys.bas.bg

[2] Instituto de Astronomía y Geodesia (CSIC-UCM). Universidad Complutense de Madrid. Facultad de Matemáticas. 28040 Madrid, Spain. arnoso@iagmat1.mat.ucm.es, vieira@iagmat1.mat.ucm.es

(Paper submitted to Computers & Geosciences)

Abstract

The paper deals with a new computer program, named VAV, for the analysis of any kind of tidal data. VAV can be applied on unevenly spaced data without any interpolation. The basic algorithm consists in a transformation of the data from the time domain into a time/frequency domain. This is done through filtration of data intervals without overlapping. This operation eliminates a rather flexible model of the drift. The filters used are orthogonal and in the case of unevenly spaced data, they are adaptable in the time domain. After the transformation, the tidal parameters are estimated through the method of the least squares that is applied in the time/frequency domain. Since the noise of the data is correlated, VAV provides frequency dependent estimates of the precision. The program is specially orientated towards the search of various anomalies of the data, which may be useful, eventually, for earthquake and volcano monitoring.

Influence of different processing methods on the retrieval of gravity signals from GGP data

J. Hinderer, S. Rosat, D. Crossley*, M. Amalvict, J.-P. Boy & P. Gegout

EOST/IPGS (CNRS-ULP)
5, rue Descartes 67084 Strasbourg Cedex France

* On leave from Dept. Earth and Atmospheric Sciences, Saint Louis University,
3507 Laclede Ave., St. Louis, MO 63103, USA

jhinderer@eost.u-strasbg.fr

Abstract

This study is devoted to the investigation of different processing methods of superconducting gravimeter (SG) data as available from the GGP network. We will use two different periods for our investigation: the first is a test period from March to December 1997 where we compare the impact on residual noise levels of 3 different processing procedures and the second is an interval going from March 1997 to February 2002 where we focus on the impact of instrumental drift and on the superposition with absolute gravimeter (AG) data.

1. Introduction

We intend to investigate here different processing methods of SG data as available from the GGP network since July 1997 (Crossley et al. 1999). Of course, any gravity set has to be pre-processed because there is a need for correcting the disturbances (spikes, steps, gaps) which would degrade any further treatment such as tidal analysis or spectral estimation. The problem of data gaps is in fact different from spikes and steps because the information is missing rather than corrupted leading to unevenly spaced data sets with all the inherent restrictions in using standard codes such as ETERNA (Wenzel 1998) or simply an FFT.
The main reason for this investigation is to measure the impact of any specific treatment in terms of noise levels of the gravity data. Another reason is to test the possibility of using a fully automatic method (or at least a semi-automatic treatment with final manual step adjustments) which could be extremely helpful in the pre-processing of a large number of SG data sets as available in the GGP data base. It is quite obvious that the work presented here, on a limited period (9 months in 1997) for only one station (Strasbourg), is time consuming and cannot be extended without tremendous effort to all the GGP stations.

Many different processing methods are available and in fact any SG group has its own strategy to pre-process the data. Even when using the same processing tool, there are however often personal factors that enter the treatment. For example, if some of the corrections can be set automatically by introducing a specific threshold for spike detection and removal, other problems such as small amplitude steps (offsets) need a visual inspection and a personal decision whether to correct or not. Usually the classical preliminary step is to compute the residual gravity data using the following sequence:

- correction for local pressure effects using a standard barometric admittance – 3 nm s^{-2} /hPa, (see Crossley et al. 1995), or any other fitted value from a previous tidal analysis;
- correction for (solid Earth and ocean) tides by subtracting a so-called local tide computed from the luni-solar tidal potential with tidal gravimetric amplitude and phase factors originating from a previous tidal analysis at the same station. If such an analysis is not available, then one can use nominal factors for the solid Earth (e.g. Dehant et al. 1999) and ocean loading contributions (e.g. Scherneck 1991).

These two steps lead to the gravity residuals which are usually small amplitude signals which permit an easier detection of problems than the full gravity series.

We list hereafter some of the available methods for dealing with further problems:
- the slew rate method (Crossley et al. 1993) which is based on the application of a specific threshold to the time-derivative of the gravity residuals in order to detect non-physical samples. Rejected values can then be replaced by zero values which means that the gravity signal is replaced by the local theoretical tide;
- the PRETERNA pre-processing program by Wenzel (1994) using a threshold directly on the gravity residuals;
- the TSOFT program by Vauterin (1998) which consists in an automatic and/or manual corrections for spikes, gaps and steps applied on the gravity residuals;
- the least squares spectral analysis method by Pagiatakis (1999, 2000) which relies on a completely different philosophy namely that there is no need to interpolate bad data (samples can be unevenly spaced) and that there is a statistical estimate on the steps.

2. Test period: Strasbourg data from March 1997 to December 1997

We have tried here to compare 4 different methods applied to the gravity residuals:

1. a slew rate detection approach (Crossley et al. 1993) on 1 min samples but with manual correction for steps (data set provided by Jean-Paul Boy and method named JPB); the threshold was fixed to 2 nm s^{-2}/min to reject gravity data;
2. a semi-automatic treatment on raw data (2 sec) day by day (data set provided by David Crossley and method named DC); step 1 (DC 1) is essential cleaning to remove major disturbances and step 2 (DC 2) is final cleaning correcting smaller offsets and disturbances; data are then decimated to 1 min with the J9 filter which is the low-pass decimation filter we are using in Strasbourg;
3. a TSOFT-based method (data set provided by Séverine Rosat and method named SR) applied to 2 sec samples and further decimated to 1 min with J9 filter;
4. a TSOFT-based method either on 2 sec or 1 min samples and in a fully automatic or semi-automatic way (threshold of 10 nm s^{-2}) using the TSOFT tools (data set provided by Jacques Hinderer and method named JH); 2 sec samples are decimated to 1 min using a TSOFT decimation filter.

The evolution of the gravity residuals due to these four different pre-processing methods is shown in Figure 1. We began the time series by superposing the data and, because of different assumptions about the subsequent offset corrections, one sees that there is a cumulative divergence of the residuals at the end of the series.

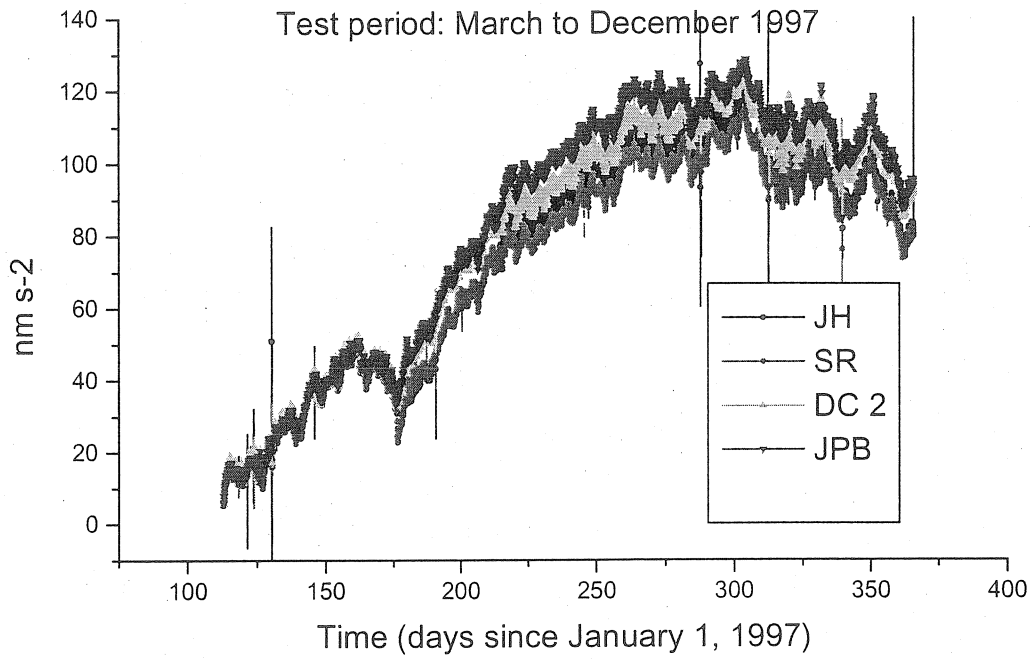

Figure 1. Gravity residuals during the test period in Strasbourg according to the 4 different pre-processing methods (JH, SR, DC 2, JPB).

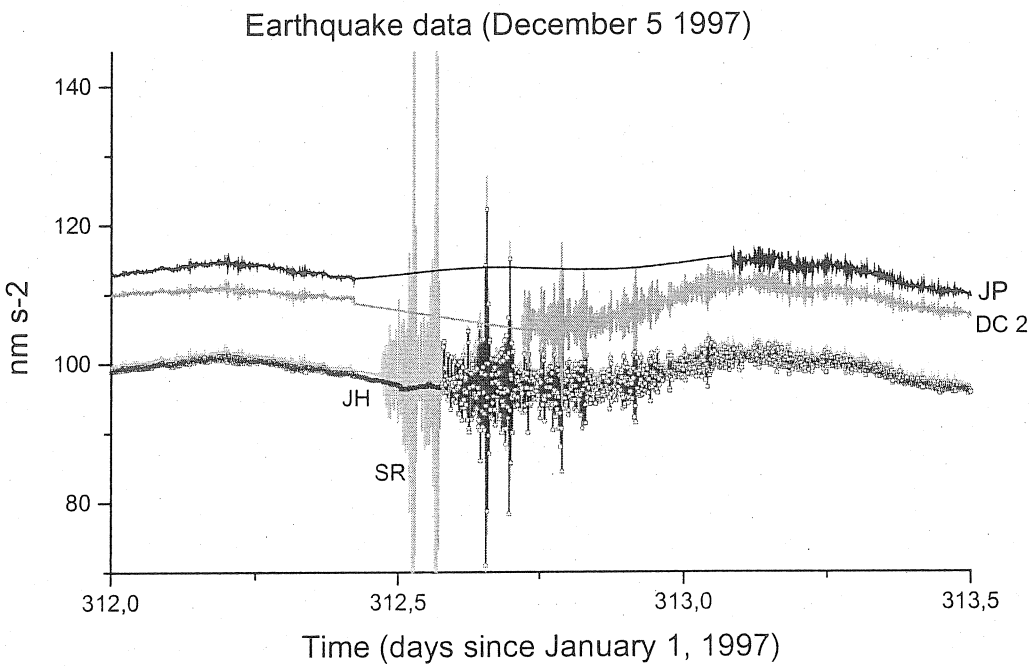

Figure 2. Different corrections of the gravity data during an earthquake (December 5, 1997).

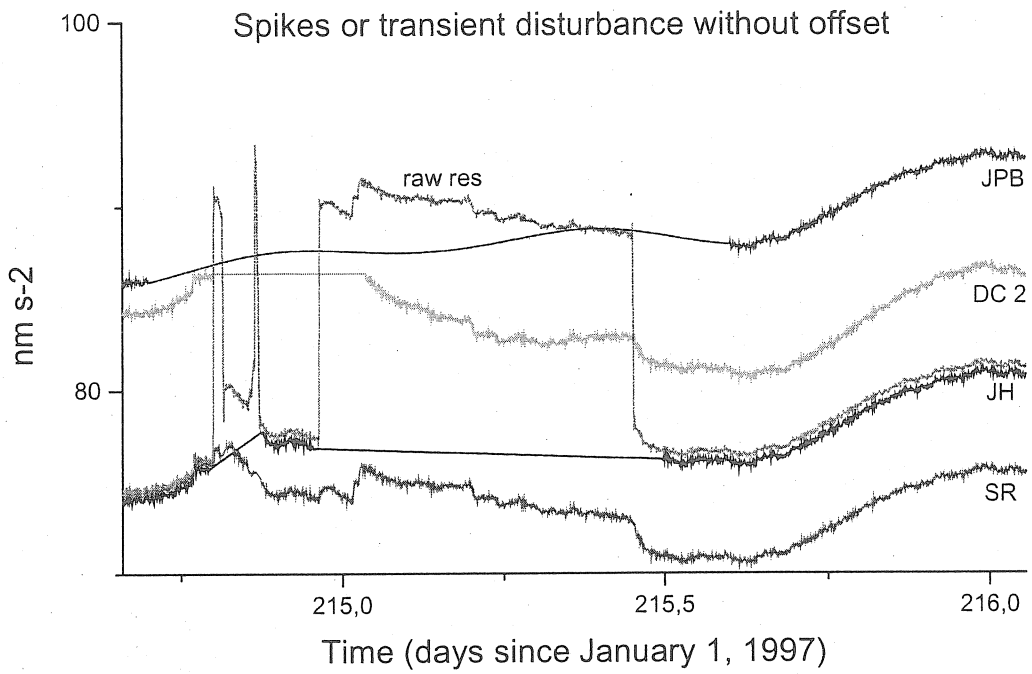

Figure 3. Corrections of spikes or transient disturbances without cumulative offset.

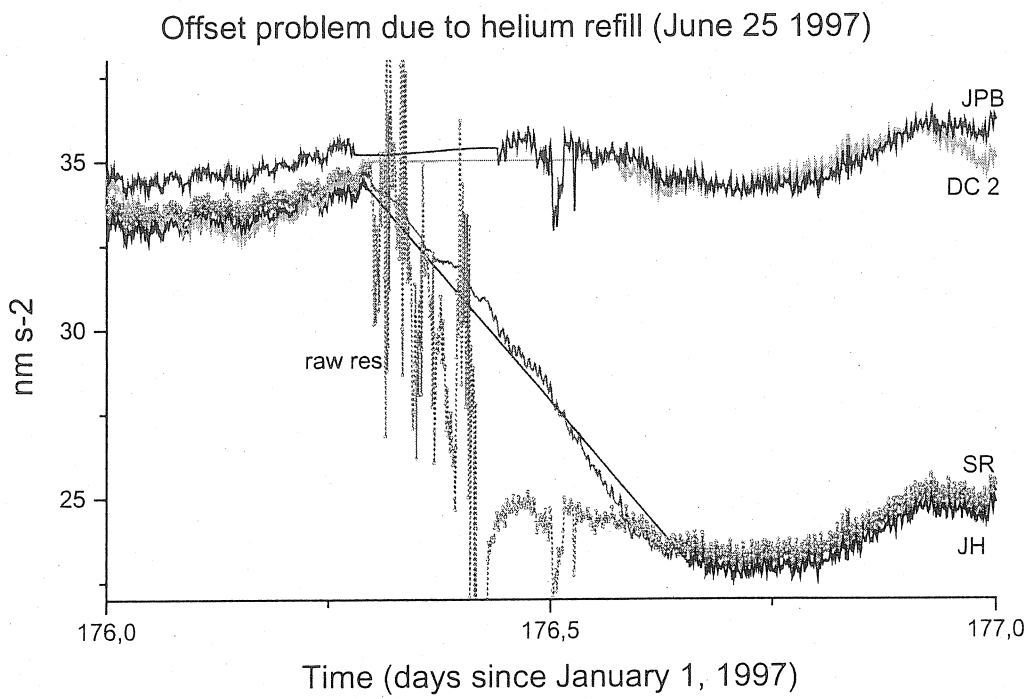

Figure 4 . Corrections of gravity data during a transfer of liquid helium in June 1997.

Other examples of problems we are facing with gravity data are shown in accompanying figures. The corrections of the data during an earthquake (December 5, 1997) are shown in Figure 2 and one sees clearly that the amount of rejected data, depending on the philosophy of dealing with earthquakes, is highly variable from one author to the other.

The case of spikes or transient disturbances (mechanical or electrical) is shown in Figure 3 and again the changes differ according to the method (the raw residuals are also shown with a dotted line).

The final example is given in Figure 4 and concerns a possible offset problem related to a transfer of liquid helium. It is evident that two methods (JH and SR) do not correct for an offset, whereas the two other authors consider an offset to have occurred.

We have used the different time series in order to compute power spectral densities (PSD) (expressed in (nm s^{-2})^2 Hz^{-1}) for inter-comparing the noise levels in various frequency bands. A general view of these noise levels is given in Figure 5 for the 5 different processing methods (DC 1 and DC 2, JH, SR, JPB); the legend is labelled according to decreasing power levels (e.g. DC 1 is the most noisy signal and the least noisy is JPB).

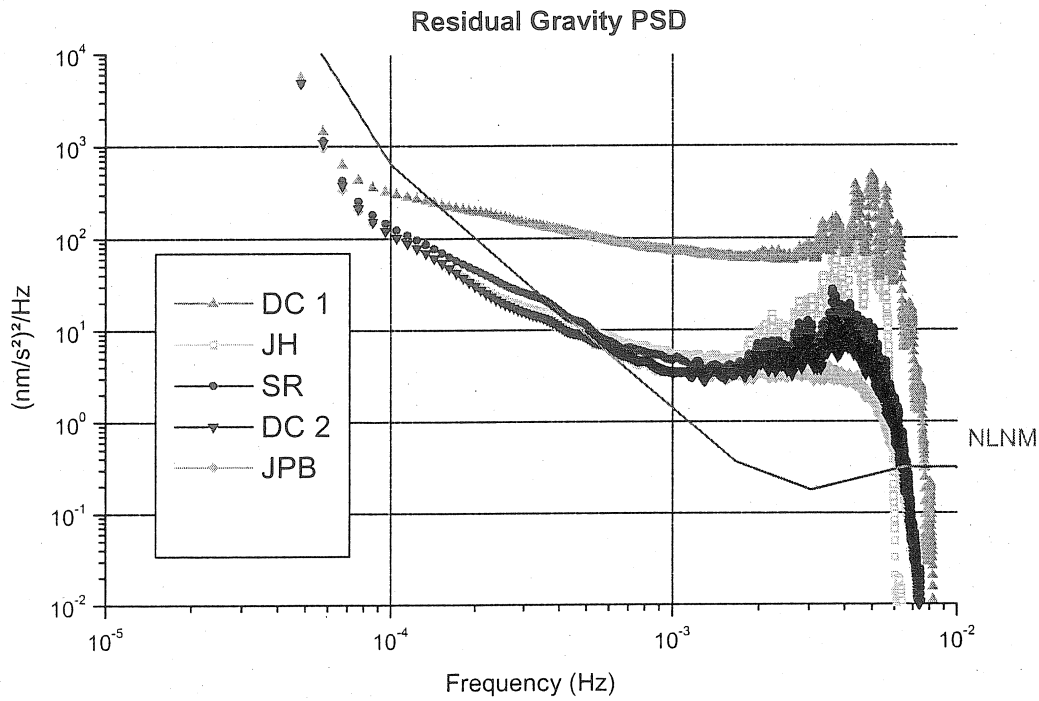

Figure 5. Power spectral densities of 5 residual gravity series, according to different methods of processing the data.

The continuous line is the New Low Noise Model (NLNM) of Peterson (1993) inferred from all the seismological records worldwide. For a more general discussion on the noise levels of the various GGP stations, we refer to Banka & Crossley (1999) and to Rosat et al. (2002). The decrease at the right end (high frequencies) is entirely caused by the decimation filters from 2 sec

to 1 min data. The left end shows that there is a convergence in the noise levels (for frequencies below 5. 10^{-5} Hz) which means that the tidal analysis of the corrected data would lead to almost the same results whatever the correction method. In the intermediate part, between 10^{-4} and 6. 10^{-3} Hz concerning the seismic and subseismic bands, the levels vary according to the method; DC 1 is much higher (by a factor 10) in PSD but this is not surprising because only the major gaps and offsets have been treated. The four other methods lead to similar noise levels for low frequencies but to different levels in the high frequency part mostly because of different amount of rejected data after earthquakes. This is why the lowest noise curve (JPB) corresponding to the highest number of rejected seismic data (see Figure 2) is also the one exhibiting almost no normal modes in the seismic band.
A zoom of Figure 5 focussing on the band (10^{-3} - 10^{-2} Hz) is given in Figure 6.

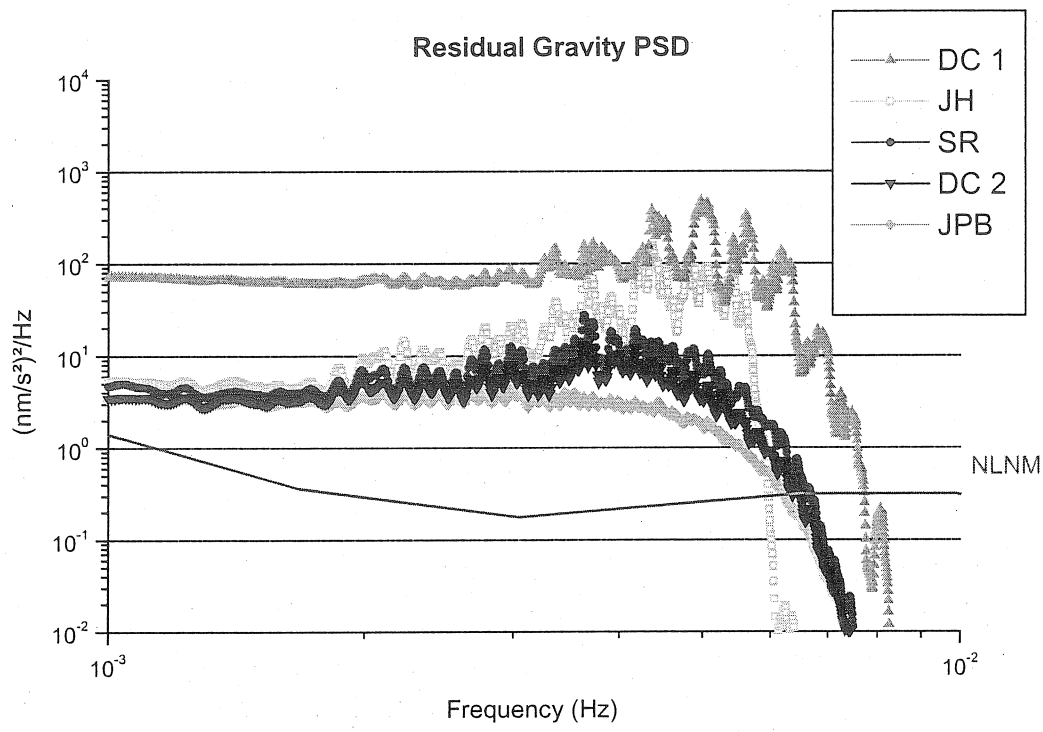

Figure 6. A zoom of Figure 5 for frequencies between 10^{-3} and 10^{-2} Hz. Note that there is a factor of 10 between the lowest and highest noise levels.

We will now show more specific results on the effects of some steps in the pre-processing. In all the remaining figures in this section, the different residual gravity PSD are computed with data from the JH method based on TSOFT. First, the role played by the decimation filter (from 2 sec to 1 min) is illustrated in Figure 7 where we compare the J9 filter (our own low-pass filter) to the filter implemented in TSOFT. The major difference is in the high frequency attenuation before the Nyquist frequency which is 8.33 10^{-3} Hz (for 1 min sampling); the different cut-off frequency also slightly alters the seismic band. Clearly the TSOFT filter is superior to the J9 one but one has to keep in mind that the length of these filters also differs.

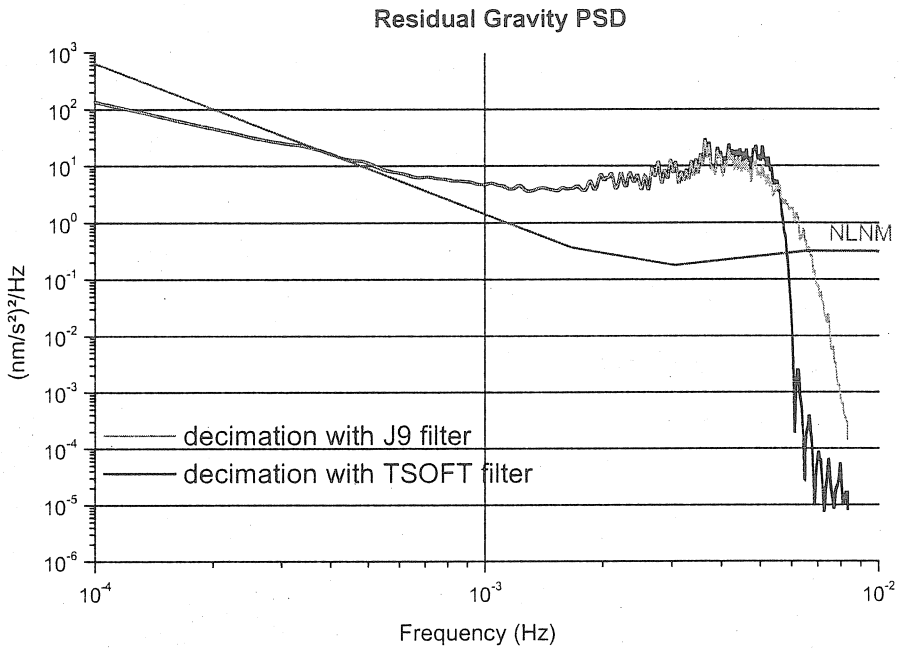

Figure 7. Residual gravity PSD of manually corrected 2 sec samples, one decimated with TSOFT and the other using the J9 digital decimation filter.

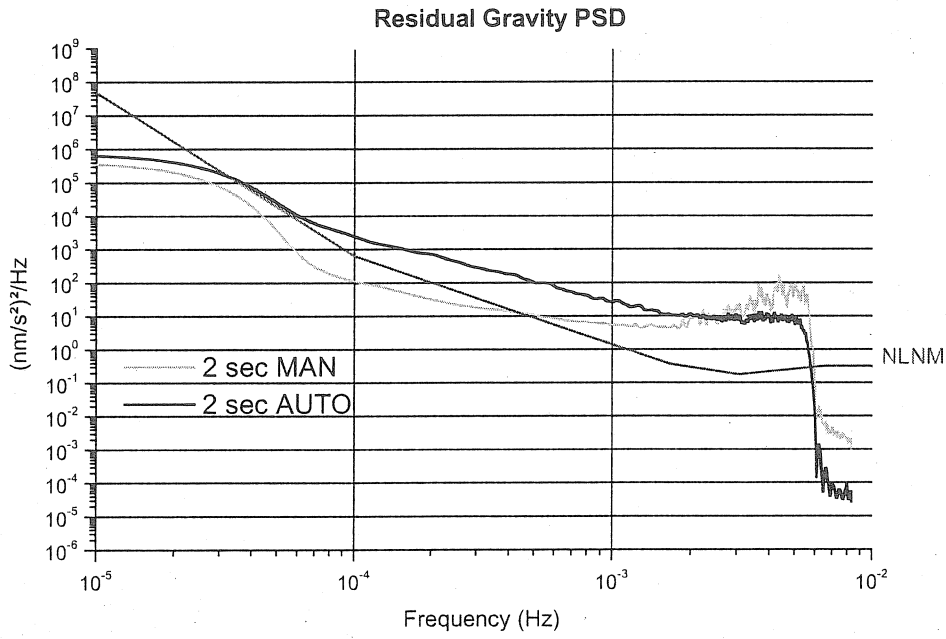

Figure 8. Residual gravity PSD according to automatic or manual corrections on 2 sec samples before 1 min decimation (both using the TSOFT filter).

The impact of using automatic or manual corrections on the 2 sec data is shown in Figure 8 and points out the rather large noise level changes which can arise in the seismic and subseismic bands; clearly this figure shows only one possible outcome because there is a specific threshold (in our

case 10 nm s^{-2}) that can be used for the automatic spike rejection and that the manual corrections are depending on the author (in this case JH).

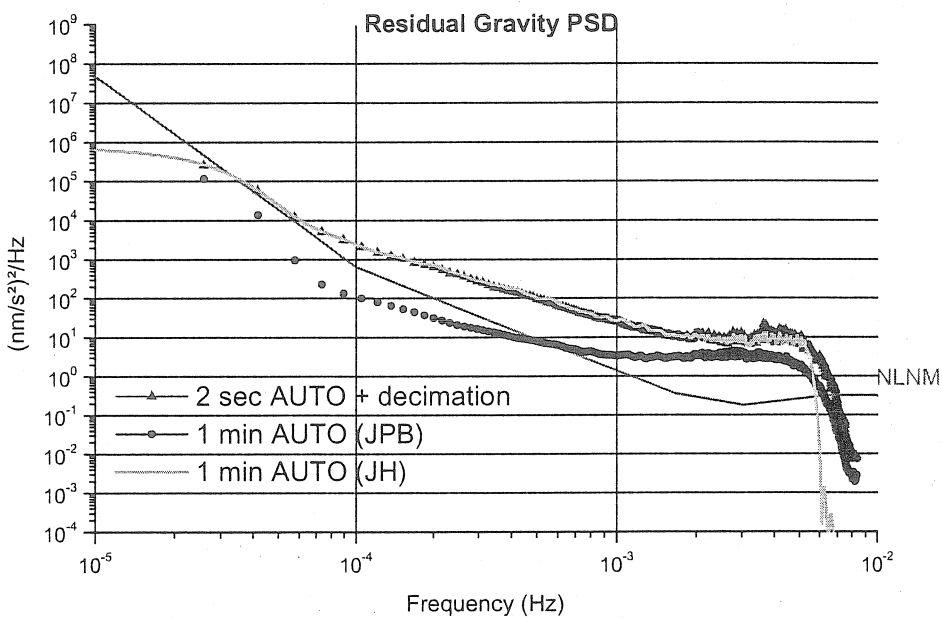

Figure 9. Residual gravity PSD for 3 different automatic correction procedures. One uses 2 sec samples before decimation, and the other two use 1 min samples from two different authors.

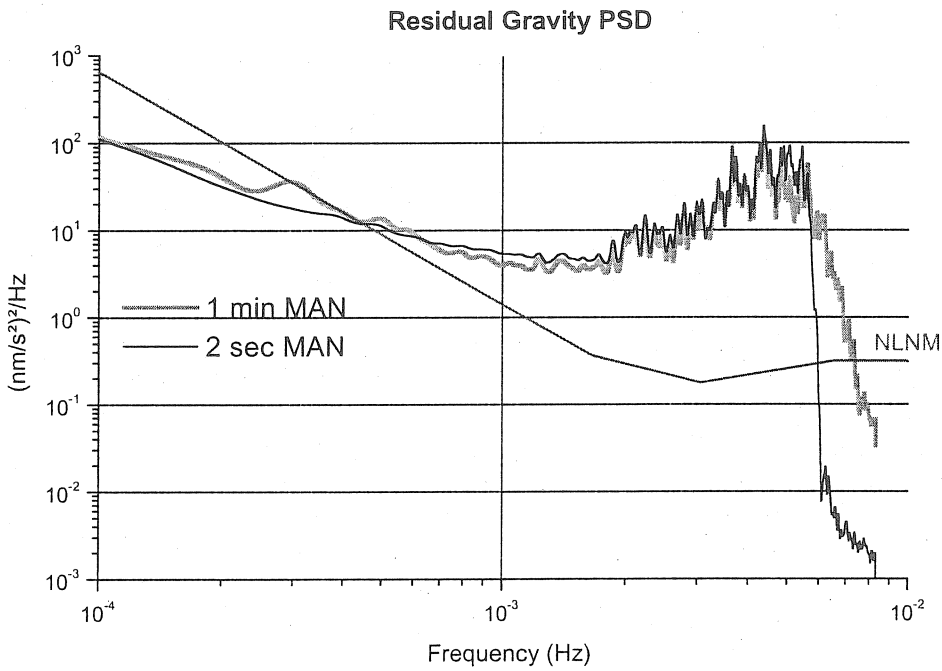

Figure 10: Residual gravity PSD according to manual corrections either on raw 2 sec data (further decimated using TSOFT filter) or on 1 min data.

The question of dealing automatically with raw samples (2 sec) or 1 min data is answered by Figure 9 where one sees that the dominant effect is the choice of the threshold rather than the sampling rate of the data in the automatic correction procedure; indeed JPB method with its lower threshold rejects more data than JH method and this leads to significantly lower noise level whereas the level difference between the two automatic methods (on raw or 1 min samples) (JH) is much weaker.

The use of different sampling rates in the manual correction procedure leads to Figure 10 where one can see that the low frequency levels are almost similar on the contrary to the band close to the Nyquist (because of different decimation filters).

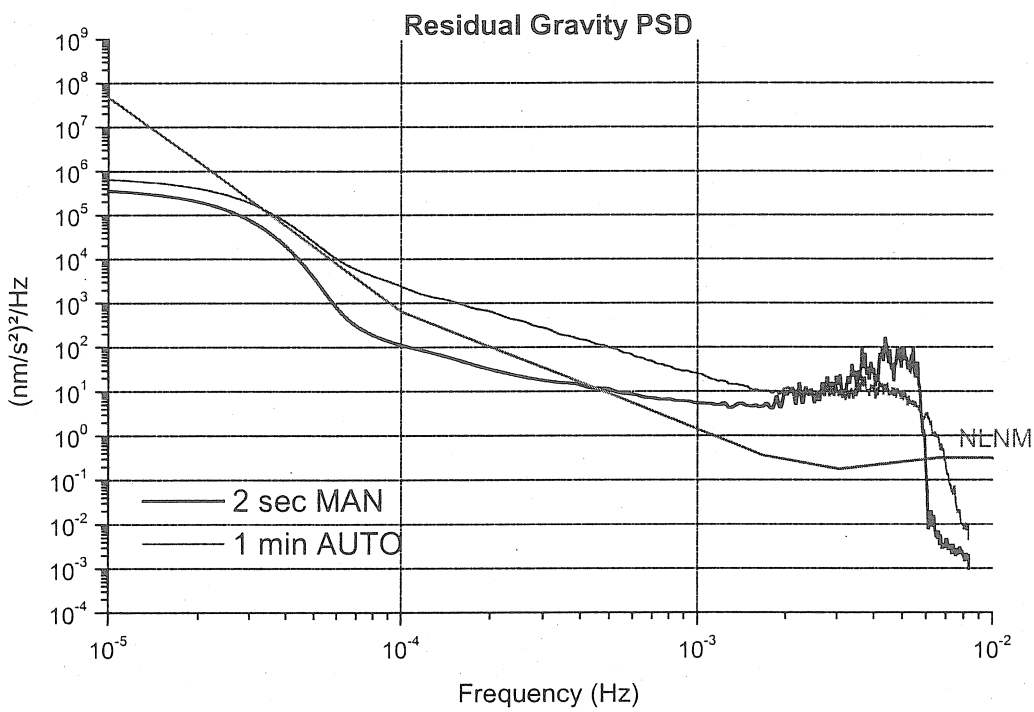

Figure 11. Residual gravity PSD according to two extreme cases: manual corrections on 2 sec samples and automatic corrections on 1 min samples.

The final comparison (Figure 11) is showing two extreme cases: on the one hand, a very time consuming procedure where the 2 sec samples are all manually corrected and then decimated to 1 min; on the other hand, a very fast treatment where the 1 min samples are automatically corrected. One sees clearly the benefits of doing manual corrections on the gravity data after visual inspection rather than using an automatic procedure:

- the PSD (2 sec MAN) crosses the NLNM at a much higher frequency than the PSD (1 min AUTO) and hence has a lower noise level in the subseismic band;
- the PSD (2 sec MAN) exhibits more seismic normal modes than the other PSD and is therefore more appropriate in studies related to the hum or others.

3. Full period: Strasbourg data from March 1997 to February 2002

After having tested these different methods for pre-processing the gravity data on a limited time span in 1997, we investigate now the full available period for our instrument in Strasbourg, namely from March 1997 to February 2002 (almost 5 years). We keep only three methods, all of them being applied to 1 min samples:

1. a semi-automatic method (REPAIR) based on the slew rate detection (JPB) and using a threshold of 2 nm s^{-2} /min to reject gravity data;
2. the same method but with a different treatment of the pressure signal (SR). There is a barometer change (instrument failure) during the analysed period; JPB introduces a drift correction in the barometric pressure (~ 1.66 hPa/year) in order to have the same absolute levels when substituting one meter by the other while SR makes an offset correction in the pressure to adjust the levels (and hence in the gravity);
3. a semi-automatic method using TSOFT (JH) (as discussed in section 2).

The consequences on the evolution of the gravity residuals from March 1997 to February 2002 due to these 3 treatments are shown in Figure 12 which shows only slight overall differences.

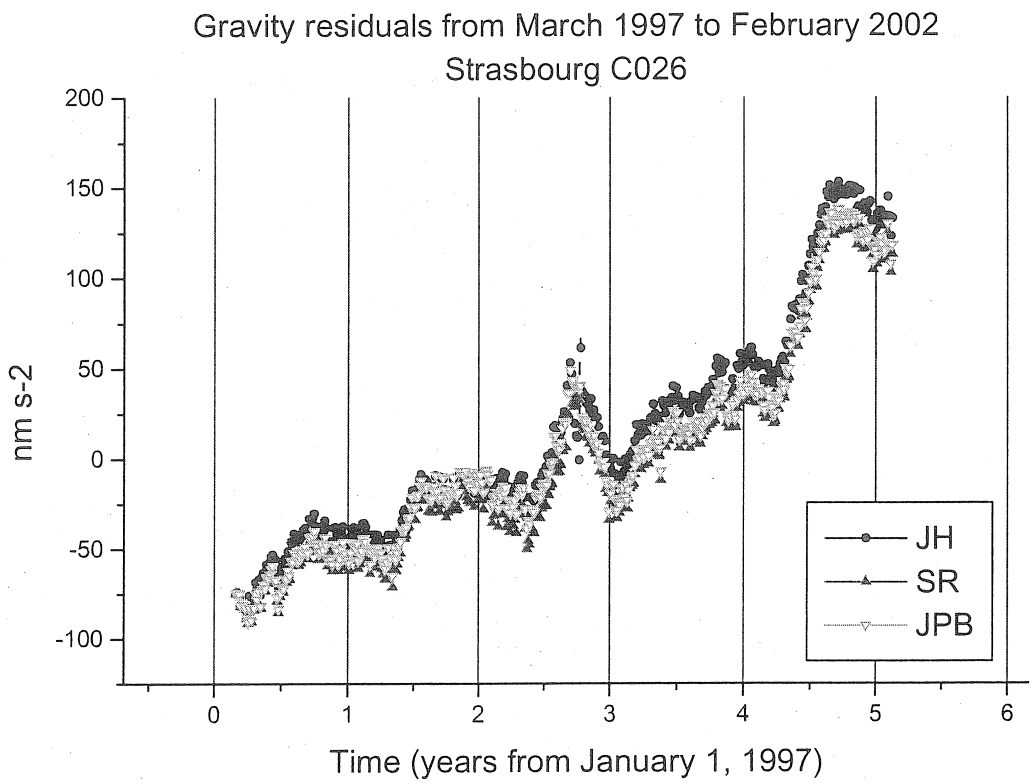

Figure 12. Time evolution of gravity residuals in Strasbourg from March 1997 to February 2002.

The differences in the gravity residuals between the JH and SR treatments are shown on Figure 13 exhibiting clearly the various offset corrections with different amplitudes.

A zoom of this difference covering several days is shown on Figure 14 and indicates a typical case of a different treatment of an offset; the oscillations are tidal constituents which originate from the use of (slightly) different tidal parameters in building up the residual signals.

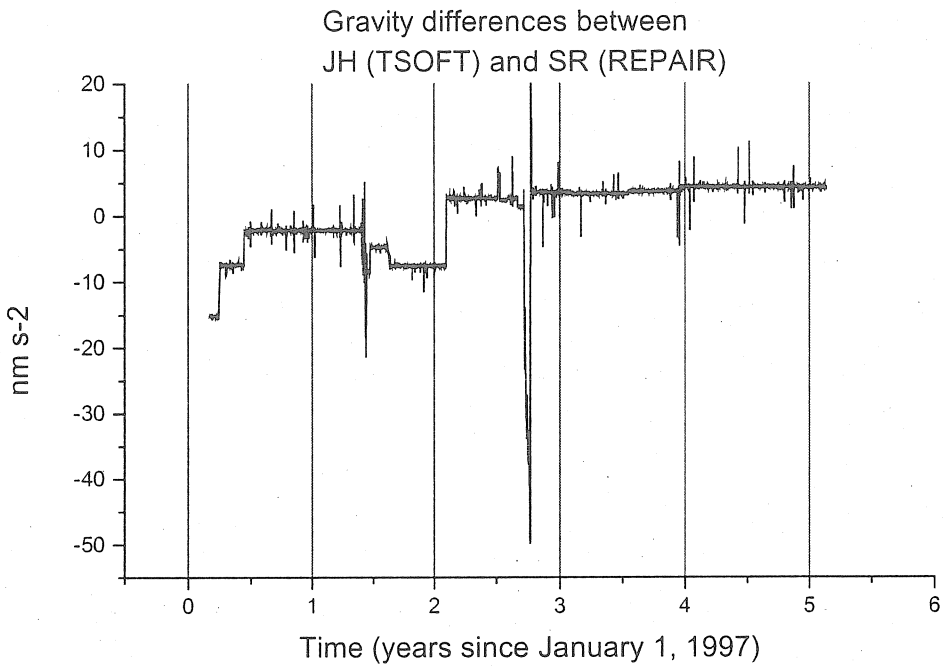

Figure 13. Difference in the gravity residuals due to two different treatments.

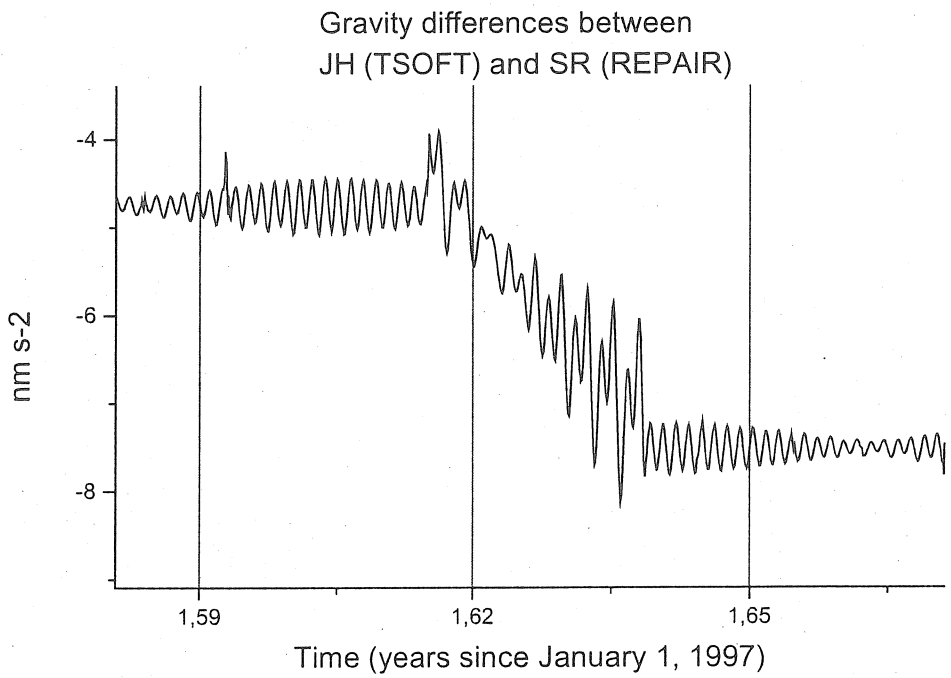

Figure 14. A zoom of figure 13 showing a probable offset over several days as well as small amplitude residual tides.

The question of removing offsets (especially the ones with small amplitudes of the order or less than 10 nm s^{-2}) has always been debated in the gravimetry community. Some can be instrumental (for

instance mechanical when you touch the instrument), but many are geophysical and it is sometimes impossible to decide which is which without precise information on the auxiliary and environmental parameters (e.g. rain). The consequences are important for the study of the long term gravity changes because of the cumulative effect of the different offset corrections. In particular, the drift estimate of the SG will be affected by this effect. One constraint can be introduced by repeated absolute gravity measurements at the same site which will clearly help in determining the physical long term gravity evolution.

Figure 15 shows the superposition of AG and SG observations (following the TSOFT (JH) and REPAIR (SR) processing methods) at our station. Previous analysis on the same station but with shorter records can be found in Amalvict et al. (1998, 1999, 2001) and Boy et al. (2001).

.

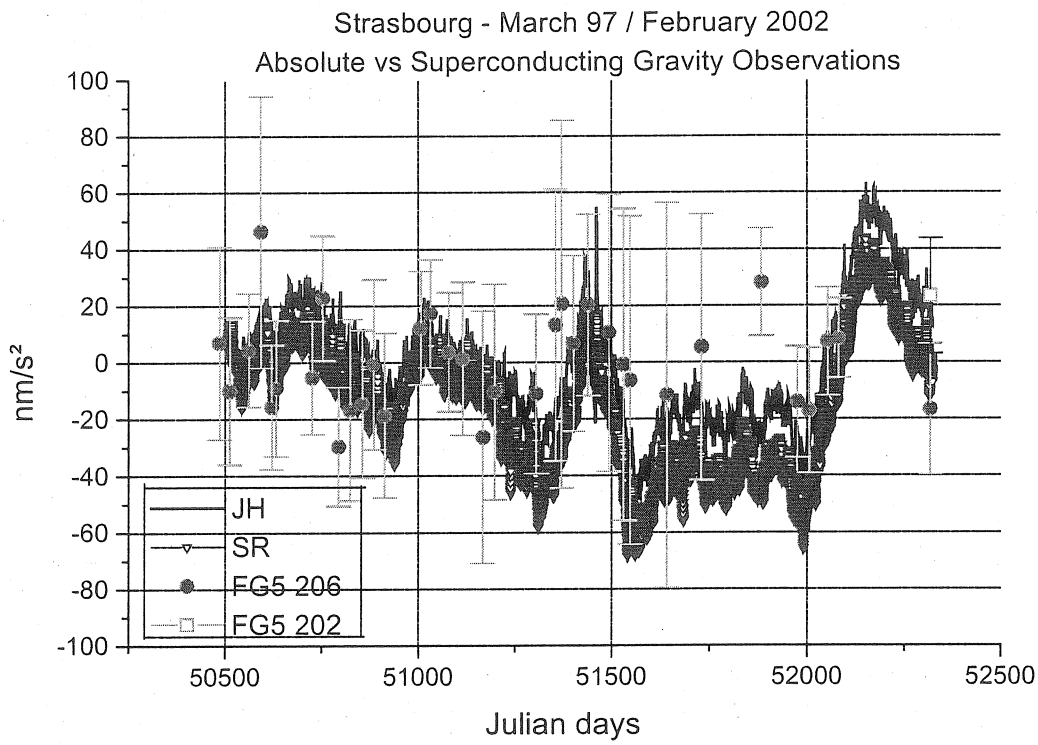

Figure 15. Superposition of absolute and superconducting gravimeter observations at Strasbourg during a 5 year time span (February 21, 1997 corresponds to Julian day 50500).

Both data sets have been corrected for the polar motion contribution using a nominal gravimetric factor 1.16; a fitted linear drift of 39.6 nm s^{-2}/year is subtracted from the SG while a fitted drift of 12.4 nm s^{-2}/year is removed from the AG. There are about 30 AG determinations with FG5#206 leading to mean g values obtained from about a week of continuous measurements for each mean value. The superposition is quite satisfying and almost all values overlap within the error bars (1 standard deviation in the case of AG). We have also indicated the February 2002 measurement with FG5#202 (done by M. Van Camp from ROB, Belgium) when our instrument came back from a factory maintenance and upgrade. A zoom of Figure 15 on the last 320 days of our gravity series is given in Figure 16. One can notice that:

1. the two processing techniques (REPAIR and TSOFT) lead to a 20 nm s^{-2} cumulative offset over the 5 year period (integrated effect of positive and negative offset corrections);

2. there is also a 30-40 nm s^{-2} gravity difference between FG5#202 and FG5#206 during the intercomparison test at the end of the record in February 2002 (with identical processing).

Because both residual curves show no offset correction during this time span, the TSOFT residual curve which is coincident with the three AG determinations in 2001 before the upgrade of the instrument favours the FG5#202 determination with respect to FG5#206 in February 2002 (after the upgrade). This example also shows the importance of having regularly AG measurements to follow the long term continuous evolution in gravity at an SG station. However there is a mutual advantage of using both types of measurements (AG versus SG) because the continuous SG monitoring can also help to reject extreme AG values (provided the drift of the SG is accurately known). In practise a proper treatment of both data sets requires simultaneous determinations of the offsets and the long term drift of the SG.

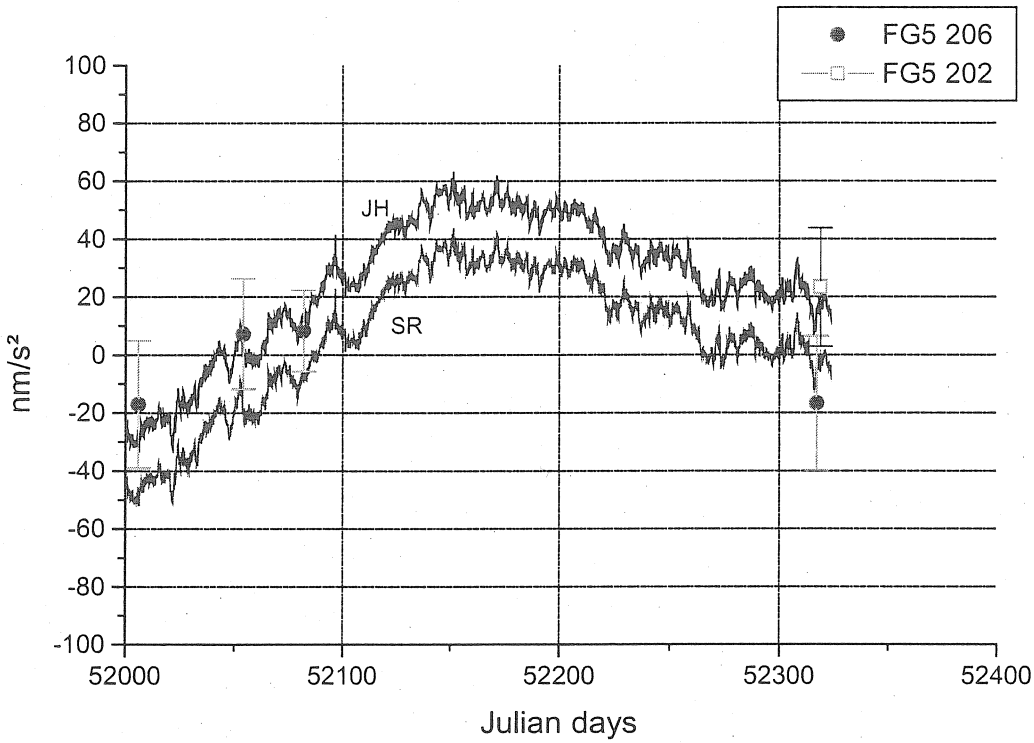

Figure 16. A zoom of Figure 15 showing the AG/SG superposition during the last 320 days of the 5 year period in Strasbourg.

4. Conclusion

This paper is devoted to the impact of different pre-processing methods on GGP gravity data. In the first part, we used a data set from March to December 1997 to test 5 different methods based either on 2 sec raw samples or 1 min data as provided in a standard form to the GGP data base. All the methods are based on a treatment of the disturbances left in the gravity residuals (observed gravity – local synthetic tide including solid and ocean loading tides – local pressure correction). Some of the methods are fully automatic with the help of the TSOFT pre-processing package and are able to remove spikes and offsets and to fill up gaps. Some other methods use the same TSOFT software to detect the problems but need a manual decision for applying the suggested corrections.

One method uses the slew rate detection algorithm (time derivative of gravity residuals) to point out the disturbances left in the signal. We assembled the gravity residual curves according to these various processing techniques and also computed the PSD to show the remaining noise levels in various frequency bands.

We could therefore address the problem of the importance of correcting raw data (in our case 2sec) or standard 1 min data and we could point out the role played by the decimation filters. The manual inspection of the data reveals the differences according to the author and we could also evaluate the price to pay when using a fully automatic method based on a specific threshold for spikes. No automatic offset correction was done in this study and we emphasize the difficulty of correcting small amplitude (less than 10 nm s^{-2}) apparent offsets. One important impact of offset corrections is that there is a cumulative effect with time.

We did then a similar analysis on a 5 year data set from March 1997 to February 2002. Again the importance of the cumulative offset corrections appears and reaches 20 nm s^{-2} at the end of the investigated period. There is a subsequent consequence in the drift estimate of the SG therefore possibly altering the retrieval of polar motion and seasonal contributions. Because of these offsets, there is a difficulty in using SG data to check AG data to better than several tens of nm s^{-2} (typically 20 to 30); we provide an example with FG5#202 and FG5#206 differences in February 2002.

The pre-processing of the GGP data is important in almost every frequency band of interest. The noise levels in the long period seismic and sub-seismic bands are strongly depending on the chosen procedure. It is less clear in the tidal bands where apparently only small differences are expected. Finally, the long term gravity time series retrieved from SG observations are crucially depending on the amount of corrected offsets, for the determination of the polar motion and the seasonal components.

Acknowledgements

This is EOST contribution N° 2002-14-UMR7516.

References

Amalvict, M., J. Hinderer, O. Francis and J. Mäkinen, 1998. Comparisons between absolute (AG) and superconducting (SG) gravimeters. In: R.Forsberg, M. Feissel and R. Dietrich (eds), Geodesy on the Move. Gravity, Geoid, Geodynamics, and Antarctica. IAG Scientific Assembly, IAG Symposia, **119**, 24–29.

Amalvict, M., Hinderer, J., and Boy, J.P., 1999. A comparative analysis between an absolute gravimeter (FG5-206) and a superconducting gravimeter (GWR C026) in Strasbourg: new results on calibration and long term gravity changes, Boll. Geofisica Geodetica, **40**, n°2-3, 519-525.

Amalvict, M., Hinderer, J., Boy, J.-P., and Gegout, P., 2001. A 3 year comparison between a superconducting gravimeter (GWRC026) and an absolute gravimeter (FG5#206) in Strasbourg (France) , Journal of Geodetic Society of Japan, **47**,.334-340.

Banka, D. and Crossley, D.J., 1999. Noise levels of superconducting gravimeters at seismic frequencies, Geophys. J. Int., **139**, 87-97.

Boy, J.-P., Hinderer, J., Amalvict, M., and Calais, E., 2000. On the use of long records of superconducting and absolute gravity observations with special application to the Strasbourg station, France, Bull. Inf. Marées Terrestres, **133**, 10377-10393.

Crossley, D., Hinderer, J., Jensen, O. and Xu, H., 1993. A slewrate detection criterion applied to SG data processing, Bull. Inf. Marées Terrestres, **117**, 8675-8704.

Crossley, D., Jensen, O.G. and Hinderer, J., 1995. Effective barometric admittance and gravity residuals, Phys. Earth Planet. Int., **90**, 221-241.

Crossley, D., Hinderer, J., Casula, G., Francis, O., Hsu, H.-T., Imanishi, Y., Jentzsch, G., Kaarianen, J., Merriam, J., Meurers, B., Neumeyer, J., Richter, B., Shibuya, K., Sato, T., and T. van Dam, 1999. Network of superconducting gravimeters benefits a number of disciplines, EOS, Transactions, AGU, **80**, no11, 121, 125-126.

Dehant, V., P. Defraigne, and Wahr, J.M., 1999. Tides for a convective Earth, J. Geophys. Res., **104**, B1, 1035-1058.

Hinderer, J., Crossley, D. and Xu, H., 1995. The accuracy of tidal gravimetric factors and nearly diurnal free wobble resonance parameters in superconducting gravimetry, Proc. 12th Int. Symp. Earth Tides, ed. H.T. Hsu, Beijing, China, 289-295.

Pagiatakis, S., 1999. Stochastic significance of peaks in a least-squares spectrum, J. Geodesy, **73**, 67-78.

Pagiatakis, S., 2000. Application of the least squares spectral analysis to superconducting gravimeter data treatment and analysis, Bull. Inf. Marées Terrestres, **133**, 10415-10426.

Rosat, S., Hinderer, J., and Crossley, D., 2002. A comparison of the seismic noise levels at various GGP stations, Bull. Inf. Marées Terrestres, submitted.

Scherneck, H. G., 1991. A parameterized Earth tide observation modeland ocean tide loading effects for precise geodetic measurements, Geophys. J. Int., **106**, 677-695.

Vauterin, P., 1998. Tsoft: graphical and interactive software for the anlysis of Earth tide data, Proc. 13th Int. Symp. Earth Tides, eds. B. Ducarme & P. Pâquet, Brussels, Belgium, 481-486.

Wenzel, H.-G., 1994. PRETERNA- a preprocessor for digitally recorded tidal data, Bull. Inf. Marées Terrestres, **118**, 8722-8734.

Wenzel, H.-G., 1998. Earth tide data processing package ETERNA 3.30: the nanogal software, Proc. 13th Int. Symp. Earth Tides, eds. B. Ducarme & P. Pâquet, Brussels, Belgium, 487-494.

Comparison of Earth Tides Analysis Programs

O. Dierks and J. Neumeyer

GeoForschungsZentrum Potsdam, Division 1,
Telegrafenberg, 14473 Potsdam, Germany

dierks@gfz-potsdam.de

1 Introduction

The increasing accuracy of gravimeters especially of those with superconducting technology and the comparison between many stations and working groups in projects like the "Global Geodynamic Project (GGP)" lead to the problem that possible differences in the results occur from differences in used analysis programs. This article describes three of the widely used analysis programs for earth tide analysis and shows the results of some comparing investigations made at the GFZ Potsdam for a diploma thesis.

2 Preprocessing

Before the tidal analysis can be performed the raw gravity data have to be repaired and filtered. This is done by using a pre-processing software. Two of these programs were also tested (PRETERNA 3.30 and TSOFT 1.1.4).

The preprocessing can be divided into several parts:

- calibration of the data
- calculation of the gravity residuals
- removing of spikes, steps and interfering signals
- filling of data gaps by theoretical values
- filtering and decimation to the required sampling rate for the tidal analysis software.

Central step is the correction of the data. The automated and hand made correction of steps and spikes is different for both programs. The automatically correction of large or multiple steps is not possible with both programs. In program PREGRED from the ETERNA-package it is difficult to overlook the data set with the small zoom functions. Corrected and uncorrected signals are visible in program TSOFT. Each correction can be rejected. Many mathematical and stochastically calculations can be applied on the data. A lot of datasets can be managed and handled in the program simultaneously. The user can program an automation of the correction without loosing visible control.

Within the other steps of the preprocessing the two programs behave equal. ETERNA-package is in some parts even more powerful by using the newest tidal potential catalogue and tuned digital numerical filters. The program TSOFT computes the filter coefficients each time they are needed according to the settings by the user. But this great choice possibly bears errors.

3 Description of the Analysis Programs

The following three widely used analysis programs were tested in this work:

- Program ANALYZE from the ETERNA-package, version 3.30, by H. - G. WENZEL [WEN-96a], [WEN-96b]
- Program BAYTAP-G in the version from 15.11.1999 by Y. TAMURA [TAM-91]
- Program VAV in the version from April 2002 by A. P. VENEDIKOV et. al [VEN-01]

The changing gravitational forces from sun, moon and the planets affect the earth. In the earth's centre of mass this gravitational force is compensated by the centrifugal forces due to the motion of the earth around the sun and due to the motion of the earth around the barycentre of the moon-earth system respectively. Centrifugal acceleration is constant in every point of the earth but gravitational acceleration is different due to spatial extent of the earth. The small resulting acceleration is called tidal acceleration. The tidal acceleration in a fixed point of the earth changes with time because of earth rotation and movement of the participating bodies.

The changes of the tidal acceleration in a fixed point can be recorded by the use of e. g. a gravimeter. But the recorded data series y(t) does not only consists of the observed tidal gravity signal w(t) but also contains further information:

$$y(t) = w(t) + d(t) + \alpha \cdot a(t) + \varepsilon(t). \quad (1)$$

Term d(t) describes the drift of the gravimeter. Term a(t) is a time series with meteorological or hydrological data. Coefficient α describes the influence of this additional parameter onto the gravity measurement. Further signals and measurement errors are combined in term $\varepsilon(t)$.

An analysis program corrects the observed signal y(t) by eliminating the drift series and the influence of the meteorological and hydrological signals. Using the coordinates of the station and a tidal potential catalogue a theoretical tidal gravity signal is computed. A comparison between this theoretical and the observed tidal gravity signal is used to estimate a set of tidal parameters (amplitude factor and phase lead) for the station. The tidal parameters amplitude factor and phase lead cannot be determined for each wave noted in the tidal potential catalogue. Following the RAYLEIGH-criterion the waves of the used tidal potential catalogue are stacked together to wave groups [VEN-61]. For each of these groups the tidal parameters amplitude factor and phase lead are estimated.

After some general comments on each program its methods are described to compute tidal parameters, influence of additional signals and accuracy of the results.

3.1 ANALYZE

The program is based on a method developed by CHOJNICKI [CHO-73] and improved by SCHÜLLER [SCH-76] and WENZEL [WEN-96a]. A least square adjustment is used to estimate the tidal parameters, the meteorological and hydrological regression parameters, the pole tide regression parameters and the TSCHEBYSCHEFF polynomial bias parameters for drift determination. The amount of data is nearly unlimited. Every kind of earth-tide data (gravity, strain, tilt and displacement) and up to eight channels with meteorological and hydrological data can be analysed.

The user can determine the range of up to 85 wave groups. One tidal potential catalogue out of seven including the newest from HARTMANN and WENZEL [HAR-95] can be chosen to calculate the theoretical tidal signal. On the other hand the requirements on the format of the data and the parameter file are very stringent [WEN-96b].

The model used for least square adjustment is:

$$\ell(t) + v(t) = \sum_{j=1}^{q} \left(\hat{X}_j \cdot CO_j + \hat{Y}_j \cdot SI_j \right) + \sum_k \hat{D}_k \cdot T_k(t_n) + \sum_m \hat{R}_m \cdot z_{m(t)} \qquad (2)$$

where $\ell(t)$ = Observed gravity signal

$v(t)$ = Improvements to the observations

X_j, Y_j = Linear form of unknown tidal parameters H_j (amplitude factor) and $\Delta\Phi_j$ (phase difference) for each wave group j:
$X_j = H_j \cdot \cos\Delta\Phi_j$
$Y_j = H_j \cdot \sin\Delta\Phi_j$

CO_j, SI_j = Factor of theoretical tidal parameters A_j (amplitude) and Φ_j (phase) for each wave i in the wave group j, starting with wave a_i and ending with wave e_i:

$$CO_j = \sum_{i=a_i}^{e_i} H_i^* \cdot A_i \cdot \cos(2\pi f_i t + \Phi_i)$$

$$SI_j = \sum_{i=a_i}^{e_i} H_i^* \cdot A_i \cdot \sin(2\pi f_i t + \Phi_i)$$

H_i^* = Amplification factor from digital highpass filter (equal 1 if drift is approximated by polynomials)

D_k, T_k = Coefficients (D_k) of TSCHEBYSCHEFF-polynomials T_k of degree k

R_m, z_m = Regression coefficients (R_m) of additional channel number m (z_m)

A possible drift in the data is eliminated by highpass filtering or is approximated by TSCHEBYSCHEFF–polynomials (T_k) whose coefficients (D_k) are also estimated in the least square adjustment. The filter coefficients for different numerical digital filters are included in the ETERNA-package. But the method of high pass filtering can only be used when no long periodic waves shall be determined. Together with the analysis of long periodic waves the drift has to be eliminated by an approximation through TSCHEBYSCHEFF-polynomials.

The influence of the air pressure data (or other meteorological or hydrological signals $z_m(t)$) onto the gravity measurement is determined by a linear regression. In the case of highpass filtering the air pressure data are filtered too and the regression is computed with the filtered data.

The accuracy of each parameter is determined in the least square adjustment in the form of standard deviations. The standard deviations of the tidal parameters are too optimistic and therefore corrected. They are multiplied by a factor that is derived from the spectrum of the residuals [WEN-96b].

3.2 BAYTAP-G

This program is based on a method called Bayesian prediction, developed in 1976 by HARRISON and STEVENS [HAR-76]. The method has been modified in Japan since 1983 for the use with earth-tide data. All kinds of earth-tide data can be analysed, but only three additional channels with meteorological or hydrological data are possible. The requirements are very stringent to the format of data and parameter files. The arrangement of the tidal wave groups is done automatically depending on the length of the time series, but the user can change the wave group boundaries by editing the corresponding file [TAM-90], [TAM-91]. The tidal potential catalogues from TAMURA [TAM-87] or CARTWRIGHT-TAYLOR-EDDEN [CAR-73] can be used.

Tidal parameters, drift and meteorological parameters are estimated through an iterative method similar to least square adjustment by minimizing the term [TAM-90]

$$
\begin{aligned}
&\sum_{i=1}^{n}\left[y_i - \sum_{m=1}^{M}\left(A_m C_{mj} + B_m S_{mj}\right) - d_i - \sum_{k=0}^{k_{max}} b_k \cdot x_{i-k\cdot\Delta t}\right]^2 \\
&+ D^2 \sum_{i=1}^{n}\left[d_i - 2\,d_{i-1} + d_{i-2}\right]^2 \qquad (3)\\
&+ \mathrm{WEIGHT}^2 \sum_{m=2}^{M}\left(\left(A_m - A_{m-1}\right)^2 + \left(B_m - B_{m-1}\right)^2\right).
\end{aligned}
$$

A_m and B_m are the linear expressions of the unknowns amplitude factor and phase lead for each m of the M wave groups at all. C_{mj} and S_{mj} are computed from the tidal potential catalogue using all j waves contained the m^{th} wave group. This tidal part is subtracted from each observation y_i (n datapoints in total) together with the drift-value d_i and the term describing the influence of additional channels x(t) onto the measurement (see equation (5)). D and WEIGHT are called hyperparameters and can be defined in the parameter file.

The second line of equation (3) is used for drift computation. Within this program the drift is not approximated by low degree polynomials. Here the drift is computed separately in each datapoint. The drift behaviour is characterized by the formula:

$$d_i = 2d_{i-1} - d_{i-2} + u_i \qquad (4)$$

Here u_i is the stochastic part denoting a white noise sequence. d_i is the drift value at the current datapoint; d_{i-1} and d_{i-2} are the drift values in the two previous datapoints. The hyperparameter D can be used to fit the drift model to the data. A large value for parameter D causes an almost linear drift model; a small value leads to a drift model bending close to the data.

A similar possibility is given with hyperparameter WEIGHT in the third line of equation (3). Here the variability of the tidal parameters can be chosen. But this option is only useful if too many tidal parameters shall be estimated from too poor data.

The influence onto gravity measurement is computed by regression for maximum three additional signals. But exceeding a simple linear regression the influence of more datapoints than the actual datapoint can be used:

$$\sum_{k=0}^{k_{max}} b_k \cdot x_{i-k\cdot\Delta t} \qquad (5)$$

Here parameter k gives the number of computation points for regression and Δt the time lag between the computation points if $k > 0$.

Within the iterative search the hyperparameter D is adjusted to get the best combination between parameters, measured data and tidal parameters. At the end of each turn an ABIC-value (ABIC = AKAIKE Bayesian Information Criterion) is computed. The solution with the smallest ABIC-value is the final one where data, parameter and drift fit each other best. This ABIC-value is also the only useful accuracy statement. A standard deviation is computed but following the author of this program it is simply derived from the ABIC-value. So this standard deviation is not comparable to standard deviations from the other programs.

3.3 VAV

Program VAV is based on a method called MV66 [VEN-66a], [VEN-66b] and an improvement of program NSV [VEN-97]. The data file can be adopted from program ANALYZE, but program VAV has its own format for data files and uses own input files for tidal wave grouping and parameter settings. The wave group arrangement is done automatically depending on the length of the data set. Also a grouping variant can be chosen from a special input file. The used tidal potential catalogue is from TAMURA [TAM-87].

The fundamental idea of the program NSV [VEN-97] is a filtration of the original data containing an elimination of the drift and the separation into several pairs of series (step 1). Each pair contains signals from one main tidal species (D, SD or TD). The unknown tidal parameters for each tidal species are determined simultaneously but separately (step 2). This leads also to a frequency dependent accuracy statement (AKAIKE Information Criterion (AIC-value) and standard deviation). Both steps are also contained in program VAV but the separation in step 1 is not restricted to main tidal species. Here a wide spectrum of frequencies can be chosen by the user. Step 2 is using all the separated tidal species in a single least squares adjustment. An improvement of program VAV is the possibility to use data with different sampling rates and with several gaps in the same run without the need for interpolation [VEN-01].

The original data set $\mathbf{Y}$ is divided into N intervals $\mathbf{y}_i$ of equal length. Each set contains n data points (n· N = M = total number of data points). n differs between the intervals, if the data are unequally spaced. Tidal parameters and air pressure regression coefficient are determined in a least squares fit together with the drift polynomial coefficients by minimisation of the following expression:

$$\mathbf{AX} + \mathbf{PZ} + \mathbf{E} = \mathbf{Y} \qquad (6)$$

where $\mathbf{AX}$ is the tidal model including terms for the air pressure correction. Vector $\mathbf{X}$ is the vector of unknowns. Matrix $\mathbf{E}$ is the noise of the measurement. The model of the drift $\mathbf{PZ}$ is explained next.

In each interval $\mathbf{y}_i$ the drift is approximated by a polynomial of low degree (0 k 3). The matrix-notation of this looks like

(7)
$$\underset{M,N(k+1)}{P} = \begin{bmatrix} p_1 & & 0 \\ & \ddots & \\ & p_i & \\ & & \ddots \\ 0 & & p_N \end{bmatrix} \qquad \underset{N(k+1),1}{Z} = \begin{bmatrix} z_1 \\ \vdots \\ z_i \\ \vdots \\ z_N \end{bmatrix}$$

with P containing the known polynomials depending on the time in each interval and Z containing the unknown polynomial coefficients representing the drift.

For each interval μ matrixes c are created. Each matrix represents one of the chosen frequencies for filtering and separation

(8)
$$\underset{n,2}{c_{ij}} = \begin{bmatrix} \cos \varpi_j t_1 & \sin \varpi_j t_1 \\ \vdots & \vdots \\ \cos \varpi_j t_n & \sin \varpi_j t_n \end{bmatrix}$$

With j running from 1 to μ denoting the angular frequencies used for separation and i running from 1 to N denoting the intervals. t_1, t_2, ... t_N is the time series in each interval. The matrixes c_{ij} are transformed to f_{ij} and than merged together for each frequency to

(9)
$$\underset{M,2N}{F_j} = \begin{bmatrix} f_{1j} & & 0 \\ & \ddots & \\ & f_{ij} & \\ & & \ddots \\ 0 & & f_{Nj} \end{bmatrix}$$

All μ F-matrixes are merged together with matrix P to a matrix called D so that

(10)
$$\text{size } (D) = (M,M) \text{ and } D^T D = D D^T = I$$

The resultant identity-matrix depends already on the transformation of the c-matrixes.

Throughout filtering and separation we get

(11)
$$U = F^T Y = \begin{bmatrix} u(\varpi_1) \\ \vdots \\ u(\varpi_\mu) \end{bmatrix} \quad \text{with} \quad u(\varpi_j) = F_j^T Y = \begin{bmatrix} f_{1j}^T y_1 \\ \vdots \\ f_{Nj}^T y_N \end{bmatrix}$$

The least squares fit (6) can than be changed into one using the filtered values

(12)
$$GX + E' = U$$

without changing the results as shown in [VEN-01], but with estimation of more realistic accuracy statements.

Beside this standard deviation from the least square adjustment an AIC-value is computed. This value is used to compare different solutions of the same dataset with different parameter settings. The solution with the smallest AIC-value is the best one.

4 Comparative analysis with synthetic data

For comparing of the three tidal analysis programs a theoretical benchmark series (limited to degree 3) has been calculated and kindly provided by Bernard Ducarme (Royal Observatory of Belgium). The ten-year dataset of synthetic tidal acceleration (1 hour sampling rate) was computed for the SG-station BE (Brussels, Belgium). The used series with disturbed data is also a benchmark series with added red noise from Bernard Ducarme. The real data analysed in the next chapter was measured at SG-station SU (Sutherland, South Africa). The benchmark series are analysed with the three programs ANALYZE, BAYTAP-G and VAV. The obtained results were compared to the theoretical tidal parameters included in the benchmark series (amplitude factor = 1.0, phase lag = 0.0).

4.1 Analysis of pure synthetic data

The first tidal analysis of each program was started with the standard parameter settings (default values) offered by the programs (see end of chapter 4.2 for finally used values). All analyses have been carried out with the TAMURA catalogue [TAM-87].

The following figures show the differences of the resolved amplitude factors (DAF) against 1.0 and the resolved phase leads (or their difference against 0.0; DPL). Figures 4.1, 4.2, 4.5 and 4.6 show the results for the three programs and the 31 used tidal wave groups. 31 wave groups is the maximum number of wave groups to be used with program BAYTAP-G. The spaces between the wave groups on the horizontal scale are due to figures 4.3, 4.4, 4.7 and 4.8. Here additional a fine wave group splitting with 54 tidal wave groups is used.

Because of the absence of any perturbation in the input data (synthetic tidal acceleration) the programs should calculate the same tidal parameters as included in the input data. The difference between the amplitude factors (DAF) or phase lead (DPL), respectively are shown in figure 4.1 and figure 4.2 for the 31 selected wave groups.

a) ANALYZE

The difference of the amplitude factors DAF is smaller than 0.00015 for all the selected wave groups (maximum: 0.00014 for wave groups S1 and PSI1). For the phase lead the difference DPL is smaller than 0.016° (2N2). The application of the HANN-window or a change of the numerical highpass filter lead to nearly no changes.

b) BAYTAP-G

The deviations of the amplitude factors DAF are similar small (maximum: 0.00013). The biggest DAF are concentrated on the lower frequencies (wave groups SGMQ1, 2Q1, SIG1). The phase lead has a maximum deviation at M3 (0.051°). It is astonishing that all DAF are negative (amplitude factor smaller 1.0) and all DPL positive (phase lead greater 0.0).

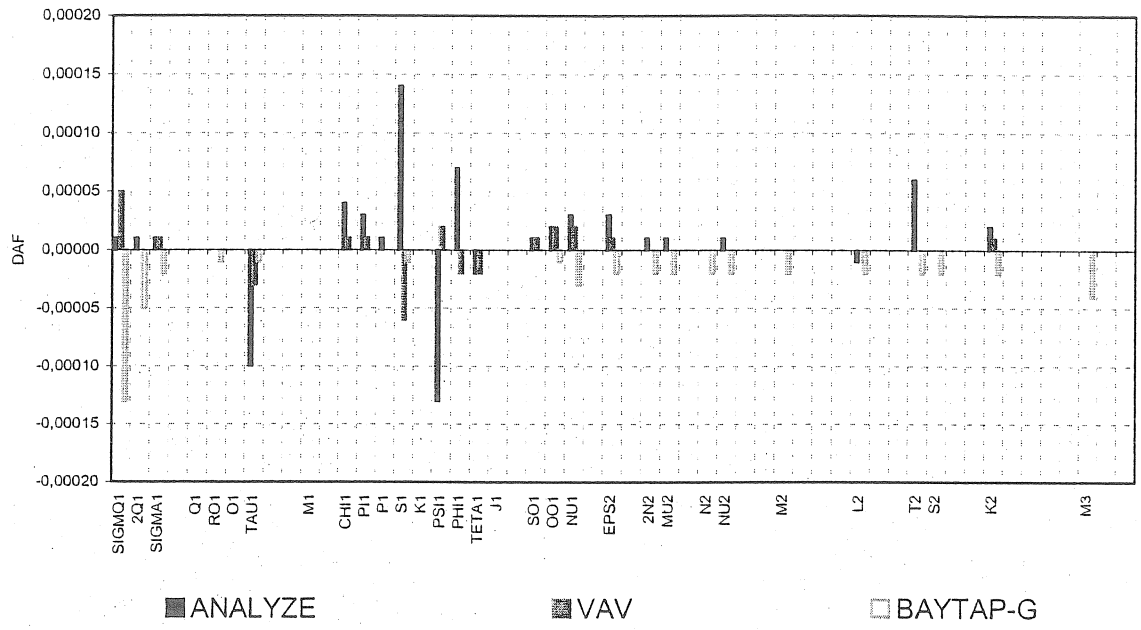

Figure 4.1: Deviations of amplitude factors for analysis of pure benchmark data

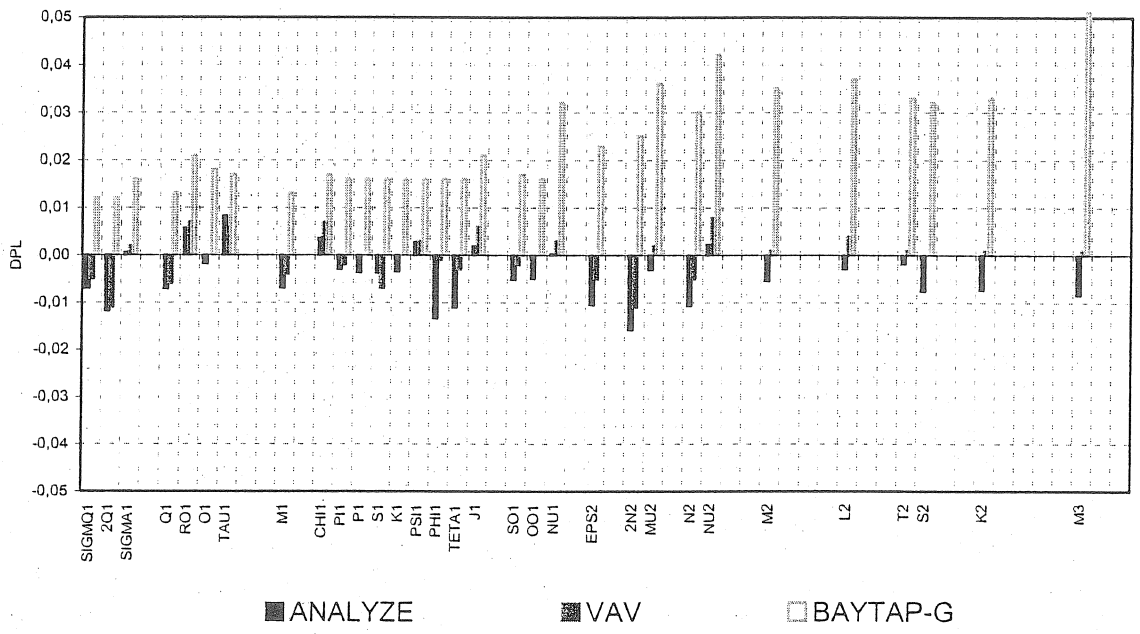

Figure 4.2: Deviations of phase leads for analysis of pure benchmark data

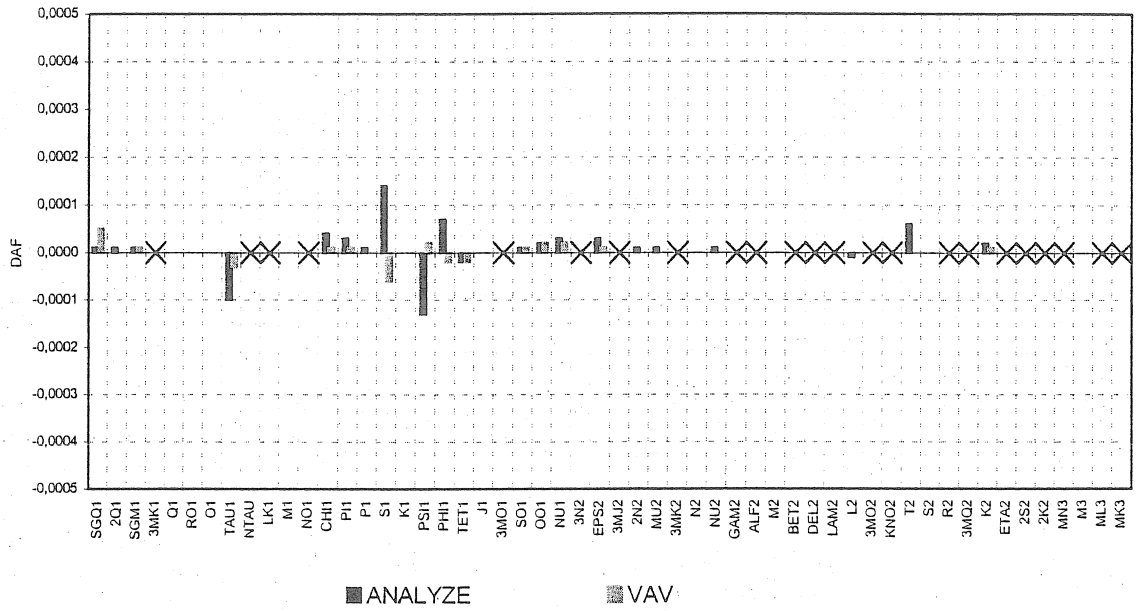

Figure 4.3a: Deviations of amplitude factors after analysis of pure benchmark data with 31 wave group

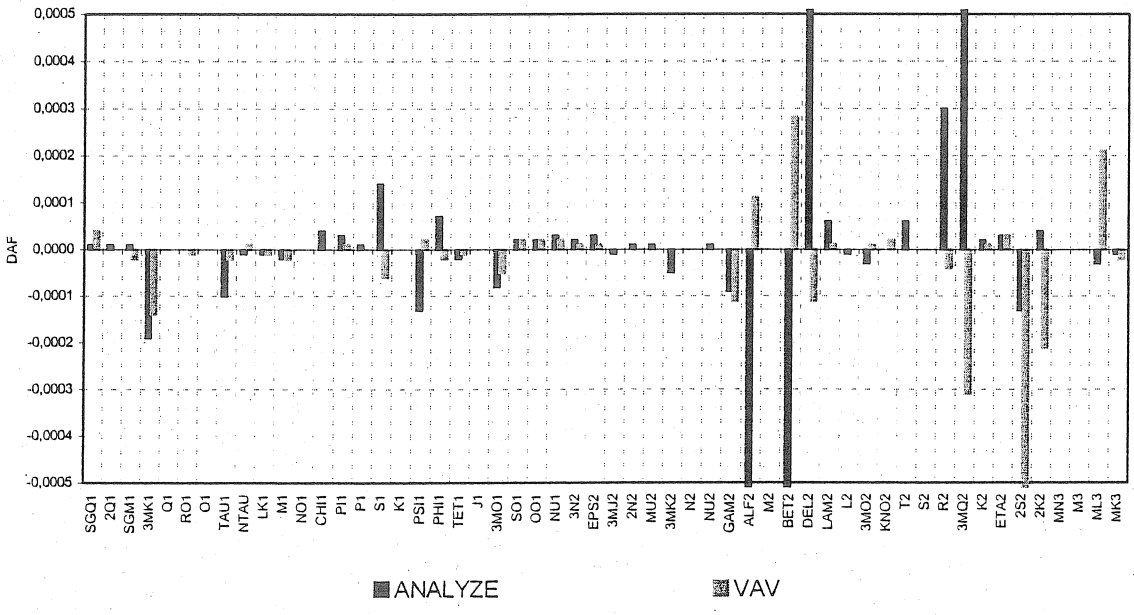

Figure 4.3b: Deviations of amplitude factors after analysis of pure benchmark data with 54 wave groups

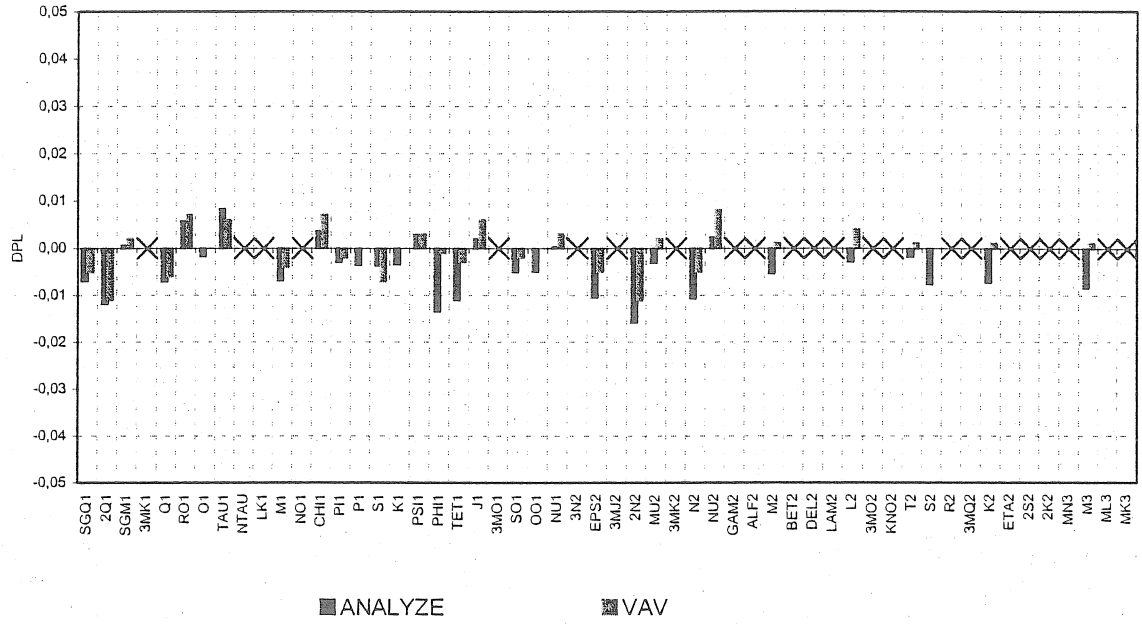

Figure 4.4a: Deviations of phase leads after analysis of pure benchmark data with 31 wave group

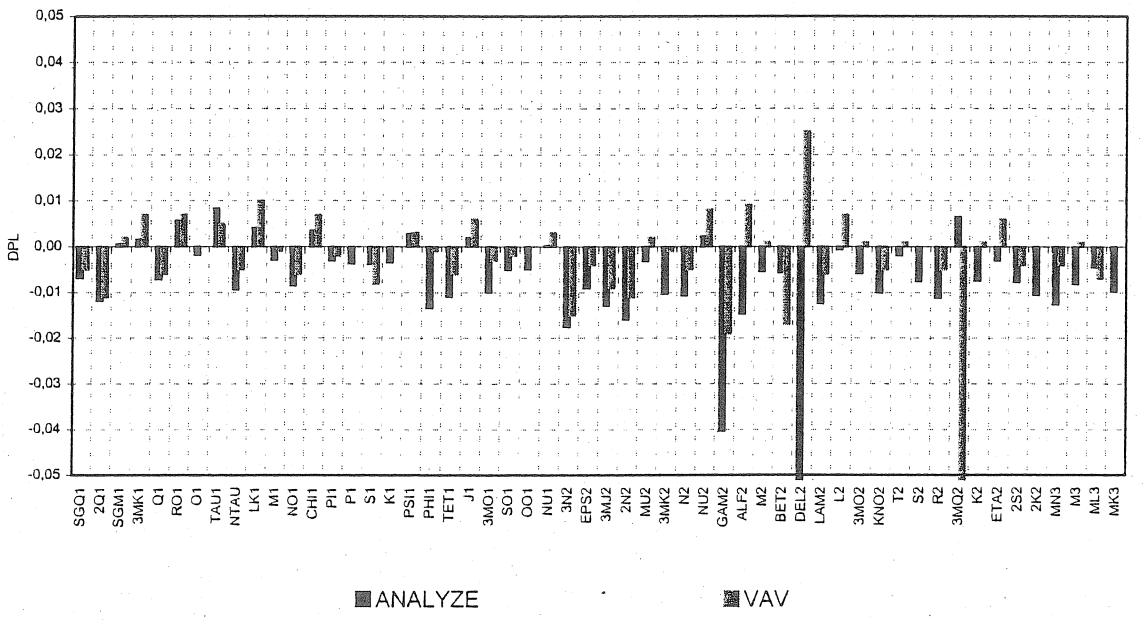

Figure 4.4b: Deviations of phase leads after analysis of pure benchmark data with 54 wave groups

c) VAV

The deviations of the amplitude factors DAF are smaller than 0.00010 (maximum: 0.00006 for wave group S1). The DPL are also comparable to the results of program ANAYLZE (maximum: 0.012° for 2N2 and 2Q1).

A further comparison was made by the use of a finer wave group splitting with 54 wave groups instead of 31. This grouping was used in a second run for the programs ANALYZE and VAV. Program BAYTAP-G is not able to use more than 31 wave groups. The comparison between programs ANALYZE and VAV is shown in the figures 4.3 (DAF) and 4.4 (DPL). In the upper part of both figures the results with 31 wave groups are shown. The wave groups marked with a cross are not analysed within this grouping. In the lower part of both figures the results of the finer grouping with 54 wave groups are shown.

The graphs are printed with the same scales to see directly any differences between the two grouping variants. As expected the differences between the two grouping variants are very small. The deviations DAF and DPL are of course high for the small, new created wave groups (e. g. 3MK1, ALF2, BET2, DEL2, 3MQ2). The results of some wave groups become a little bit better for both programs by using the finer wave grouping. For a few other wave groups they become worse.

4.2 Analysis of disturbed synthetic data

In a second test theoretical red noise was added to the synthetic tidal acceleration data. The analysis of this disturbed benchmark series leads to worse results for the three programs.

The analysis with programs ANALYZE and BAYTAP-G lead to similar results of DAF and in some parts also of DPL (figures 4.5 and 4.6). The maximal deviations are for DAF 0.009 (PSI1) and for DPL 0.6° (SIGMQ1).

The results from program VAV are different for many wave groups to both other programs. Maximum deviation for DAF is also on wave group PSI1 but with a value of 0.012. For DPL the maximum deviation is also on PSI1 (0.56°). But for many wave groups the values and also the sign of DAF and DPL are different to ANALYZE and BAYTAP-G.

In figures 4.7 (DAF) and 4.8 (DPL) the programs VAV and ANALYZE are compared again. The upper part of both figures shows again the results of the analysis with 31 wave groups, the lower parts the analysis with 54 wave groups. The results (DAF and DPL) of programs ANALYZE and VAV do nearly not change between both grouping variants except for the new created tidal wave groups and their direct neighbouring wave groups (figures 4.7 and 4.8). The small changes between both wave groupings are as uneven as in figures 4.3 and 4.4. Here DAF and DPL are very high for the new created wave groups, especially in the semi diurnal frequency band.

The following parameter settings were used within the three programs to analyse the benchmark series. The analysis of benchmark data with program ANALYZE leads to best results when using RIGIDEARTH=1, as was recommended by the author of the program. The HANN-window was not used (HANNWINDOW=0). Parameter

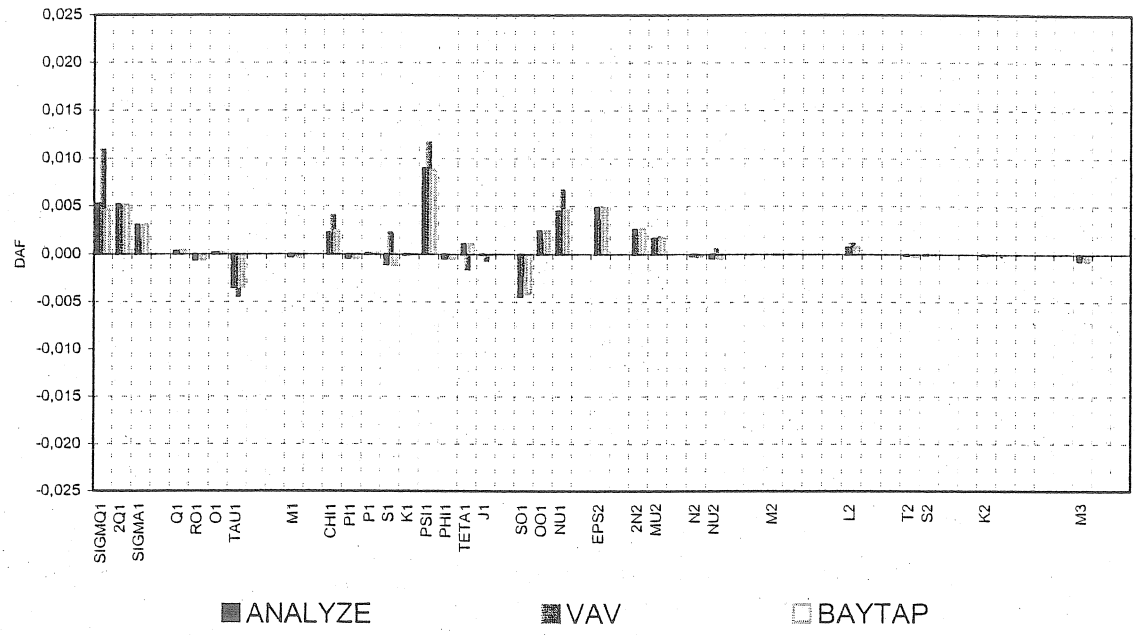

Figure 4.5: Deviations of amplitude factors for analysis of noisy benchmark

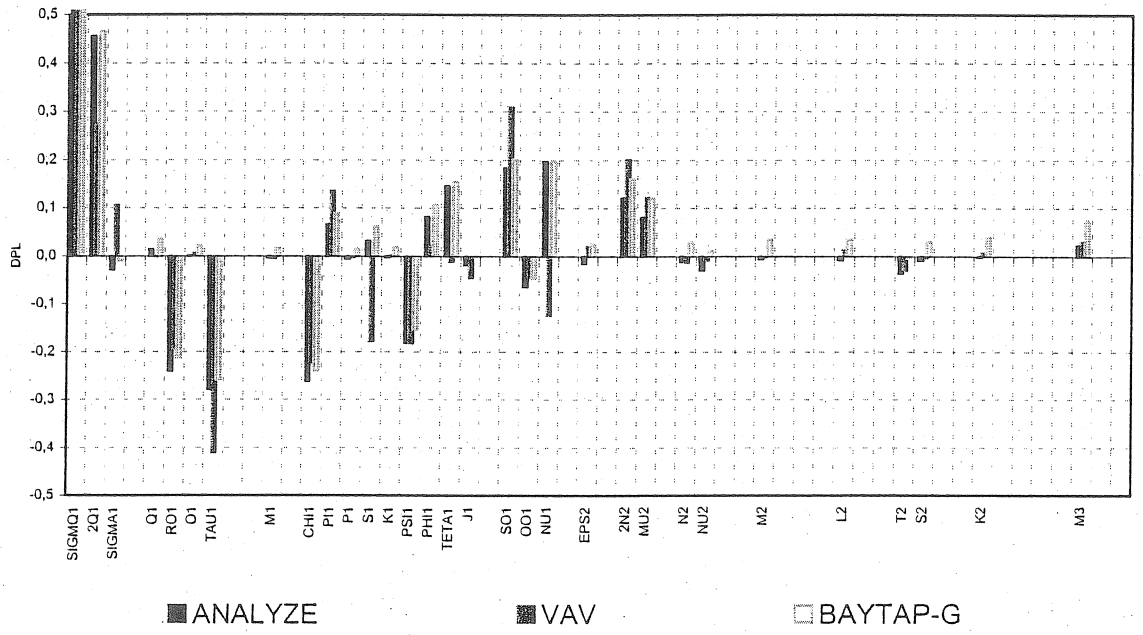

Figure 4.6: Deviations of phase leads for analysis of noisy benchmark

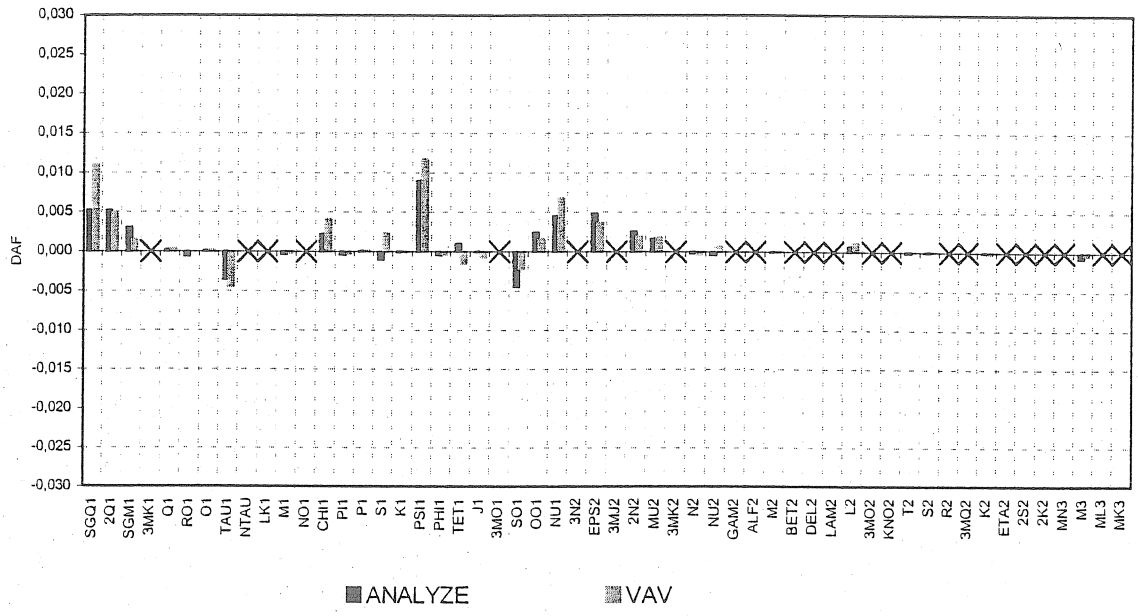

Figure 4.7a: Deviations of amplitude factors for analysis of noisy benchmark data with 31 wave groups

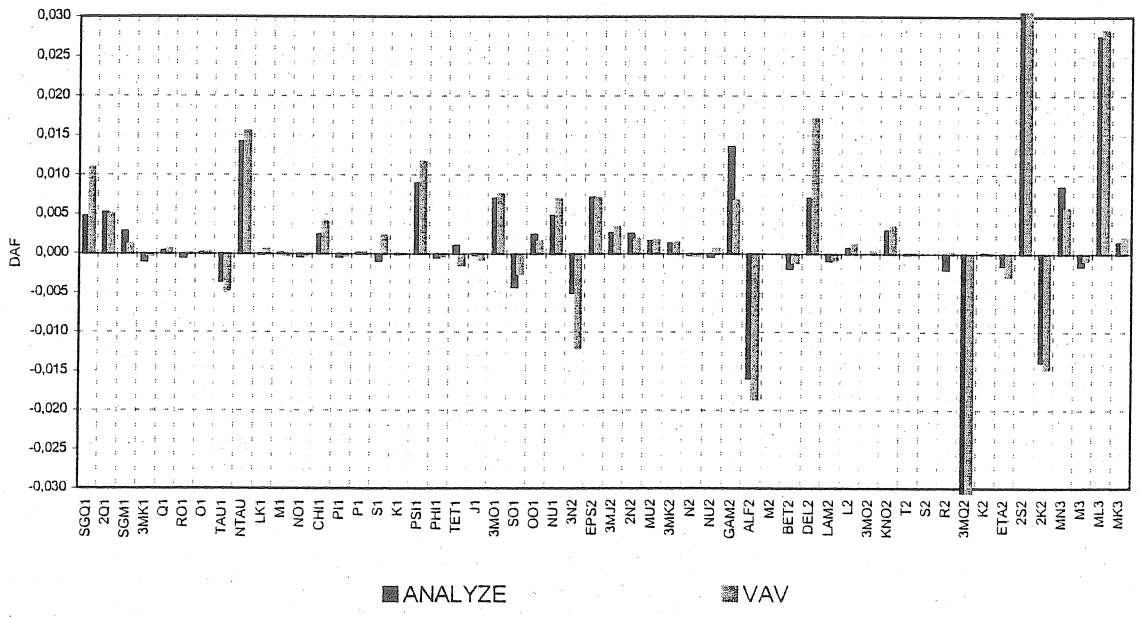

Figure 4.7b: Deviations of amplitude factors for analysis of noisy benchmark data with 54 wave groups

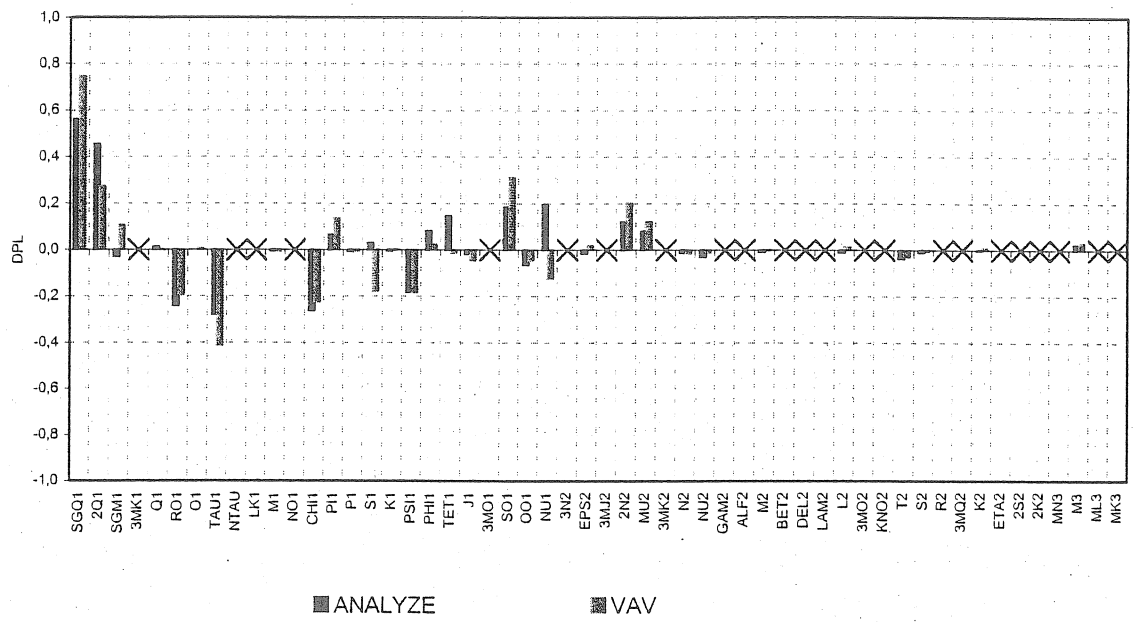

Figure 4.8a: Deviations of phase leads for analysis of noisy benchmark data with 31 wave groups

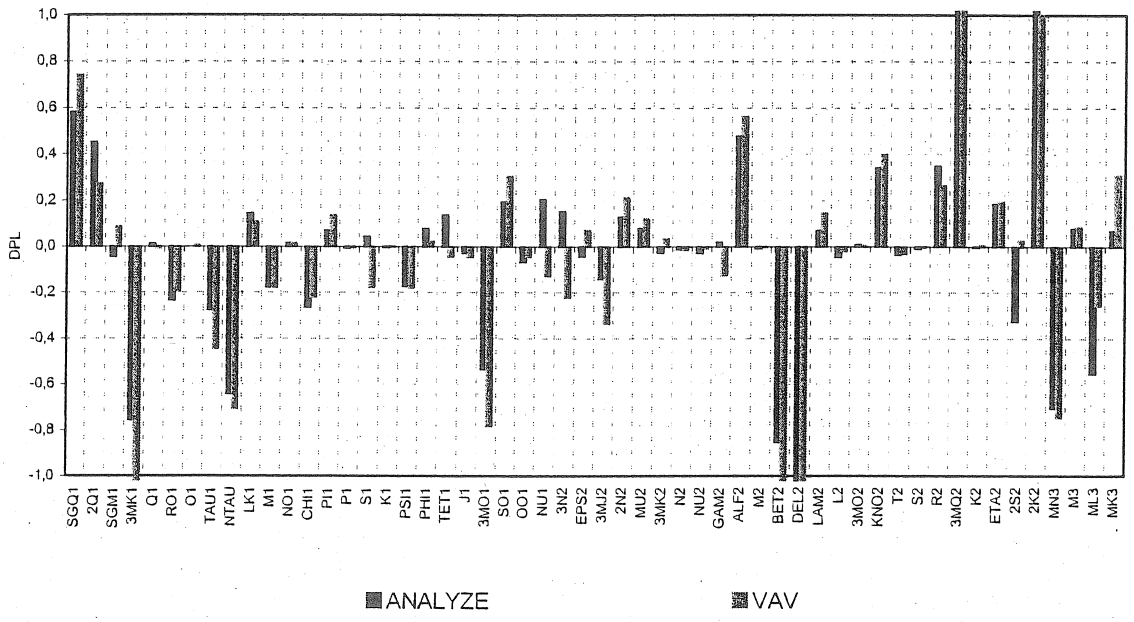

Figure 4.8b: Deviations of phase leads for analysis of noisy benchmark data with 54 wave groups

NUMFILNAME does not really have influence on the analysis (NUMFILNAME=n1h1h007.nlf and 002 were finally used). The results (DAF and DPL) get better for some wave groups for others they get worse. WAVEGROUPI and TIDALPOTEN were fixed to use the same wave grouping and tidal potential catalogue in all three programs.

Program BAYTAP-G leads to best results with LOVENM=0 (similar to RIGIDEARTH). Parameter DMIN, managing the search for the smallest ABIC-value, had to be set to something equal 0.1. Then the search for the smallest ABIC-value comes to an end. But the parameter DMIN has not much influence on the results as long as the solution with the smallest ABIC-value is detected. Parameter P4FLAG which includes the waves of potential of degree 4 is best set equal 1 (4^{th} order potential is contained) and parameter ORDER = 2 managing the variability of the drift (ORDER = 2 in the midterm of equation (3)). Parameters ITH=1 and IPOTEN=2 are fixed to use the tidal potential catalogue of TAMURA. SPAN and SHIFT were set to 0 to analyse the whole data set in just a single run.

The variety of parameters within program VAV is very big (three times as much as for programs ANALYZE and BAYTAP-G). But for the analysis of this benchmark series a lot of them are not used anyway. The time window (length of the filter intervals) had a length of 48 hours and the power of the drift polynomials was set to 3. In this drift time series the long periodic tidal waves are included. The long periodic signals cannot be eliminated by filters. The only other possibility is to analyse this long periodic waves too. The filter-frequencies were set to 15°/h, 30°/h, 45°/h. The wave grouping was the same as in the two other programs. The possibilities of separation or correction of the waves of third or fourth order potential were not used.

5 Comparative analysis of observed data

The monthly corrected and decimated datasets were connected to a long dataset with duration of ten month. After preparation of data in BAYTAP-format the wave group arrangement was adjusted so that all three programs use the same arrangement of 31 tidal wave groups together with the same tidal potential catalogue of TAMURA.

Program ANALYZE computes a regression coefficient between highpass filtered gravity data and highpass filtered air pressure data. Here no parameters can be set, the program just has to know which additional signal is supplied. Highpass filtering is applied to eliminate the drift. An approximation with TSCHEBYSCHEFF-polynomials is not used. This method only makes sense when analysing long period wave groups. Parameter RIGIDEARTH now has been set to 0 for real data and NUMFILNAME=n1h1h002.nlf and HANNWINDOW=1 led to better results.

The regression coefficient is estimated in program BAYTAP-G with the model shown in equation (5). In the analysis with the lowest ABIC-value the parameters were set to $k_{max}=\Delta t = 0$ = LAGP, IAUG = 1, LAGINT = 0 (arbitrary when LAGP = 0). As in the programs ANALYZE and VAV just a linear regression with only the actual air pressure value is computed than. Parameter LOVENM is set to 2, parameter DMIN is set as low as 0.01.

Program VAV determines also one regression coefficient for the whole frequency range to describe the influence of air pressure onto the gravity measurement. In contrast to NSV where only frequency dependent solutions were possible. Parameter >CROSS_frequency_independent_coefficient must be set to 1. The value of the regression coefficient is in good agreement with the result from program ANALYZE. The method for adjustment of a phase shift between gravity and air pressure signal is not used. The determination of one regression coefficient for each wave group species leads to good results too. Only the accuracy of wave groups S1 and S2 is a little bit worse. But now a slight decrease of the regression parameter for the influence of the air pressure with increasing frequencies can be seen. Further parameter settings: waves of potential of degree 3 and 4 are corrected and the length of the filter is set to 48 hours.

Estimated linear regression coefficients are shown in table 1. The coefficients do not differ very much and in a visually comparison between the two datasets a coefficient of –2,8 nm^{-2}/hPa was found.

Table 1: Regression coefficients between air pressure and gravity

		Coefficient in nms^{-2}/hPa	Standard deviation in nms^{-2}/hPa
ANALYZE		-2,82	0,02
BAYTAP-G		-3,16	0,02
VAV		-2,81	0,09
VAV	D	-2,94	0,11
	SD	-2,75	0,20
	TD	-2,44	0,11

The results of the analyses of real data with the three programs are shown in figures 5.1 and 5.2 (DAF and DPL). Here DAF and DPL are not the deviations of the results against 1.0 and 0.0. For each wave group amplitude factors and phase leads from the three programs are averaged. DAF and DPL are now the differences between the results of the programs and these mean values.

Obviously the differences in the frequency range of the semi- and terdiurnal waves are small, except of wave group EPS2 where the BAYTAP-results are very different from both other programs. The deviations for the diurnal wave groups are higher and very unequal between the different programs and wave groups. The air pressure with a strong diurnal variation may affect the results for S1. The best results for this wave group and also for PSI1 (nearest to 1.16 for amplitude factor and 0.0 for phase lead) were given by program BAYTAP-G.

The drift approximation with polynomials is not used in program ANALYZE. The programs BAYTAP-G and VAV compute the drift signal as a standard part of the analysis. The computed results are very similar. In both drift signals the long period waves (e. g. fortnightly wave) are contained.

A comparison of the computed standard deviations is not possible for all three programs because BAYTAP-G does not produce a comparable value. But all programs give the residuals after analysis. These residual signals were transformed to amplitude spectra with program TSOFT using FFT and a HANN-window. The spectra are shown in figures 5.3 to 5.5 (units: amplitude: nm/s^2, frequency: cpd).

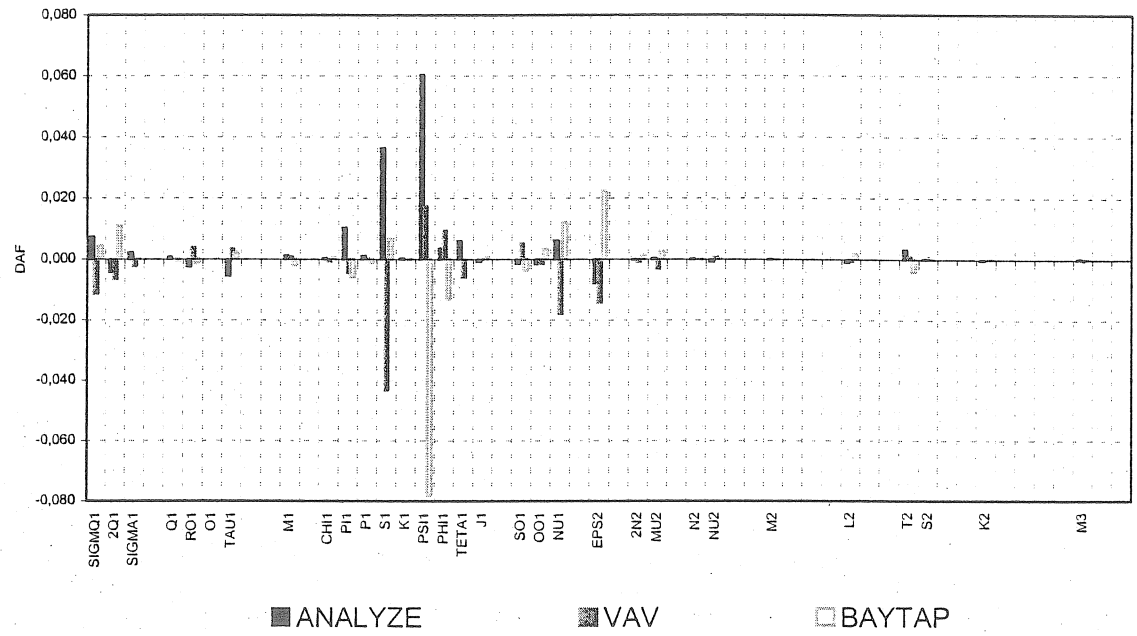

Figure 5.1: Deviations of amplitude factors for analysis of real data

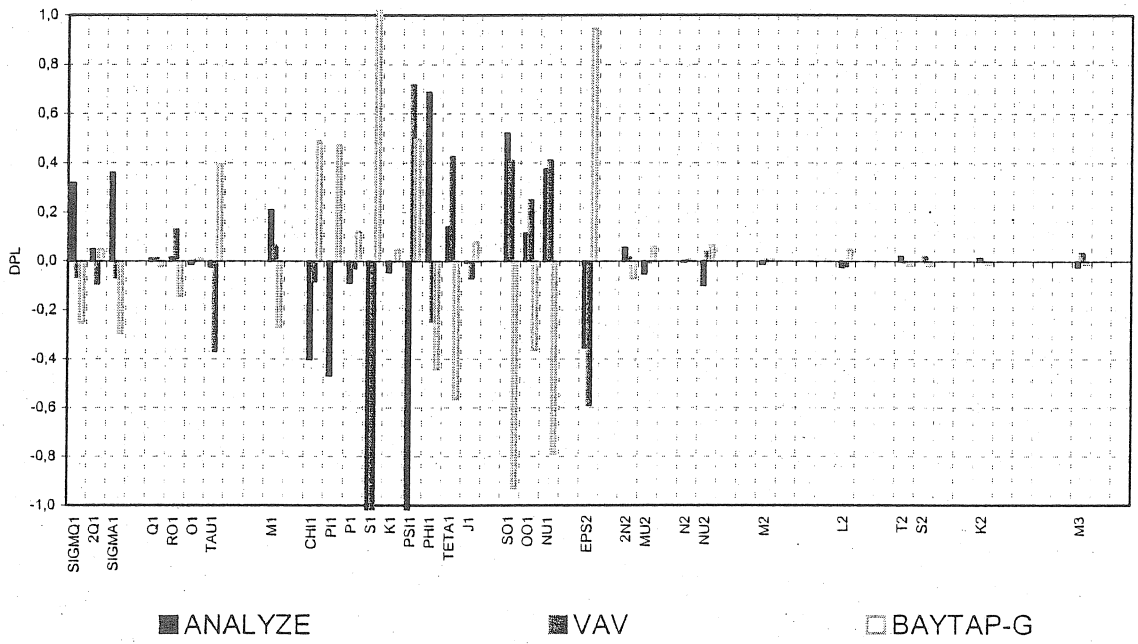

Figure 5.2: Deviations of phase leads for analysis of real data

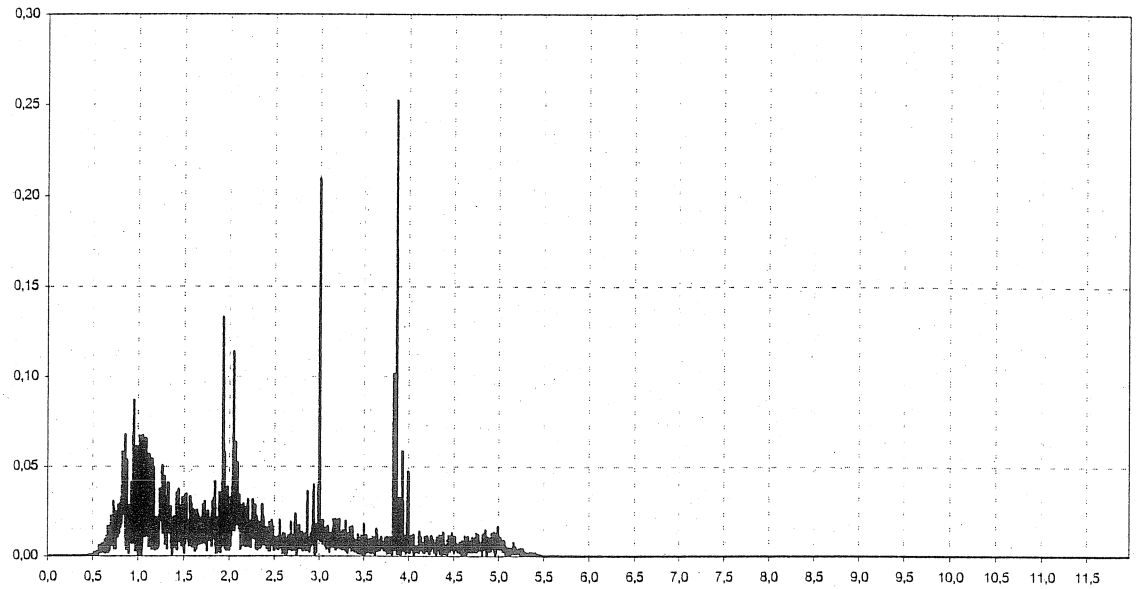

Figure 5.3: Amplitude spectrum of residuals computed by program ANALYZE

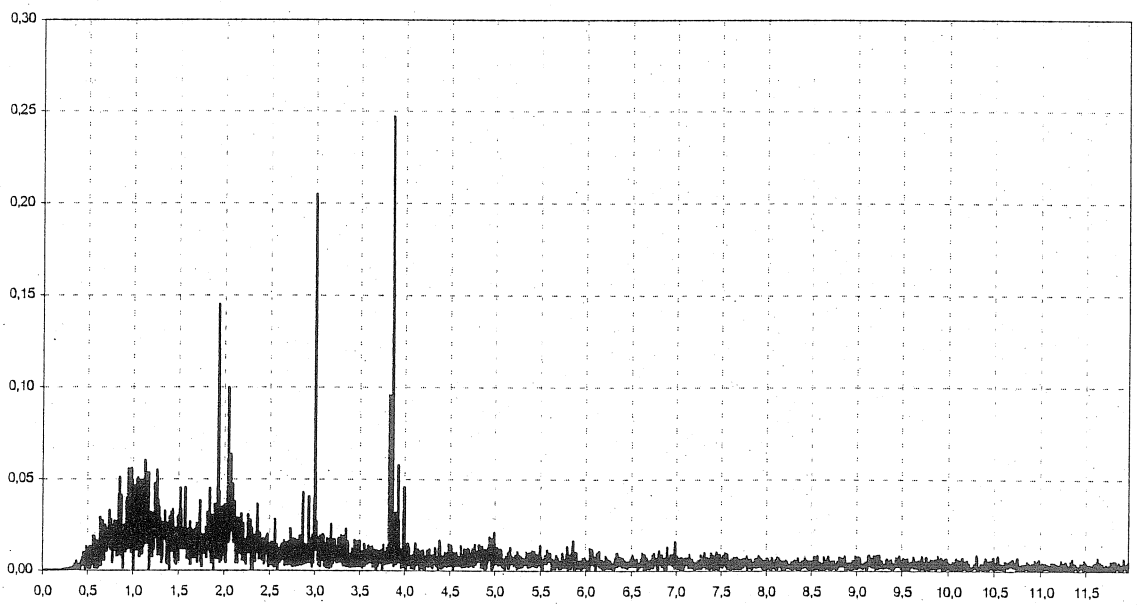

Figure 5.4: Amplitude spectrum of residuals computed by program VAV

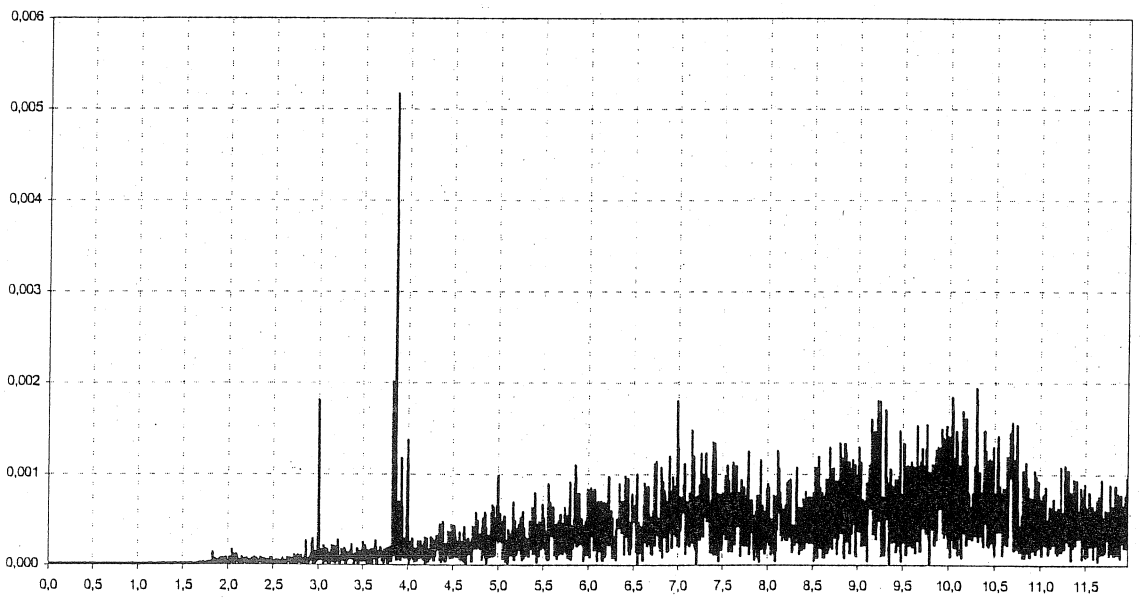

Figure 5.5: Amplitude spectrum of residuals computed by program BAYTAP-G

The spectra from the residuals calculated by ANALYZE and VAV are very similar. While the decreasing amplitude below frequencies of 0.8 cpd results from highpass filtering there is no explanation for the very small amplitudes (different scale!) and the vanishing amplitudes already below frequencies of 1.5 cpd within the spectra of the residuals from program BAYTAP-G. Both other spectra show for single frequencies more energy than for most others. These are remaining signals that could not be assigned to one of the parts named in equation (1) (e. g. air pressure, tidal signal).

6 Conclusions

Combining the direct results of the different analyses for each program does not lead to an advantage of one of these three programs. The results (DAF and DPL) of one program are not better than for another throughout the different wave groups, grouping variants and analyses. But it has to be said that all these results were obtained with special data sets, a fixed wave grouping and just one tidal potential catalogue. By using further applications (e. g. catalogue of HARTMANN and WENZEL in analyses with ANALYZE) different and possibly better results may be obtained.

Program BAYTAP-G is in the used version not able to analyse the long periodic waves. But this could be very interesting when analysing longer data sets of a superconducting gravimeter with its high stability especially in this frequency band. The program BAYTAP-L is made for this frequency range but then there may be the problem that the two frequency parts of one data set (LP and D to TD) are analysed by two separate programs.

Program ANALYZE shows up with good results during the tests (except for the very small wave groups ALF2, BET2, DEL2), a good and complete documentation and a broad output without using special parameter settings. Only this program offers the possibility to use the newest and most accurately tidal potential catalogue of HARTMANN and WENZEL [HAR-95].

The numeric results from program VAV do nearly not differ to those from program ANALYZE. And when differences occur they are small and have changing sign. A problem with program VAV is the slight documentation. There are offered more than 70 parameters to manage the program but only just very little documentation about the effects of each parameter and how to handle them. Beside the advantage of many possibilities to control the analysis there is the danger of not knowing the influence onto the computation.

Acknowledgement

Many thanks to Bernard Ducarme (Royal Observatory of Belgium) for the computation of the benchmark series and the analyses, especially with ANALYZE and to Angel Venedikov (Geophysical Institute at the Bulgarian Academy of Science) for the analyses with VAV and the support for this program.

7 References

[CAR-73] Cartwright, D. E.; Edden, A. C.: *Corrected tables of tidal harmonics*. In: The Geophysical Journal. (1973), Vol. 3, No. 33

[CHO-73] Chojnicki, T.: *Ein Verfahren zur Erdgezeitenanalyse in Anlehnung an das Prinzip der kleinsten Quadrate*. In: Mitteilungen aus dem Institut für Theoretische Geodäsie der Universität Bonn, No. 15. Bonn: 1973

[HAR-76] Harrison, P. J.; Stevens, C. F.: *Bayesian forecasting (with discussion)*. In: Journal of the Royal Statistical Society B, No. 38, pp. 205-247, 1976

[HAR-95] Hartmann, T.; Wenzel, H.-G.: *Catalogue HW95 of the Tide Generating Potential*. In: Marees Terrestres Bulletin d'Informations, No. 123, pp. 9278-9301, Paul Melchior (Edit.). Bruxelles: Association Internationale de Géodésie, 1995

[SCH-76] Schüller, K.: *Ein Beitrag zur Auswertung von Erdgezeitenregistrierungen*. In: Deutsche Geodätische Kommission bei der Bayerischen Akademie der Wissenschaften, No. 227. München: 1976

[TAM-87] Tamura, Y.: *A harmonic development of tide-generating potential*. In: Marees Terrestres Bulletin d'Informations, No. 99, pp. 6813-6855, Paul Melchior (Edit.). Bruxelles: Association Internationale de Géodésie, 1987

[TAM-90] Tamura, Y.: *BAYTAP-G Users Manual*. Mizusawa: National Astronomical Observatory

[TAM-91] Tamura, Y.; Sato, T.; Ooe, M.; Ishiguro, M.: *A procedure for tidal analysis with a Bayesian information criterion*. In: Geophysical Journal International, No. 104, pp. 507-516. Oxford: 1991

[VEN-61] Venedikov, A. P.: *Application à l'Analyse Harmonique des Observations des Marées Terrestres de la Méthode des Moindres Carrées*. In: C. R. Acad. Bulg. Sci. (1961), No. 14, pp. 671-674

[VEN-66a] Venedikov, A. P.: *Une méthode d'analyse des Marées terrestres à partir d'enregistrements des longueur arbitraires*. In: Bull. Cl. Sci., 5^{e} S., t. LIII, fasc 3, Communications de l'Observatoire Royal de Belgique, Série géoph., No. 71, pp. 463-485. Acad. Royal de Belgique, 1966

[VEN-66b] Venedikov, A. P.: *Sur la constitution de filters numériques pour le traitement des enregistrements des Marées terrestres*. In: Bull. Cl. Sci., 5^{e} S., t. LIII, fasc 6, Communications de l'Observatoire Royal de Belgique, Série géoph., No. 76, pp. 827-845. Acad. Royal de Belgique, 1966

[VEN-97] Venedikov, A. P., Vieira, R.; de Toro, C.; Arnoso, J.: *A new program developed in Madrid for tidal data processing*. In: Marees Terrestres Bulletin d'Informations, No. 126, pp. 9669-9704, Paul Melchior (Edit.). Bruxelles: Association Internationale de Géodésie, 1997

[VEN-98] Venedikov, A. P.: Output when calling the help function in NSV98. Extracted from source code <NCONI.FOR> in the version from 01. Sept. 1998

[VEN-01] Venedikov, A. P.; Arnoso, J.; Vieira, R.: *Program VAV/2000 for tidal analysis of unevenly spaced data with irregular drift and coloured noise*. In: Journal of the Geodetic Society of Japan, Vol. 47, No. 1, pp. 281-286, 2001

[WEN-94] Wenzel, H.-G.: *Erdgezeitenanalyse*. In: Bericht zum DGG-Seminar Gezeiten in Oberwolfach / Schwarzwald Oktober 1994, Sonderband II / 1995, Deutsche Geophysikalische Gesellschaft e.V. Münster 1995, pp. 19 - 38

[WEN-96a] Wenzel, H.-G.: *The nanogal software: Earth tide data processing package ETERNA 3.30*. In: Marees Terrestres Bulletin d'Informations, No. 124, pp. 9425-9439, Paul Melchior (Edit.). Bruxelles: Association Internationale de Géodésie, 1996

[WEN-96b] Wenzel, H.-G.: *ETERNA Manual*. Version 3.30, Karlsruhe: Black Forest Observatory

A comparison of the seismic noise levels at various GGP stations

Séverine ROSAT (1), Jacques HINDERER (1) and David CROSSLEY (1/2)

(1) IPGS-EOST (UMR CNRS-ULP 7516), 5, rue Descartes, 67084 Strasbourg, France.
srosat@eost.u-strasbg.fr
(2) On leave from Dept. Earth and Atmospheric Sciences, Saint Louis University, 3507 Laclede Ave., St. Louis, MO 63103, USA.

Abstract

Since 1997 a network of superconducting gravimeters (SG) has been monitoring the variations of the Earth's gravity field. Data from the network, under the coordination of the Global Geodynamics Project (GGP), allow a comparison of the noise levels of the different contributing stations. We use a standardized processing procedure to evaluate the combined instrument plus site noise in the long-period seismic band (200s-600s). Most of the stations have Power Spectral Densities (PSD) contained in a 10 dB wide range, i.e. there is a factor 3 in amplitude between the least and the most noisy station. In the high frequency part of the PSD, the decrease induced by the decimation filter to one minute affects the computation of the Seismic Noise Magnitude (SNM) for many stations. The SNM is a summary statistics introduced by Banka in 1997 to enable a quick comparison of the quality of a site-sensor combination. From T=16 min to T=3.5 h, PSD are below the New Low Noise Model of Peterson (NLNM). SG's data are therefore appropriate for studying long-period seismic and subseismic modes. Knowledge of the noise levels of each station is important in a number of studies that combine the data to determine global Earth parameters. We cite for example the stacking of the data to determine the period of the free core nutation and the Chandler wobble, and the potential use of the data in the search for the gravity variations associated with the translational mode of the inner core.

Introduction

Since 1997 a network of superconducting gravimeters (SG) (Crossley et al., 1999) has been monitoring the variations of the Earth's gravity field. Data from the network, under the coordination of the Global Geodynamics Project (GGP) (Crossley and Hinderer, 1995), allow a comparison of the noise levels of the different contributing stations.

The analysis of the noise level at a gravimeter station is well realized by the use of a Power Spectral Density of the instrument series. The PSD has the advantage of being independent of the length and sampling rate of the signal. Moreover the integration over a frequency band leads to the estimate of the mean power within this band, and the PSD is always representative of a physical phenomenon, particularly if it is aperiodic or transient. In the present study, the New Low Noise Model (NLNM) of Peterson (1993), designed for seismometers, is used as a reference level to give an estimate of the quality of the site-sensor combination. With a single instrument at a site, it is not possible to separate site noise from instrument noise.

Banka (1997) introduced a summary statistics that can be derived from the PSD. It is called the Seismic Noise Magnitude (SNM), a quantity that is based on a narrow window in the normal mode band between 200s and 600s. We divide the paper into three sections, the first deals with the processing procedure, the second is for the study of the noise level at the Strasbourg station and the third one presents a comparison of the seismic noise levels at 19 GGP stations.

1. The processing procedure for the Seismic Band, 200s-600s

The processing procedure is fully described and evaluated in Banka and Crossley (1999); here it will be only briefly summarized.
Gravity and pressure data are analysed for each day of a given year at a superconducting gravimeter station. The following steps are applied:

- amplitude calibration of raw gravity and pressure data;
- subtraction of the tides computed using an elastic reference earth model:
  the difference between using an elastic model and calculating local tides is insignificant. Banka and Crossley (1999) found that the inclusion of ocean tides does not affect the noise levels in the seismic band nor in fact the use of a highly accurate tidal potential. Besides it does not make any difference whether the FCN correction is used or not. The Xi Qinwen (1989) tidal potential with a cut-off of 0.0001 for the Doodson amplitude yielding 383 waves was used.
- reduction of the influence of the air pressure with an admittance factor of -0.3 μgal/mbar: the pressure data must have been fixed for spikes, gaps and offsets so that problems in the pressure do not get transferred into the gravity data.
- subtraction of a best-fitting 9th degree polynomial to eliminate the instrument drift and any residual tidal signal;
- computation of the RMS deviation;
- selection of the 5 quietest days (based on those with the lowest RMS);
- Fast Fourier Transform and average of the 5 amplitude spectra;
- computation of the Power Spectral Density (PSD).

In the period range 200s-600s, the Seismic Noise Magnitude is defined through the relation:

$$SNM = \log10(\text{meanPSD } (\mu gal^2/Hz)) + 2.5$$

Thus the sphere resonance mode, which usually has a period shorter than 200s, is excluded from the computation for all the superconducting gravimeters (SGs).

By taking the log of the PSD and normalizing it so the NLNM is zero, we are able to use a single figure that acts as a quality factor for site-instrument noise. Such a figure clearly contains much less information than the PSD, but in some cases, it may be useful in quickly comparing the high-frequency performance of instruments.

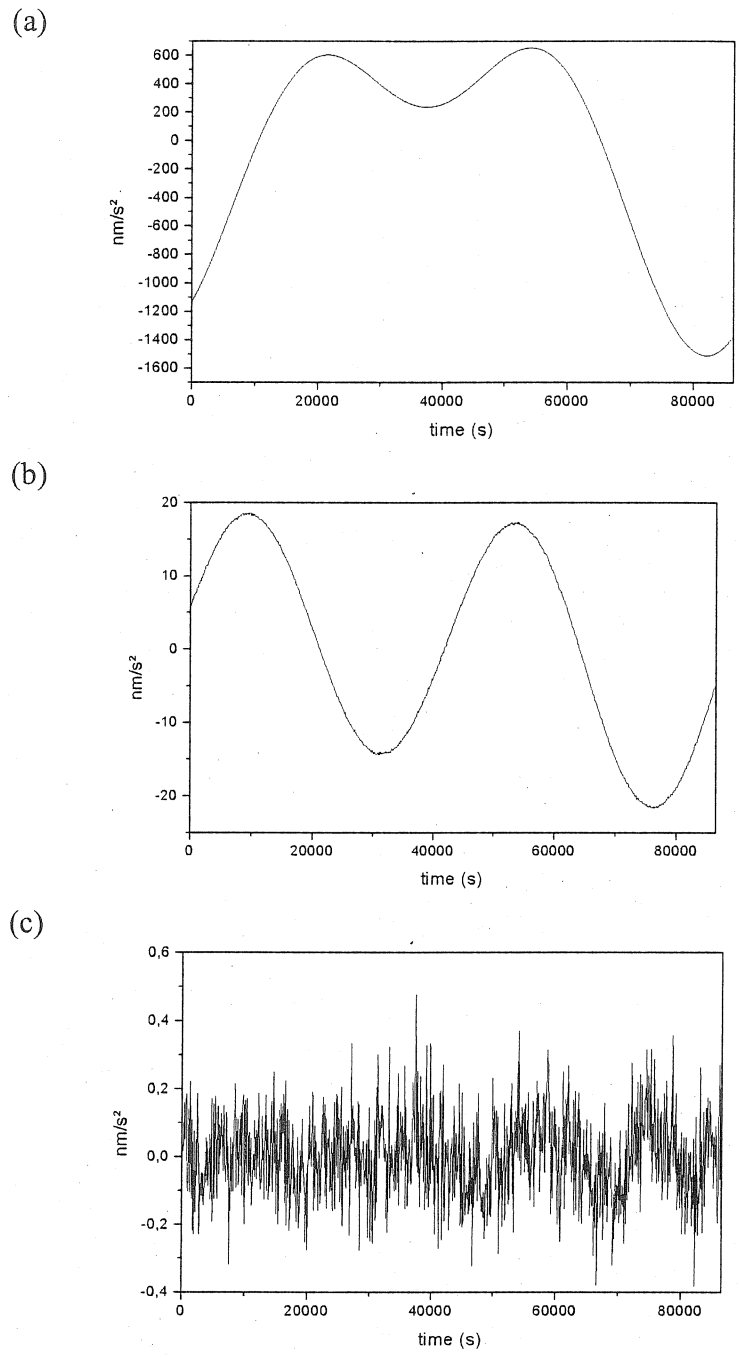

Figure 1: Example of procedure at Strasbourg for one day (98/01/26)
(a) Raw gravity (b) Tides and pressure subtracted (c) a 9th degree polynomial subtracted

For instance at Strasbourg station, the amplitude of the raw gravity signal is about 200μgal (Figure 1 (a)). After tide and pressure correction, it is about 4μgal (Figure 1 (b)) and after the subtraction of a ninth degree polynomial the amplitude is of the order of 0.01μgal (Figure 1 (c)).

2. The Power Spectral Density at Strasbourg

The procedure was first applied to the original 2 second sampling data of Strasbourg. The sphere resonance of this SG appears at 2 minutes (8 mHz), see Figure 2.
The high frequency decrease of the PSD is due to the GGP2 anti-aliasing filter, shown in Figure 3. The smooth diminution in the long period part of the PSD is caused by the subtraction of the 9th degree polynomial.

The procedure was then carried out on the 1 minute decimated data. The influence of the low pass filter has a small but noticeable effect in the seismic band 200s-600s used for our Seismic Noise Magnitude computation (Figure 3 (a)). For Strasbourg, the decrease in the SNM due to the attenuation of the decimation filter is only about 4%, Figure 3 (b).

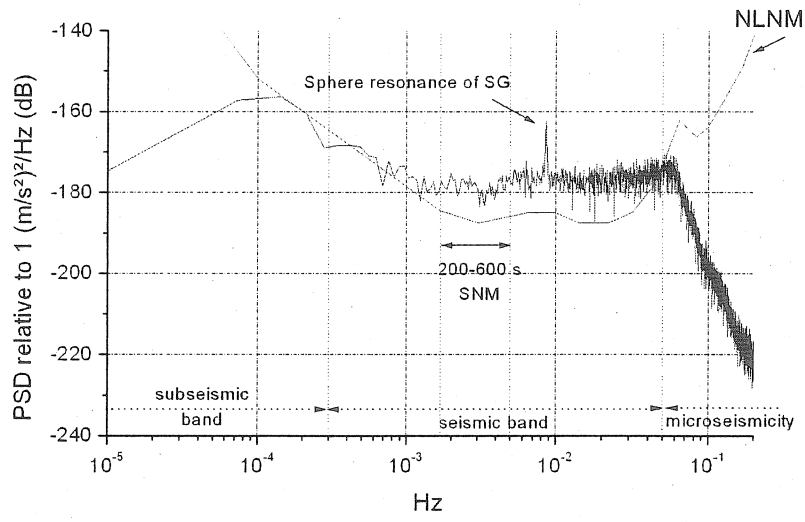

Figure 2: Power Spectral density of 5 quiet days at Strasbourg, 1998. The raw data are sampled at 2 seconds.

(a)

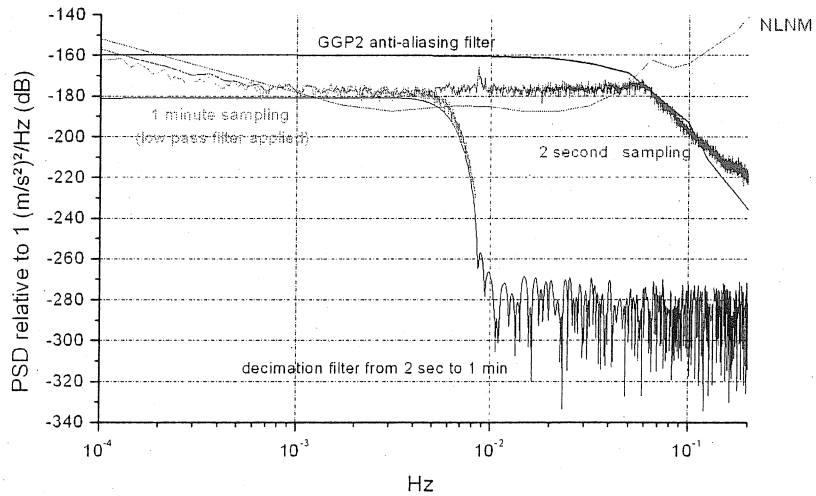

(b)

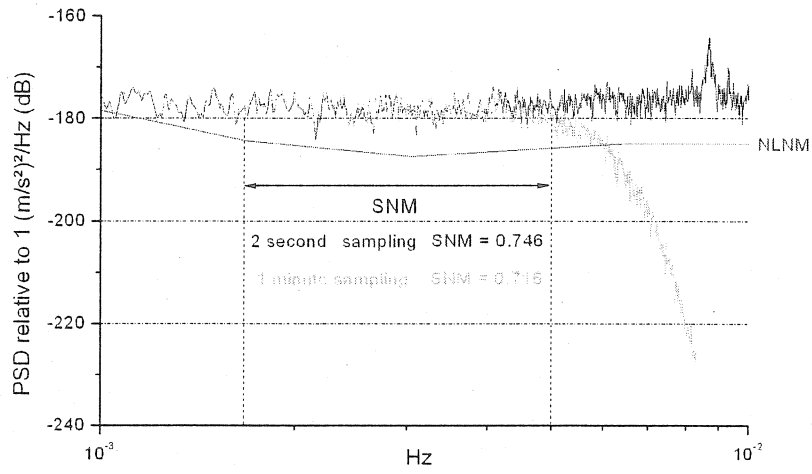

Figure 3: Power Spectral Density of 5 quiet days at Strasbourg. (a) shows the effect of the GGP2 and decimation filters, (b) shows the influence of the decimation filter from 2 seconds to 1 minute on the Seismic Noise Magnitude.

Table 1 points out the stability of the SNM in Strasbourg with time. The data are plotted in Figure 4 and show that from 1997 to 2001 the noise magnitude decreased by 4.8%.

Table 1. SNM for Strasbourg, various years.

Year	The 5 quietest days	Range of RMS for 5 days (nm/s^2)	SNM
1997	271, 192, 65, 257, 66	0.13-0.14	0.757
1998	26, 39, 129, 37, 277	0.12-0.13	0.737
1999	73, 72, 89, 326, 70	0.11-0.13	0.731
2000	73, 78, 91, 14, 1	0.13-0.14	0.723
2001	91, 213, 112, 244, 90	0.12-0.14	0.720
All years	99073, 98026, 99072, 01091, 01213	0.11-0.12	0.708

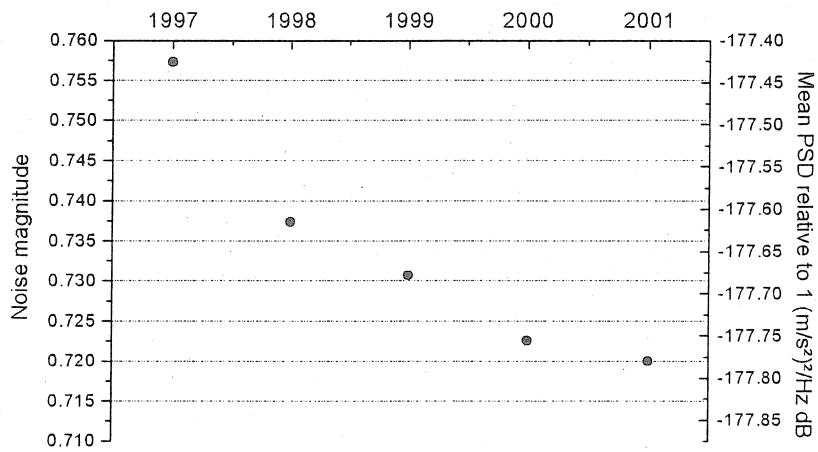

Figure 4: Evolution of the Seismic Noise Magnitude in Strasbourg from 1997 to 2001.

The distribution of RMS deviations for year 1998 is represented in Figure 5. It is a non-Gaussian distribution with a median value of 0.28 nm/s². Notice that the value corresponding to the 5 best days is of course smaller (0.12 nm/s²).

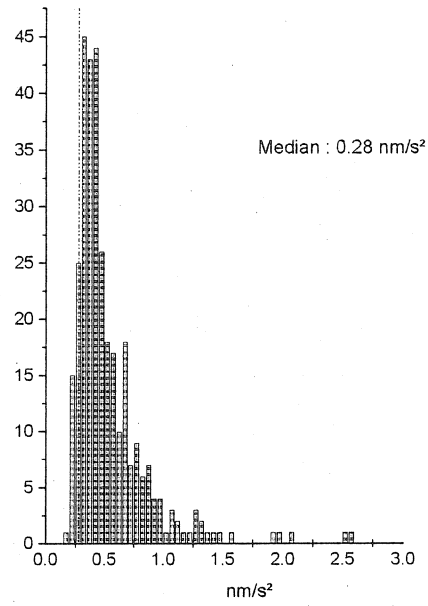

Figure 5: Histogram of RMS deviations in 1998 at Strasbourg

Figure 6 reveals the evidence of the good correlation between RMS deviation and mean PSD in our case. Indeed these selection criteria are only equivalent because the high-frequency micro-seismic noise is cut-off by the decimation filter and because the 9th degree polynomial has removed the long-period signals (Figure 7). For instance, if there was no high frequency filtering, the micro-seismic noise would be added to the seismic noise and would make the new selection of quiet days unsuitable to compute the seismic noise levels.

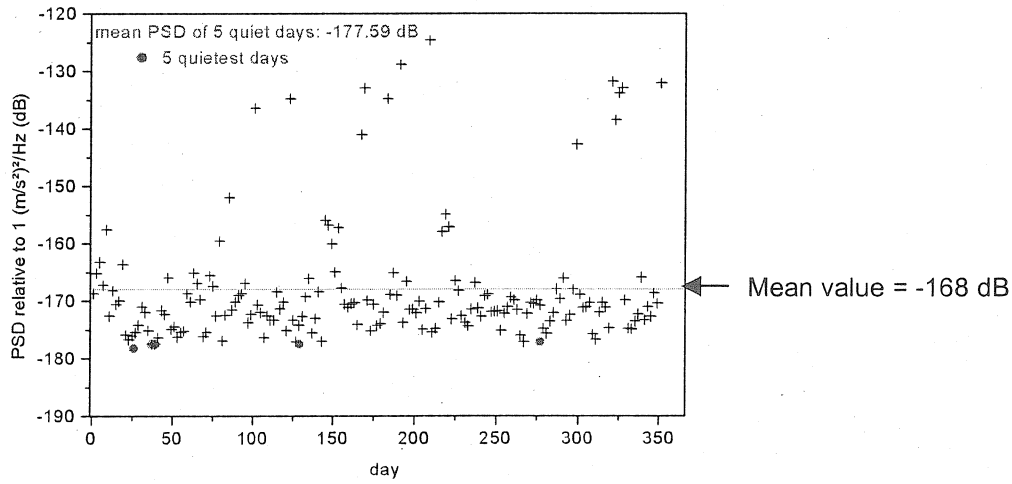

Figure 6: Mean Power Spectral Density values for each day of 1998 at Strasbourg. The mean PSD corresponding to the 5 quietest days (with lowest RMS deviations) are represented with circles.

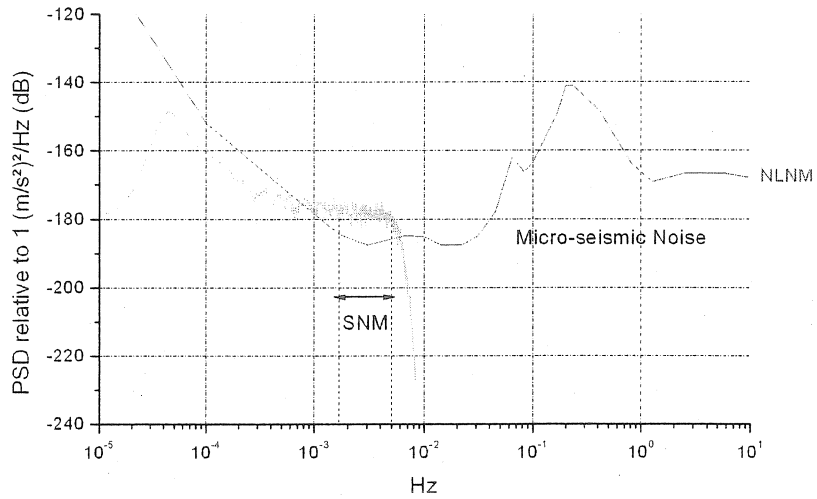

Figure 7: Power Spectral Density of 5 quietest days in 1998 at Strasbourg showing the attenuation in the long period band due to the 9th degree polynomial and the high frequency filtering due to the decimation to 1 minute.

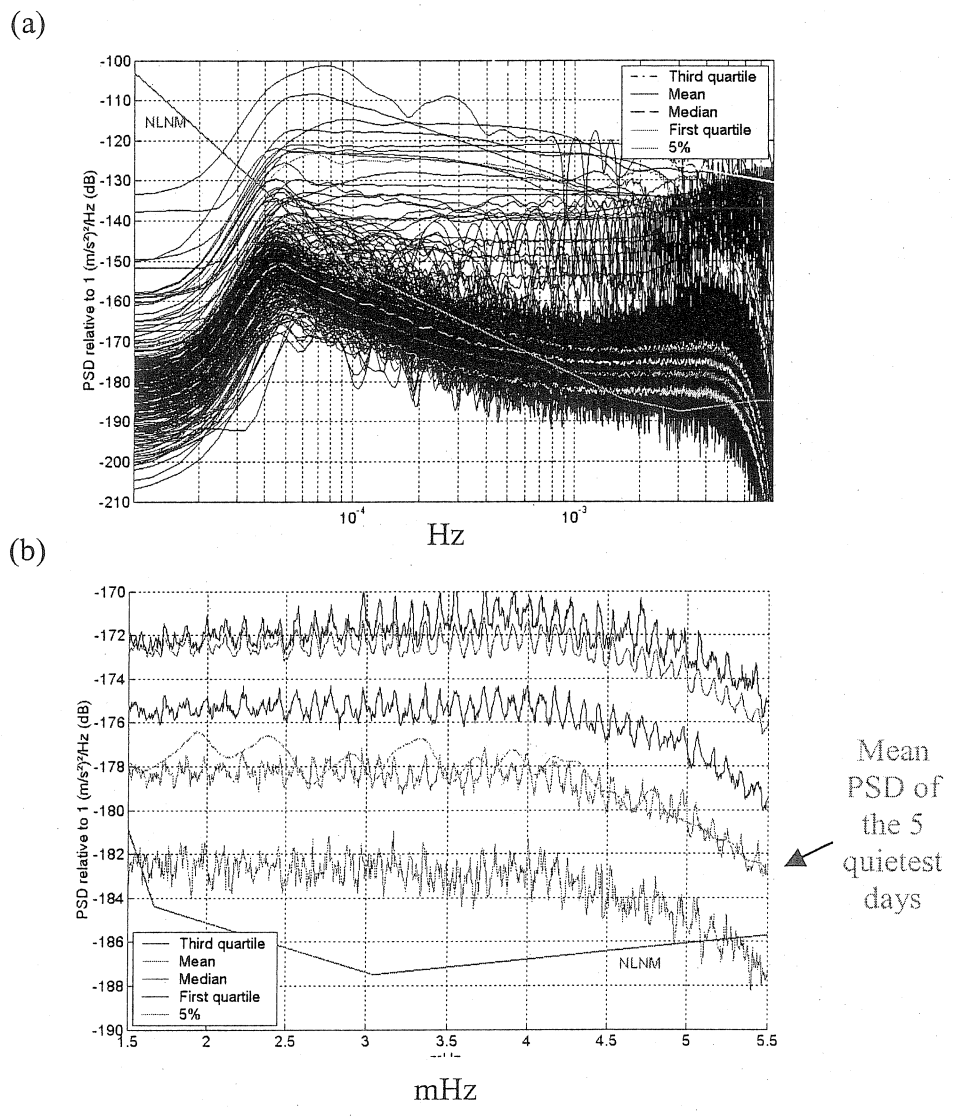

Figure 8: Statistics on all the daily PSD at Strasbourg for 1998. (a) shows all the individual spectra. The 5%, first quartile, median, mean and third quartile are plotted in (a) and (b).

Statistics on the PSD for each day of a year at Strasbourg are represented in Figure 8. The mean PSD of the 5 quietest days is at the same level as the first quartile. The mean and the third quartile levels are close and they are the highest levels. They seem to show some organized oscillations that are the background free oscillations or "hum" (Nawa et al., 2000). The mean and the median values are different which indicates a non-Gaussian distribution of the RMS deviations.

It was already noticed in previous studies (Freybourger et al., 1997 – Zürn and Widmer, 1995) that the pressure correction with an admittance is not efficient at high frequencies on seismic data. It can be seen in Figure 9 that the air pressure correction has however a substantial effect at frequencies less than 1 mHz.

(a)

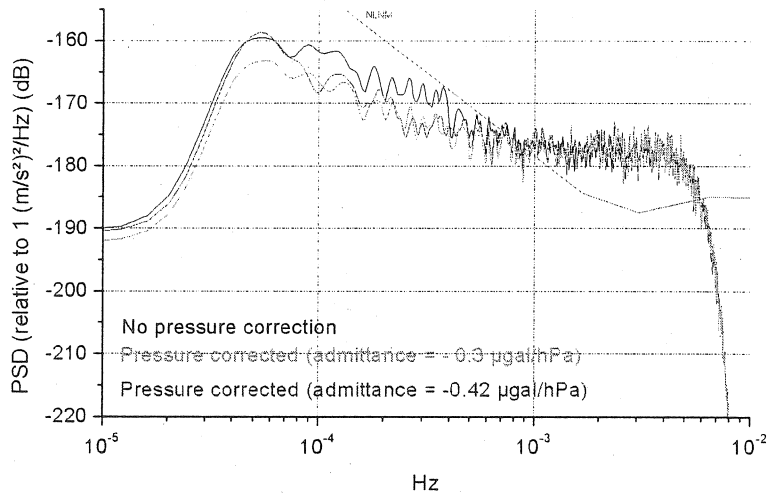

(b)

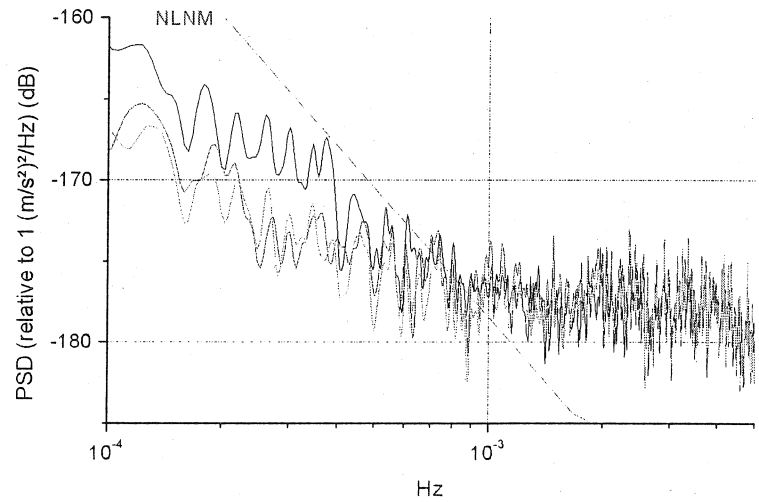

Figure 9: Influence of pressure reduction on the PSD levels, Strasbourg, 1998. (b) is an enlargement of (a) showing the pressure effect more clearly.

3. The Power Spectral Densities at GGP stations and the Seismic Noise Magnitudes

The processing procedure summarized in part 1 was applied to 19 GGP stations in order to make a comparison of the different noise levels. The stations considered were Bandung (BA), Brussels (BE), Brasimone (BR), Boulder (BO), Canberra (CB), Cantley (CA), Esashi (ES), Kyoto (KY), Matsushiro (MA), Membach (MB), Metsahovi (ME), Moxa (MO), Potsdam (PO), Strasbourg (ST), Sutherland (SU), Syowa (SY), Vienna (VI), Wetzell (WE) and Wuhan (WU). The PSD were smoothed in the frequency domain with a 501-point Parzen window in Figure 10 and with a 2001-point Parzen window in Figure 11.

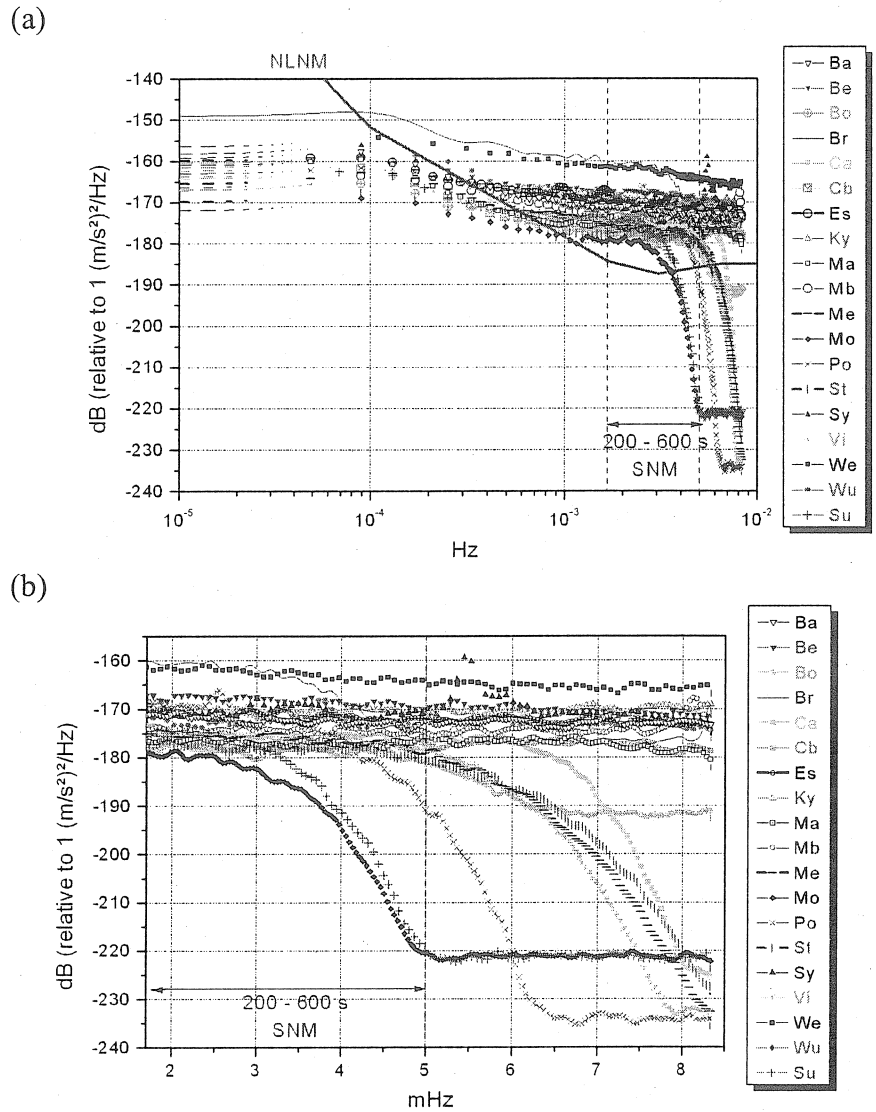

Figure 10: Power Spectral Densities of the 5 quietest days of a year at 19 GGP stations. (b) is a zoom in the seismic band. The PSD are smoothed with a 501-point Parzen taper.

Figure 10 underlines the decimation filter used at each station. Moxa and Sutherland have low pass filters that attenuate the fastest and the steepest, so their SNM computed in the 200s-600s band will be altered towards lower values by the decimation. We must keep this in mind when comparing all the 19 SNM. It will be the case also for Potsdam. Concerning Strasbourg which has the next steepest decimation filter, the decrease introduced by the attenuation is of 4% (as seen in section 2). The sphere resonance is clearly visible at Syowa.

Most PSD are contained in a 10 dB range corresponding to a factor of 3 in amplitude between the least and the most noisy stations.

Figure 11 presents a comparison of the levels in the seismic band 200s-600s. Four stations have their noise levels considerably altered by their decimation filters in that band. They are Brasimone, Potsdam, Sutherland and Moxa. The levels at Boulder, Strasbourg, Metsahovi and Vienna are also slightly affected. The other stations have roughly constant levels over the whole band.

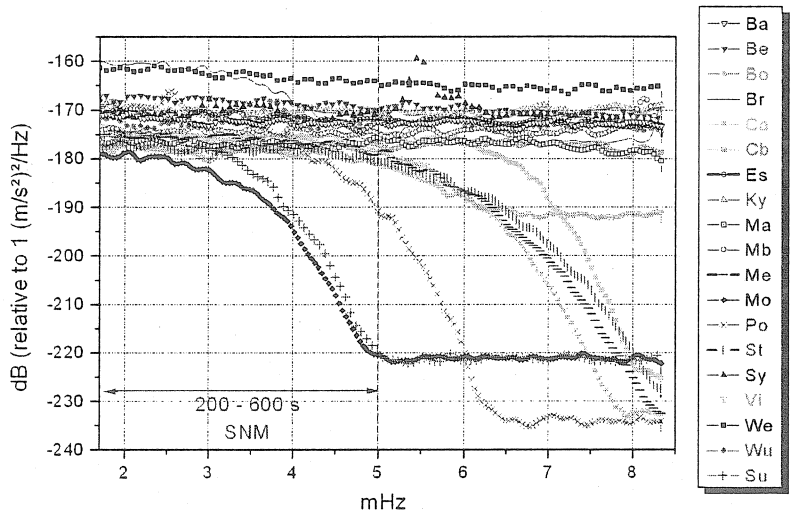

Figure 11: Power Spectral Densities of the 5 quietest days of a year at 19 GGP stations in the seismic band 200s-600s. The PSD are smoothed with a 2001-point Parzen window.

A quick comparison in the seismic band 200s-600s can be obtained by computing the Seismic Noise Magnitudes; these are plotted in Figure 12. The SNM computed by Banka (1997) for a STS-1 seismometer at the Black forest Observatory (BFO) is also indicated for comparison. The former SG at Strasbourg (TT070) is represented to show the important improvement realized with the new instrument C026 since 1996. The SNM decreased by 51% from the TT070 to the present SG at Strasbourg.

Moxa has the lowest SNM, however it must be underlined again that this value is lowered by 63% by the decimation filter.

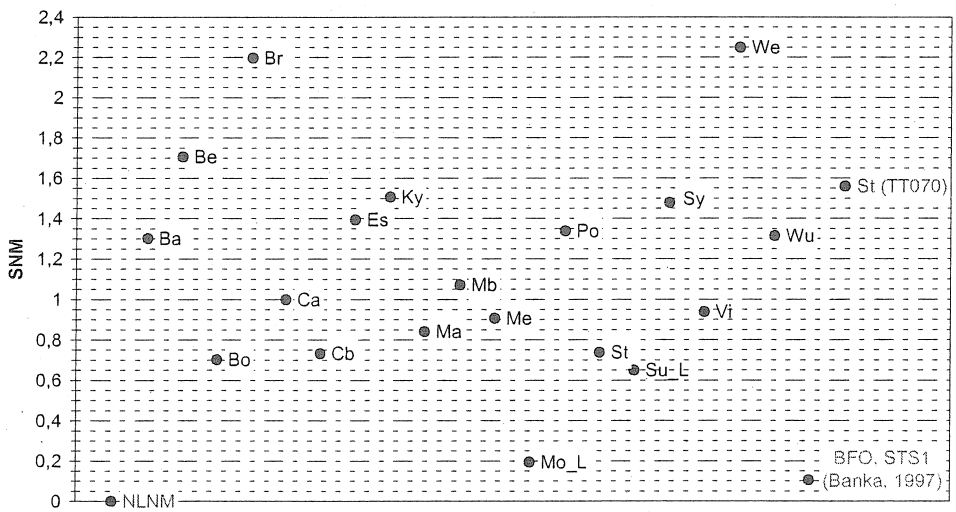

Figure 12: Noise Magnitudes in the frequency band 200s-600s for the 19 GGP stations.

Conclusions

In the high frequency band the decrease induced by the GGP2 anti-aliasing filter on raw gravity data was presented. In the seismic band, the decimation filter from raw sampling rate to one minute data alters the Seismic Noise Magnitude computation. A link between RMS and PSD was stressed; in particular, there is a strong correlation when the micro-seismic noise has been filtered out. The effect of pressure reduction is noticeable at frequencies less than 1 mHz. The PSD of 19 GGP stations were plotted and most of them are contained in a 10 dB range. The SNM was also computed for these stations.

In general, GGP stations have very low noise levels in the long period seismic band, except Brasimone and Wettzell (instrument SG103) that show large Seismic Noise Magnitude values.

The knowledge of all GGP decimation filters appears to be necessary to understand the high frequency trends of the Power Spectral Densities.

GGP station levels are crossing the New Low Noise Model from T=16min to T=3.5h. Superconducting gravimeters are therefore excellent instruments for studying long period signals. In that purpose, a pressure correction is necessary to further decrease the noise level.

A comparison of the noise levels in the subseismic band and in the tidal bands of GGP stations has to be carried out in the future, leading to a selection of the quietest stations for optimal stacking in the search for the Slichter mode (Slichter, 1961).

Acknowledgements

The authors are grateful to all the GGP station managers for providing their data sets. This study was supported by CNRS (Intérieur de la Terre). This is EOST contribution N° 2002 -10 - UMR 7516.

References

Banka, D., 1997. Noise levels of superconducting gravimeters at seismic frequencies, *PhD thesis*, GDMB-Informationgesellschaft mbH, Clausthal, Germany.

Banka, D. and Crossley, D.J., 1999. Noise levels of superconducting gravimeters at seismic frequencies, *Geophys. J. Int.*, **139**, 87-97.

Crossley, D. & Hinderer, J., 1995. Global Geodynamic Project – GGP: Status report 1994. In CONSEIL DE L'EUROPE: *Cahiers du Centre Européen de Géodynamique et de Séismologie*, volume 11, pages 244-274.

Crossley, D., Hinderer, J., Casula, G., Francis, O., Hsu, H.T., Imanishi, Y., Jentzsch, G., Kääriäinen, J., Merriam, J., Meurers, B., Neumeyer, J., Richter, B., Shibuya, K., Sato, T., Van Dam, T., 1999. Network of superconducting gravimeters benefits a number of disciplines, EOS, **80**, 11, 121/125-126.

Freybourger, M., Hinderer, J. & Trampert, J., 1997. Comparative study of superconducting gravimeters and broadband seismometers STS-1/Z in subseismic frequency bands, *Phys. Earth planet. Inter.*, **101**, 203-217.

Nawa, K., Suda, N., Fukao, Y., Sato, T., Tamura, Y., Shibuya, K., McQueen H., Virtanen, H. & Kääriäinen, J., 2000. Incessant excitation of the Earth's free oscillations: global comparison of superconducting gravimeter records, *Phys. Earth planet. Inter.*, **120**, 289-297.

Peterson, J., 1993. Observations and modelling of seismic background noise, Open-File Report 93-332, U.S. Department of Interior, Geological Survey, Albuquerque, New Mexico.

Qinwen, Xi, 1989. The precision of the development of the tidal generating potential and some explanatory notes, *Bull. Inf. Mar. Terr.*, **105**, 7396-7404.

Slichter, L. B., 1961. The fundamental free mode of the Earth's inner core, *Proc. Nat. Acad. Sci.*, **47** (2), 186-190.

Zürn, W. & Widmer, R., 1995. On noise reduction in vertical seismic records below 2 mHz using local barometric pressure, *Geophys. Res. Lett.*, **22**, 3537-3540.

What can Superconducting Gravimeters contribute to normal mode seismology?

R. Widmer-Schnidrig

Black Forest Observatory, Heubach 206, D-77709 Wolfach, Germany
e-mail: widmer@geophys.uni-stuttgart.de

1. Introduction

Superconducting gravimeters (SGs) currently deployed in the sparse GGP network [*Crossley et al.*, 1999] hold the promise to achieve lower instrumental noise levels over sensors currently deployed in the Global Seismographic Network (GSN) and used in studies of the Earth's free oscillations.

This position paper attempts to review the current situation in observational normal mode seismology: both from the point of view of instrumental challenges and challenges related to the illumination of the Earth's large-scale structure.

Particular attention is given to 1-D and 3-D density structure and how this structure is encoded in the observable normal mode spectra. The reason for concentration on density structure is that the frequency band where SGs compare most favorably with seismic sensors coincides with the band where the modes have increased sensitivity to laterally heterogeneous as well as 1-D density structure through the mechanism of self-gravitation. Since our ability to learn about Earth structure is always a question of signal-to-noise ratio (SNR) in our data we have organized the paper into a discussion of instrumental and environmental noise followed by a discussion of normal mode signals.

The paper concludes with an assessment of where SGs can make a difference in our quest to learn about deep Earth structure.

2. Vertical Seismic Noise

2.1. Global Noise Models

The level of background seismic noise limits our ability to detect small seismic signals which have propagated through the Earth and which carry information about both their source and the structure of the medium through which they propagated. Comprehensive studies of typical and of minimum noise levels have been carried out to asses station performance, to help in site selection, and in negotiations of nuclear test ban treaties [e.g. *Agnew and Berger*, 1978; *Peterson*, 1993; *Astiz and Creager*, 1995]. Figure 1 shows the new Low Noise Model of *Peterson* [1993] which is the lower envelope of noise levels found at GSN stations. A number of different sensors are deployed at the GSN stations, however, below 30 mHz the NLNM is largely defined by the Streckeisen STS-1 seismometer.

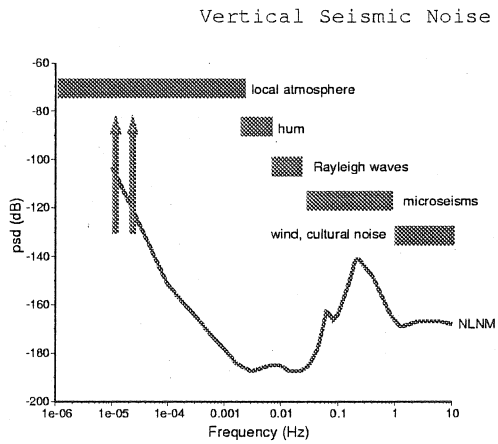

Figure 1. Dominant sources of seismic noise on vertical component sensors (*i.e.* gravimeters and vertical seismometers) together with the New Low Noise Model (NLNM) of *Peterson* [1993]. The NLNM is the lower envelope of noise spectra at GSN sites and represents the least expected noise level for seismic observatories. The NLNM is given in power spectral densities in units of dB relative to 1 $(m/s^2)^2/Hz$.

Many of the large features of the NLNM are well understood. At frequencies below 2 mHz the Newtonian attraction of moving air masses in the local atmosphere above the seismic sensor is the principal source of noise [e.g. *Warburton and Goodkind*, 1977; *Zürn and Widmer*, 1995].

In the band 2-7 mHz the NLNM exhibits a slight minimum near 3 mHz but is otherwise relatively flat. Recent studies of the noise floor in this band with high frequency resolution have revealed that the noise floor contains a well defined structure consisting of ~50 regularly spaced peaks whose frequencies coincide with the fundamental spheroidal modes, ${}_0S_\ell$ [e.g. *Suda et al.*, 1998]. This structure in the noise floor is termed background free oscillations or simply *hum*. Since free oscillations are a global phenomenon the hum constitutes a lower bound for observable signals at any site on the Earth's surface. The hum amplitude has also been found to be very stable in time with only a small semi-annual harmonic component. In the band 7 - 30 mHz the NLNM exhibits a local maximum near 10 mHz.

The cause for the generally level noise floor between 2 and 30 mHz is still not understood. However *Nishida et al.* [2002, manuscript in preparation] were able to demonstrate that in the band adjacent to the hum (7-30 mHz) the background noise consists of globe circling Rayleigh waves much like the hum [*Ekström*, 2001]. The physical process involved in the hum excitation is still a matter of debate with turbulence in the atmosphere and/or hydrosphere being the favored candidates.

One problem with identifying the source is the small size of the signal: to drive one of the spheroidal multiplets at the observed *rms* amplitudes (~ 1 ngal or 5×10^{-10} m/s at 300 seconds period, a quality factor of the mode of $Q \sim 300$ and an effective mass of the upper mantle of $m \sim 10^{24}$ kg) requires approximately 10 Watts of power! Another more serious problem is that the hum signal is very close to the detection limit of current sensors (see below).

In the band 30 mHz - 1 Hz background noise levels are dominated by the marine microseism with a peak around 0.14 Hz. The cause of the microseism are the swell- and surf-induced pressure fluctuations at the bottom of the water column which excite seismic waves in the solid Earth. It is very fortunate for the study of normal modes that the normal mode band (0.3 - 20 mHz, fig. 6) and the band of microseism (30 mHz - 1 Hz) do not overlap considering that noise levels in the microseism band are often 60 dB higher than in the band of the hum.

2.2. Noise levels at BFO

The Black Forest Observatory is particularly suited for noise studies because of two reasons: (1) noise levels at BFO have been repeatedly shown to be among the

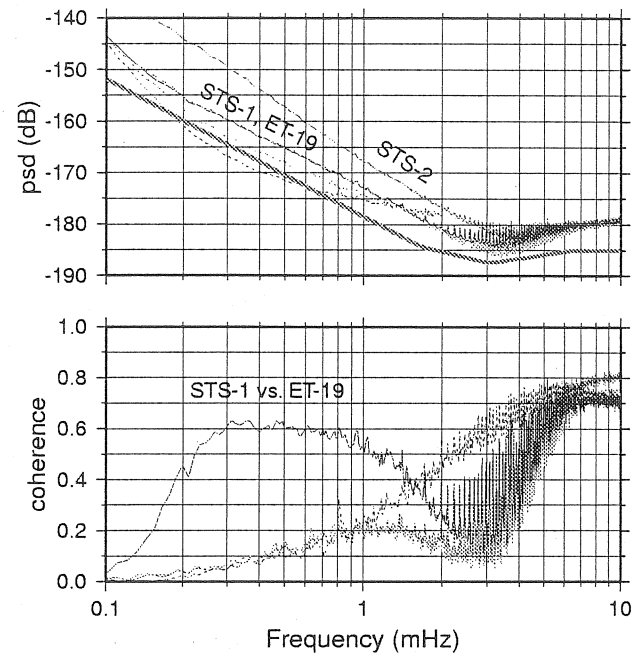

Figure 2. Comparison of the three vertical component seismic sensors installed at BFO: LaCoste-Romberg gravimeter ET-19 and Streckeisen STS-1 and STS-2 seismometers. Shown are the noise levels averaged over the 895 selected windows. The dashed curves are the pressure corrected STS-1 and ET-19 noise levels [*Zürn and Widmer*, 1995]. For the STS-2 the pressure correction is ineffective. The NLNM is shown for reference.
The lower panel shows average pairwise coherencies: STS-2 vs. STS-1 (red), STS-2 vs. ET-19 (green) and STS-1 vs. ET-19 (blue). The coherencies between the STS-2 and either STS-1 or ET-19 is low below ~5 mHz due to the increased noise levels in the STS-2. In the Band 2-4 mHz the coherency between STS-1 and ET-19 is also very low which shows that in this band the self-noise levels of these two sensors are comparable to the level of the (coherent) signal.
The dashed curve in the lower panel is the coherency between the pressure corrected spectra of ET-19 and STS-1. Its low value for frequencies less than 1 mHz shows that at least one of the sensors (the STS-1) is limited by self-noise after the pressure correction. Since the pressure correction is marginally efficient for the STS-1 and since uncorrected noise levels of STS-1 and ET-19 are practically identical, we conclude that the NLNM in this band is defined by the barometric effect. The increase of the pressure corrected coherency above 1 mHz is an artefact of the pressure correction, which only reduces noise levels below 1.5 mHz. Finally, we note the small peak in the pressure corrected coherency at 0.81 mHz - the frequency of ${}_0S_0$.

lowest of the GSN [e.g. *Zürn et al.*, 2000] and (2) these low noise levels have been achieved simultaneously with up to four different sensors [*Richter et al.*, 1995].

Thus one can attempt to answer the question to what extent the NLNM is defined by the instrumental noise of the sensors or by seismic noise. While this distinction is impossible to make with a single sensor, it is also dangerous to conclude from global studies such as the one by *Peterson* [1993] that the universality of the NLNM is a feature of the Earth's seismic background. Considering that the NLNM below 20 mHz relies primarily on data from STS-1 seismometers it is conceivable that the NLNM reflects (at least in some bands) the instrumental noise of the STS-1.

With multiple co-located sensors it is possible to separate sensor noise from seismic noise. Seismic noise should be common to all sensors while sensor noise should be uncorrelated between the different sensors.

To get a robust and representative estimate of seismic noise at BFO we have selected data from the vertical component STS-1 seismometer (VHZ) recorded on a 24 bit channel of the IDA Mk7 data logger, the TIDE channel of the LaCoste-Romberg ET-19 gravimeter (UGZ) recorded on a 16 bit auxiliary channel of the IDA Mk7 logger and the long-period channel (LHZ) of the STS-2 seismometer of the German Regional Seismic Network (GRSN) recorded with 24 bits on a Quanterra Q680 data logger. Continuous data for a 3 year window (1996:206 - 1999:179) was chopped into 24 hour long, overlapping segments with start times at midnight and at noon. Segments were only retained if data from all three sensors was complete. Power spectral densities were computed and integrated between 3 - 5 mHz to give a single number representative of noise level in the normal mode band. Based on a histogram of these noise levels a selection of 895 quiet windows was made for which all three sensors simultaneously meet our noise criterion. Thus 60 % of the windows were rejected.

Fig. 2 (top) shows the average power spectral densities for the three sensors. At frequencies below 2 mHz the psd of the STS-1 and the ET-19 sensors are very similar. This is probably because both instruments are sensitive enough to record the gravity signal from the moving air masses in the atmosphere above the station. If we apply the barometric correction [*Zürn and Widmer*, 1995], however, psd levels drop by different amounts. Histograms of regression coefficients for the three sensors are given in fig. 4. At 0.3 mHz the pressure correction reduces psd levels by $\sim$ 2 dB for the STS-1 but by as much as 7 dB for ET-19. Thus it becomes clear that self noise of the STS-1 in this band is only slightly below the signal psd whereas for ET-19 it is well below the signal level.

The low efficiency of the pressure correction for the STS-1 cold be due to a noisy integral feedback. To check this hypothesis the electronics of the STS-1 at BFO was

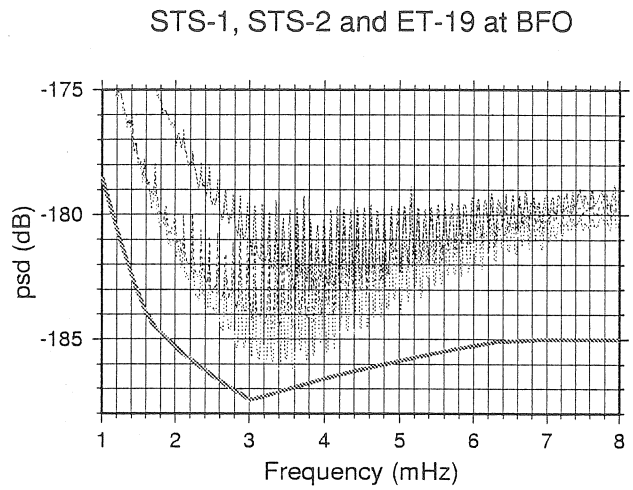

Figure 3. Blow-up of upper panel of fig 2. The lowest curve (green) is from the STS-1, followed by the ET-19 (blue, dashed) and the STS-2 (red).

modified but this modification did not lead to any improvement [*Wielandt and Zürn, pers. comm., 1999*].

The pairwise coherencies are given in the lower panel of fig. 2. In the band of the hum the STS-1 seems to be the sensor with the lowest self noise followed by the ET-19 and STS-2.

Fig. 3 zooms in on the hum part of fig 2. The comb like structure of the spectra is typical for the hum. Note the slight increase of the hum near 3.7 mHz. This amplification of the hum was noted by *Nishida et al.* [2000] and constitutes the most direct observational evidence for atmospheric excitation of the hum. Note that at 4 mHz the STS-2 is only 3 dB noisier than the STS-1 while this difference increases to 10 dB at the frequency of ${}_0S_2$ or 0.3 mHz.

2.3. Noise levels of SG meters

Since we do not operate a permanently installed SG meter at BFO we refer to published comparisons of SG meter noise levels and our permanent sensors: *Richter et al.* [1995] have compared data from the seismometers and the LaCoste-Romberg gravimeter with a temporarily installed, portable SG meter (SG102), while *Banka and Crossley* [1999] and more recently *Van Camp* [1999] compare SG meters contributing to the GGP network with our sensors.

For frequencies above 1.5 mHz these studies find that the STS-1 and ET-19 at BFO are less noisy than the SG meters. This finding has also been confirmed in studies of the hum at Canberra (Australia) where an STS-1 and an SG are co-located [*Nawa et al.*, 2000]. In the hum band average noise levels for the STS-1 are $\sim$7 dB lower than for the best SG meters while ET-19 is only 4 dB lower. (These numbers were obtained by converting the noise-magnitude estimates of [*Van Camp*, 1999] into

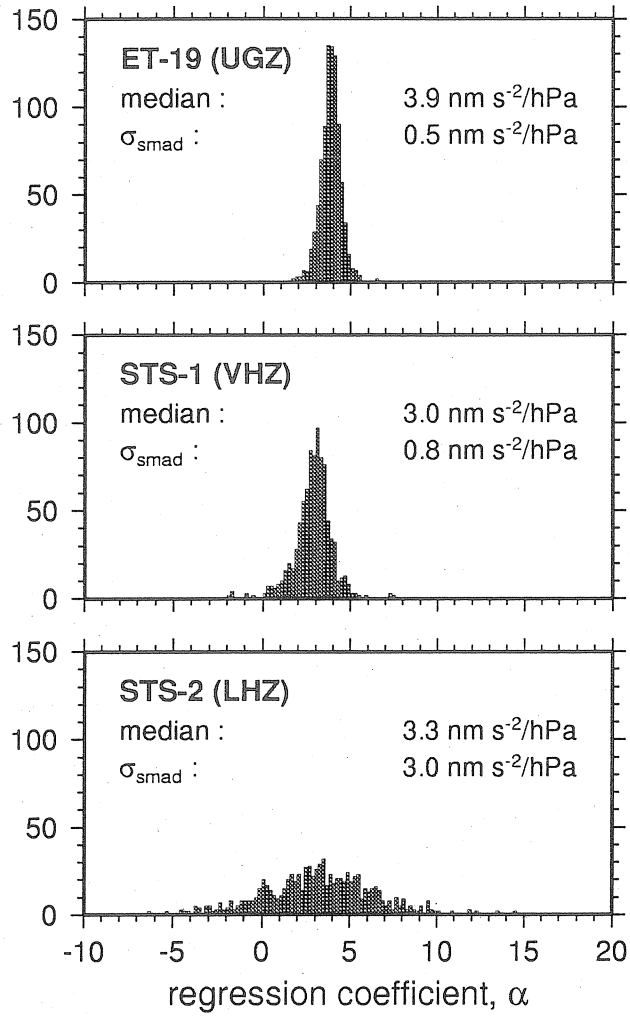

Figure 4. Histograms of 895 regression coefficients for the pressure correction. The regression was carried out in the band 0.1 - 0.5 mHz. Note the large dispersion for the STS-2. σ_{SMAD} is the scaled median absolute deviation of the median - a statisticaly robust measure of dispersion equivalent to the standard deviation.

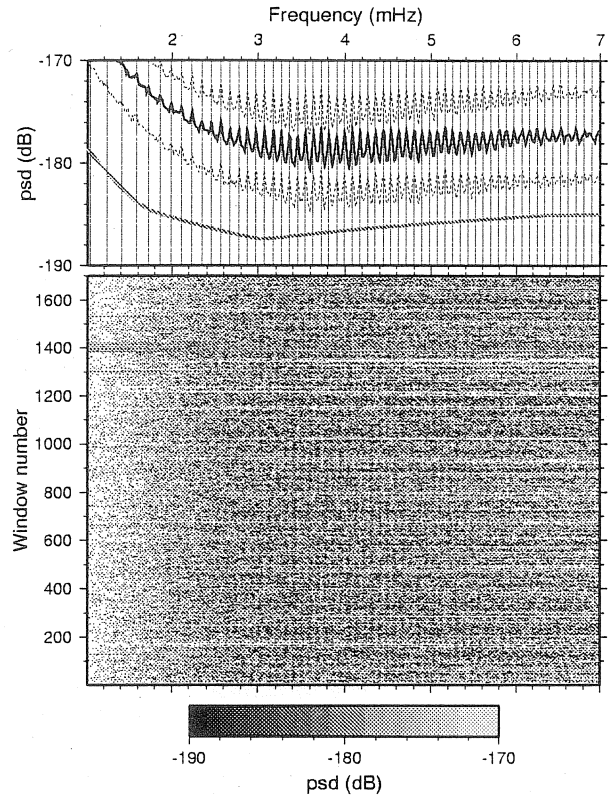

Figure 5. Time-frequency plot covering 2 years of data from the STS-2 seismometer of the German Regional Seismic Network (GRSN) at BFO. The range of the gray scale is chosen to emphasize structure in the noise during seismicaly quiet times. The upper panel shows median psd levels (black) together with the first and third quartile (dashed). The NLNM (gray) is shown for reference. The vertical dashed lines indicate the predicted frequencies of the fundamental spheroidal modes ${}_0S_\ell$ and coincide with light-grey bands in the lower panel.

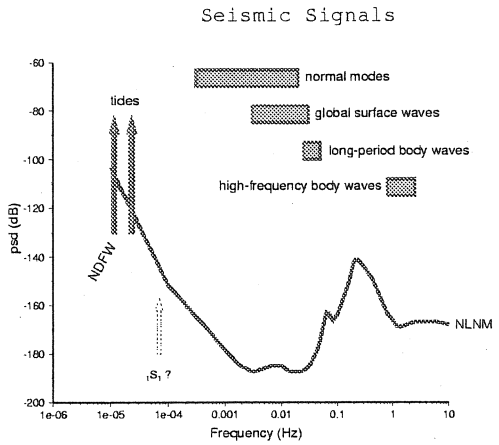

Figure 6. Principal signals in vertical seismic recordings. The suspected location of the Slichter mode, $_1S_1$ is also indicated.

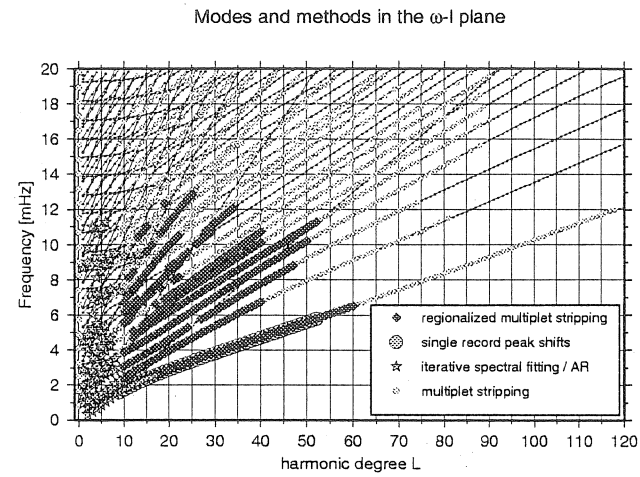

Figure 7. Spheroidal mode dispersion diagram for model PREM. The symbols used for the different modes indicates the analysis technique with which the mode was observed: regionalized multiplet stripping [*Widmer-Schnidrig*, 2002], single record peak shifts [e.g. *Smith and Masters*, 1989], iterative spectral fitting [e.g. *Ritzwoller et al.*, 1988], autoregressive method (AR) [*Masters et al.*, 2000], multiplet stripping [*Masters and Widmer*, 1995].

equivalent psd values). This difference in noise levels is also consistent with the observation that the psd levels of the best SGs intersect - after pressure correction - the NLNM at a frequency of ~1 mHz.

For frequencies below 1.5 mHz where the barometric pressure correction is efficient for gravimeters, the best SGs are less noisy than STS-1 seismometer. While SGs could still not compete with the ET-19 gravimeter in this band back in 1994 [*Richter et al.*, 1995], recent improvements in the SG meters has changed this picture. [*Zürn et al.*, 2000]. In this article data from the Balleny Islands event (1998) recorded by IRIS, GEOSCOPE and GGP networks was systematically scanned for signals of Coriolis coupled modes below 1 mHz and the highest SNR was found in the spectra of SG meters and ET-19. The most recent occasion for the observation of the gravest normal modes was the Peru event with moment magnitude M_W=8.3 on June, 23 2001 and the spectrum of the SG near Strasbourg (J9) is shown together with the spectrum of the 1977 Sumbawa event (M_W=8.3) recorded in Brasilia with the IDA gravimeter at Brasilia (BDF) in fig. 9. The spectrum from BDF was up until now the spectrum with the highest signal-to-noise ratio for the football mode, $_0S_2$. For the Peru event this mode was detected with similar SNR in spectra of SG meters located in Vienna (Austria), Metsähovi (Finland), Moxa (Germany), and Southerland (South Africa) and their heigh SNR for $_0S_2$ could not be matched with either ET-19 or any of the STS-1s of the GSN.

In other words the most recent version of SGs are now competitive with the best spring gravimeters as far up in frequency as 1.5 mHz and below ~0.6 mHz they are – after pressure correction – clearly superior to either spring gravimeters or STS-1 seismometers..

Above 3 mHz, however, it seems that the best SGs cannot compete with the STS-2 at BFO. To corroborate the low noise level of the STS-2 at BFO we show a spectrogram of 2 years of continuous data (fig. 5) together with a robust estimate of the noise levels of that sensor. While one might suspect that this low noise level of the STS-2 is due to the very elaborate shielding of the sensors at BFO, it should be noted that we detected the hum at 7 out of 14 STS-2 equipped stations of the German Regional Seismic Network (GRSN).

The low noise level of the STS-2 above 3 mHz, while higher than STS-1 or ET-19 is of some practical relevance since manufacturing of both LaCoste-Romberg ET meters as well as STS-1 seismometers has been discontinued, making the STS-2 the quietest, commercially available sensor in this band. (Note: we have not inspected data from Geotech KS-54000 borehole seismometer which are also deployed in the GSN for hum signals and are also unaware of any published hum detections for that sensor. The same is true for broad-band seismometers manufactured by Guralp).

3. Normal modes in seismic data

Before the Earth's normal modes can be detected as discrete peaks in spectra of earthquake recordings a number of criteria must be met: The earthquake source must exceed a minimum moment magnitude of M_w ~6.5.

Since the modes can be viewed as the interference of waves traveling in opposite direction around the globe,

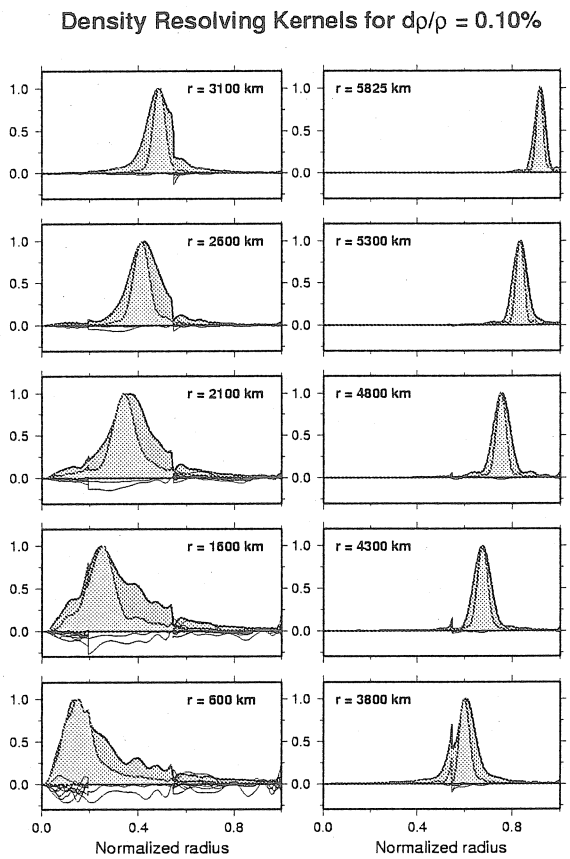

Figure 8. Backus-Gilbert type resolution analysis for the radial distribution of density. The narrower (yellow) averaging kernels include the new degenerate frequency estimates made possible by the sequence of large events in 1994. The wider (blue) averaging kernels are solely based on the degenerate frequency dataset compiled in *Masters and Widmer* [1995] which was derived from earthquake recordings prior to 1994. The width of the bell-shaped curve is a measure of the ability of the data to concentrate information regarding a particular parameter (here density) and a given variance (0.1 percent). The data of the events in 1994 have significantly improved our ability to resolve 1-D density structure.

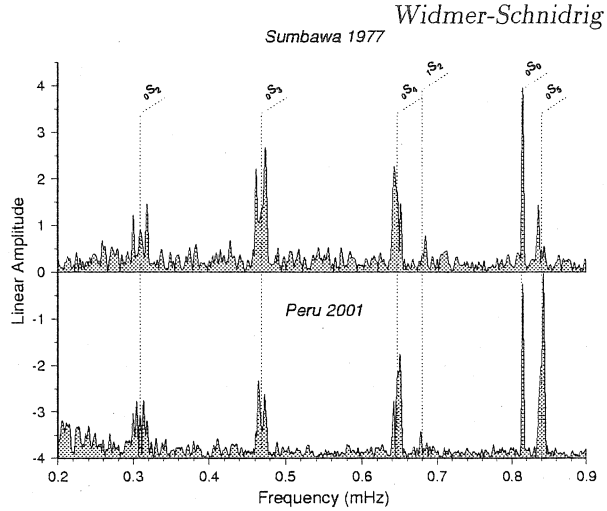

Figure 9. Comparison of two spectra from events separated by 24 years. The upper spectrum is for the 1977 Mw8.3 Sumbawa event recorded with the LaCoste-Romberg gravimeter at BDF and the lower spectrum is for the 2001 Mw8.4 Peru event recorded by the SG at J9. Record length is 150 hours for Sumbawa- and 167 hours for Peru event. Note that only the spectrum from the Peru event is pressure corrected.

the minimum time series length to Fourier analyze must be larger than the time of one orbit: ~3 hours. In order to maximize frequency resolution one has to increase the record length. In practice one faces a trade-off between frequency resolution and available signal. Increasing the time series length improves frequency resolution. However, since the modes get attenuated, there comes a point after which one adds only noise if one keeps increasing time series length. A good compromise between frequency resolution and signal-to-noise can be obtained for a record length of $1 \cdot Q$ cycles [*Dahlen*, 1979].

Earth structure is encoded in two ways in the normal mode spectra: spherically averaged Earth structure can be inferred from multiplet degenerate frequencies while aspherical structure information can be gleaned either from the splitting of individual multiplets or from the coupling between multiplets. Since the Earth is very nearly spherical one can understand that splitting and coupling of modes are subtle effects in the observed spectra and hence it should not surprise that deviations from sphericity are much less well constrained than spherically averaged earth structure.

3.1. Encoding of 1-D Earth structure in mode spectra

Estimates of multiplet degenerate frequencies can be obtained from a number of different techniques: a first set of techniques treats the effect of aspherical structure as a source of large errors and by analyzing spectra from enough earthquakes with a well distributed set of

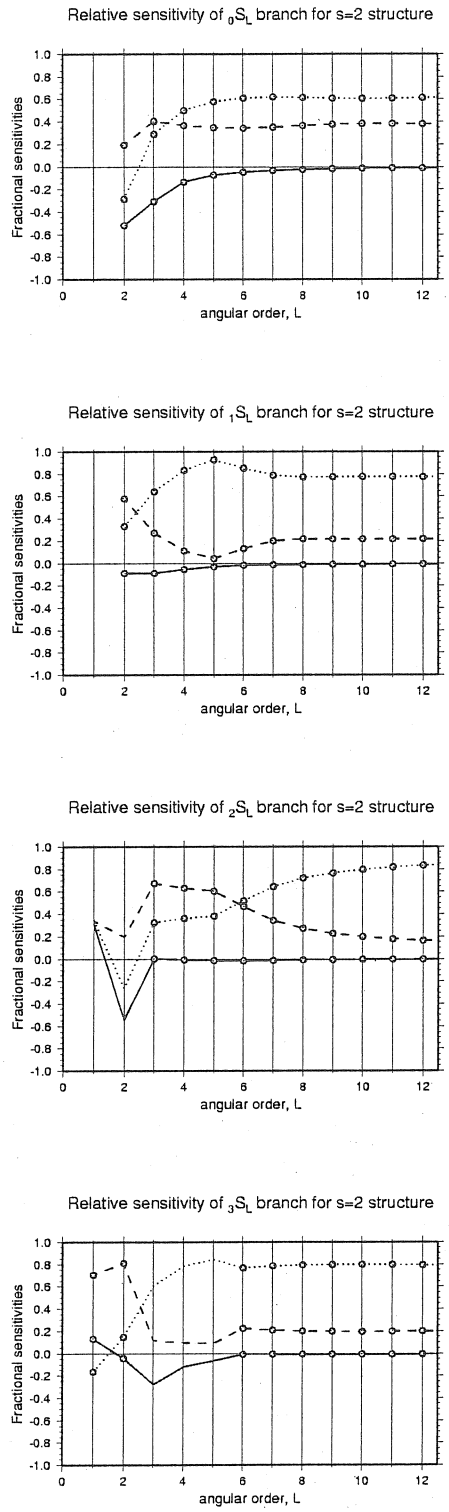

Figure 10. Relative sensitivity of aspherical structure coefficients to 3-D perturbations in Vp (dashed), Vs (dotted) and density (solid). Previously observed modes are indicated with a circular symbol. Note, that density sensitivity is only significantly different from zero for modes below 1 mHz. See also fig. 22 in *Ritzwoller and Lavely* [1995]

Table 1. Distribution of relative errors in multiplet degenerate frequency dataset used for the construction of new 1-D Earth models.

σ	$_nS_\ell$	$_nT_\ell$	$_nS_0$
$1 \times 10^{-5} - 3 \times 10^{-5}$	0	0	1
$3 \times 10^{-5} - 1 \times 10^{-4}$	56	2	13
$1 \times 10^{-4} - 3 \times 10^{-4}$	279	48	10
$3 \times 10^{-4} - 1 \times 10^{-3}$	712	198	0
$1 \times 10^{-3} - 3 \times 10^{-3}$	325	39	0

σ is the range in relative errors, $_nS_0$ are the radial modes.

stations one hopes that it will average out. (Multiplet stripping and stacking).

A second set of techniques strives to extract constraints about 3-D structure and as an aside one always also gets an degenerate frequency estimate which is largely free from bias due to effects from 3-D structure. While these techniques provide the most precise degenerate frequency estimates they can only by applied to two small subsets of modes: Histogram analysis of single record peak frequency measurements [e.g. *Smith and Masters*, 1989] while iterative spectral fitting [e.g. *Ritzwoller et al.*, 1988; *Resovsky and Ritzwoller*, 1998] and the AR method [*Masters et al.*, 2000] lend themselves only for the analysis of high-Q, low-ℓ overtones. All overtones with $\ell \geq 10$ could until recently only be analyzed with multiplet stripping. With the increasing number of high quality recordings of large earthquakes during the last decade a regionalization of the multiplet stripping technique became feasible for many high-ℓ overtones [*Widmer-Schnidrig*, 2002] which provided both improved degenerate frequency estimates as well as the first, crude 3-D constraints from these modes. Figure 7 summarizes where in the $\omega - \ell$-plane the different techniques mentioned have been applied.

The datasets used for the the analysis of high-Q, low-ℓ modes consists typically only of the ~50 records for each of the ~10 largest events. For the high-ℓ modes however much larger datasets are used: The regionalized multiplet stripping experiments were only possible because a dataset of 12000 individual traces (6000 vertical and 6000 horizontal component recordings) were available.

Table 1 gives the distribution of errors for a recently compiled dataset of multiplet degenerate frequencies. With this kind of dataset we are in a position to estimate all five elastic parameters (of a transversely isotropic medium) plus the density with high radial resolution

and very little trade-off between the parameters. Fig. 8 depicts the density averaging kernels obtained from the above dataset. The target uncertainty was set to 0.1 percent and the bell shaped kernels show over which depth range the model has to be integrated in order to achieve this error level. The target depth was varied from frame to frame and shows how resolution degrades with depth.

In fig. 8 the trade-off with other parameters becomes only noticeable in the core where the averaging kernels for the elastic parameters (drawn in black) are non-vanishing. This means that leakeage from elastic parameters biases the density estimates.

Since the density, ρ, is the geodynamically most interesting parameter any further improvement in the radial density profile should be welcome. The need to improve 1-D density models is emphasized by the observation, that for the discussion of the stability of stratification the relevant parameter is not the density, $\rho(r)$ but the less well resolved radial derivative $d\rho/dr$.

Here we recall two possible avenues to improve on 1-D density models: the observation of Zeeman splitting of individual multiplets and Coriolis coupling between spheroidal and toroidal multiplets. Zeeman splitting and Coriolis coupling are small signals and need to be observed with high precision before any new inference about Earth structure can be drawn from them. The reward however would be significant since these observables constitute linear constraints on the 1-D density profile much like the Earth's mass and moment of inertia. Thus, their interpretation is not subject to any trade-off with elastic parameters!

3.2. Splitting du to rotation - Zeeman splitting

The rotation of the Earth completely removes the degeneracy of a spheroidal multiplet, ${}_nS_\ell$. The frequencies of the $2\ell+1$ singlets become

$$\omega_m = \bar{\omega} + \delta\omega_m = \bar{\omega} + m\Omega\beta \quad \text{for} \quad -\ell \le m \le \ell \quad (1)$$

with Ω the rotation rate of the Earth, $\bar{\omega}$ the multiplet degenerate frequency, and $-\ell \le m \le \ell$ the azimuthal order of the singlet and b the Zeeman splitting parameter. If the singlet frequencies of the $2\ell+1$ singlets can be observed (such as for ${}_0S_2$ in fig. 9), one can estimate b based on eq. (1). For the kth multiplet b_k is related to the distribution of density with depth through the integral relation [*Backus and Gilbert*, 1961]:

$$\beta_k = \frac{\bar{\omega}}{\Omega} b = \frac{\int \rho[2U_k V_k + V_k^2] r^2 dr}{\int \rho[U_k^2 + \ell(\ell+1)V_k^2] r^2 dr} \quad (2)$$

where $U_k(r)$ and $V_k(r)$ are the usual scalar radial eigenfunction of the kth spheroidal multiplet. The denominator corresponds to the kinetic energy of the mode and is used to normalize the eigenfunctions to unity. One is thus left with a linear relation between the b_ks and the density.

Table 2. Zeeman-Splittingparameter of selected low-frequency spheroidal modes.

mode	f_{1066A}	b_{obs}	r	b_{1066A}
${}_0S_3$	0.468	4.67±0.16	3.4	4.621
${}_0S_4$	0.647	1.80±0.047	2.6	1.834
${}_0S_5$	0.840	0.83±0.028	3.4	0.840
${}_0S_6$	1.037	0.43±0.015	3.5	0.407
${}_1S_3$	0.940	2.728±0.053	1.9	2.632
${}_1S_4$	1.174	2.007±0.048	2.4	1.947
${}_1S_5$	1.371	1.489±0.067	4.5	1.436
${}_1S_8$	1.798	0.458±0.020	4.4	0.427
${}_2S_4$	1.377	0.087±0.107	122.0	0.280
${}_2S_8$	2.049	0.344±0.026	7.5	0.650
${}_2S_3$	1.241	0.612±0.082	14.0	0.667
${}_1S_2$	0.680	4.396±0.285	6.5	4.173

f is the multiplet degenerate frequency in [mHz] as predicted for model 1066A. b is the Zeeman splitting parameter in $[10^{-3}]$ from eq. (2), and r is the relative error in b in percent.

In a pilot study I estimated rotational splitting parameters (table 2) for spheroidal multiplets for which rotational splitting is expected to play a dominant role. While the errors in the splitting parameters are considerably larger than in the degenerate frequency dataset (see tab. 1), these parameters have the advantage to depend on density only and hence their interpretation is not subject to any ambiguity with the anisotropic elastic parameters.

Estimation of rotational splitting parameters is something that data from SG meters should be particularly suited for. Rotational splitting is largest for low-frequency multiplets because of their vicinity to the rotation frequency, Ω. The band below 2 mHz is also the band where the barometric pressure correction [*Zürn and Widmer*, 1995] is effective and where the best SG meters can outperform seismometers.

3.3. Coupling due to rotation: Coriolis coupling

Coriolis coupling between fundamental spheroidal and fundamental toroidal modes has been well observed between 1 and 3.5 mHz [*Masters et al.*, 1983] and more recently also in the band below 1 mHz [*Zürn et al.*, 2000]. In fact, apart from the spectra of the strain meter array at BFO [*Widmer et al.*, 1992], the SGs have contributed some of the best detections of the fundamental toroidal mode, ${}_0T_2$ which only shows up in vertical

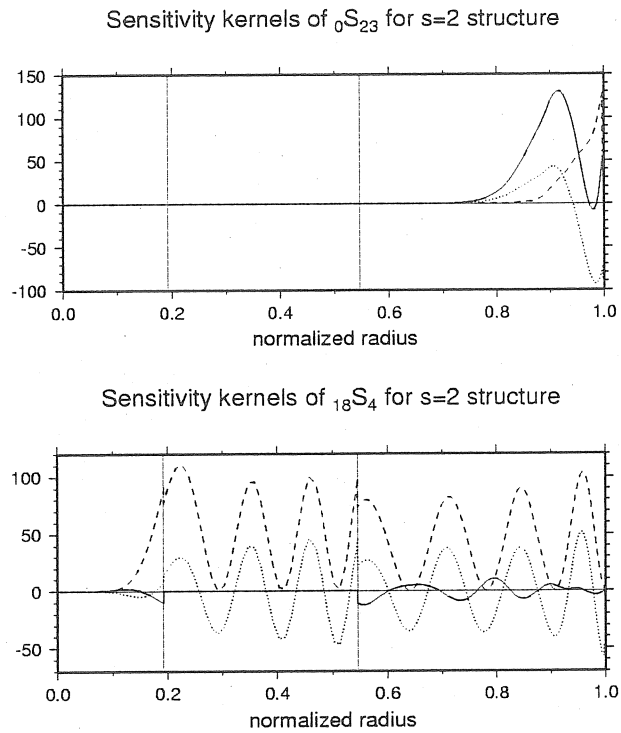

Figure 11. Sensitivity kernels for two modes with well observed structure coefficients: the fundamental mode $_0S_{23}$ and the overtone $_{18}S_4$. The Vp-kernels (dashed) and for $_0S_{23}$ also the Vs-kernel (solid) have a positive mean value while the density kernels (dotted) oscillate for both modes around a zero mean value. $_{18}S_4$ is a PKIKP-equivalent mode ans as such it is not expected to have much sensitivity to Vs structure.

component recordings through Coriolis coupling with nearby spheroidal multiplets.

Here, we only like to repeat what was already pointed out by *Zürn et al.* [2000], namely that Coriolis coupling provides linear constraints on the density profile, very similar to Zeeman splitting.

3.4. Encoding of 3-D Density structure in mode spectra

The reduced symmetry of aspherical Earth models has as a direct consequence the removal of the degeneracy of the singlet eigenfrequencies - the multiplets are split. Within the framework of first order perturbation theory this splitting can be linearly related to aspherical structure. Consider the k-th multiplet $_nS_\ell$. Its splitting can be described with the so called aspherical structure coefficients, c_s^t. The structure coefficients are linearly related to aspherical structure of harmonic degree, s, and azimuthal order, t, through [*Woodhouse and Dahlen*, 1978]:

$$ {}_kc_s^t = \int_0^a \left({}_kP_s \frac{\alpha_s^t}{\alpha_0} + {}_kS_s \frac{\beta_s^t}{\beta_0} + {}_kD_s \frac{\rho_s^t}{\rho_0} \right) dr \qquad (3) $$

where $\alpha_s^t(r)$, $\beta_s^t(r)$, $\rho_s^t(r)$ are the sought spherical harmonic expansion coefficients of Vp, Vs and density, ρ and quantities with subscript zero refer to the spherically symmetric reference model. Furthermore, $_kP_s(r)$, $_kS_s(r)$ and $_kD_s(r)$ are the kernels relating the relative volumetric perturbations of harmonic degree s to the mode splitting as represented by the aspherical structure coefficients.

The kernels of the modes $_0S_{23}$ and $_{18}S_4$ are shown in fig. 11. While Vp, Vs and density kernels are all of similar amplitude they differ in one very important aspect: Vp and Vs kernels have (at least for one of the two modes) a positive mean value while the density kernels oscillate for both modes around a zero mean. This situation is representative for all modes for which the structure coefficients, c_s^t, could be estimated. For the linear inverse problem posed in eq. 3 this means that any model with a non-zero mean for a particular spherical harmonic degree s and order t lies outside the space spanned by the set of kernels that belong to our structure coefficients! Hence our data do not allow us to make any inference on such models. To give an example: a model with a constant excess ellipticity in density of 1% ($\rho_2^0(r)/\rho_0(r) = -0.01$) leads to no additional mode splitting and cannot by reconstructed from our structure coefficients. The only exceptions are the hand full of modes below 1 mHz for which the density kernels do not integrate to zero (see fig. 10).

For completeness we mention that inversions for 3-D perturbations can also be carried out in the parameter space (μ, K, ρ). The sensitivity kernels in this representation are significantly different from the kernels in a (Vp, Vs, ρ)-representation [eq. A6 in *Ritzwoller and Lavely*, 1995]. However it turns out, that in that representation μ and ρ are well constrained model parameters while incompressibility K is as ill constrained as ρ in the (Vp, Vs, ρ)-representation. [see fig. 31 in *Ritzwoller and Lavely*, 1995].

In other words - independent of the chosen parameterization we are largely unable to estimate three independent parameters. The only exception to this bleak situation are the splittings of modes below 1 mHz which - through the effect of self-gravitation - posses additional sensitivity to density.

Whether 3-D density structure can be estimated independently of Vp and Vs structure is hotly debated in the literature. On the one hand *Ishii and Tromp* [1999] claim to succeed in the endeavor while [*Masters et al.*, 2000] present a number of inversion experiments to show that no significant improvement in the fit to the observed structure coefficients can be achieved by allowing for 3-D density structure.

The observation that density kernels in the (Vp, Vs, ρ)-representation are essentially zero mean for modes above 1 mHz constitutes a strong argument in favor of the conclusions by *Masters et al.* [2000].

4. Conclusions

We have shown, that below 1.5 mHz the most recent generation of superconducting gravimeters are competitive with the best spring gravimeters and seismometers and that for the modes below 0.6 mHz they have produced spectra with some of the highest signal-to-noise ratio sofar. The band in which SGs excel is also the band where splitting of modes possesses comparatively high sensitivity to 3-D density structure in the Earth's mantle and Core. To observe this splitting and constrain lateral density structure is one avenue of research for which SGs are uniquely suited.

Acknowledgments. I thank Walter Zürn for numerous discussions and critical inputs and Jacques Hinderer for the SG meter data from J9. The network centers of the German Regional Seismic Network, SZGRF at Erlangen and the IRIS/DMC at Seattle for archiving and distributing the data from the different sensors at BFO are greatfully acknowledged.

References

Agnew, D., and J. Berger, Vertical seismic noise at very low frequencies, *J. Geophys. Res.*, *83*, 5420–5424, 1978.

Astiz, L., and K. Creager, Noise study for the federation of digital seismic stations, *FDSN Station Book*, *1*, –, 1995.

Backus, G., and J. Gilbert, The rotational splitting of the free oscillations of the earth, *Proc. Natl. Acad. Sci.*, *47*, 362–371, 1961.

Banka, D., and D. Crossley, Noise levels of superconducting gravimeters at seismic frequencies, *Geophys. J. Int.*, *139*, 87–97, 1999.

Crossley, D., et al., Network of superconducting gravimeters benefit a number of disciplines, *EOS Trans. AGU*, *80*, 125–126, 1999.

Dahlen, F., The spectra of unresolved split normal mode multiplets, *Geophys. J. R. Astron. Soc.*, *58*, 1–33, 1979.

Ekström, G., Time domain analysis of the earth's background seismic radiation, *J. Geophys. Res.*, *106*, 26,483–26,494, 2001.

Ishii, M., and J. Tromp, Normal-mode and free air gravity constraints on lateral variations in velocity and density of the Earth's mantle, *Science*, *285*, 1231–1236, 1999.

Masters, G., J. Park, and F. Gilbert, Observations of coupled spheroidal and toroidal modes, *J. Geophys. Res.*, *88*, 10,285–10,298, 1983.

Masters, G., G. Laske, and F. Gilbert, Matrix autoregressive analysis of free-oscillation coupling and splitting, *Geophys. J. Int.*, *143*, 478–489, 2000.

Masters, T. G., and R. Widmer, Free-oscillations: frequencies and attenuations, *Global Earth Physics: A Handbook of Physical Constants*, *American Geophysical Union*, 104–125, 1995.

Nawa, K., N. Suda, Y. Fukao, T. Sato, Y. Tamura, K. Shibuya, H. McQueen, H. Virtanen, and J. Kääriäinen, Incessant excitation of the earth's free oscillations: global comparison of superconducting gravimeter records, *Phys. Earth Planet. Int.*, *120*, 289–297, 2000.

Nishida, K., N. Kobayashi, and Y. Fukao, Resonant oscillations between the solid earth and the atmosphere, *SCIENCE*, *287*, 2244–2246, 2000.

Nishida, K., N. Kobayashi, and Y. Fukao, Origin of earth's ground noise from 2 to 20 mhz, *Geophys. Res. Lett.*, *in press*, –, 2002.

Peterson, J., Observations and modeling of seismic background noise, *U. S. Geol. Surv., Open-file Rep.*, *93-322*, 1–45, 1993.

Resovsky, J., and M. Ritzwoller, New and refinded constraints on the three-dimensional earth structure from normal modes below 3 mhz, *J. Geophys. Res.*, *103*, 783–810, 1998.

Richter, B., H.-G. Wenzel, W. Zürn, and F. Klopping, From chandler wobble to free oscillations: comparison of cryogenic gravimeters and other instruments in a wide period range, *Phys. Earth Planet. Int.*, *91*, 131–148, 1995.

Ritzwoller, M., and E. Lavely, Three-dimensional seismic models of the earth's mantle, *Reviews of Geophysics*, *33*, 1–66, 1995.

Ritzwoller, M., G. Masters, and F. Gilbert, Constraining aspherical structure with low frequency interaction coefficients: Application to uncoupled multiplets, *J. Geophys. Res.*, *93*, 6369–6396, 1988.

Smith, M., and G. Masters, Aspherical structure constraints from free oscillation frequency and attenuation measurements, *J. Geophys. Res.*, *94*, 1953–1976, 1989.

Suda, N., K. Nawa, and Y. Fukao, Earth's background free oscillations, *Science*, *279*, 2089–2091, 1998.

Van Camp, M., Measuring seismic normal modes with the GWR C021 superconducting gravimeter, *Phys. Earth Planet. Inter.*, *116*, 81–92, 1999.

Warburton, R. J., and J. M. Goodkind, The influence of barometric pressure variations on gravity, *Geophys. J. R. Astron. Soc.*, *48*, 281–292, 1977.

Widmer, R., W. Zürn, and G. Masters, Observation of low order toroidal modes from the 1989 Macquarie rise event, *Geophys. J. Int.*, *111*, 226–236, 1992.

Widmer-Schnidrig, R., Application of regionalized multiplet stripping to retrieval of aspherical structure constraints, *Geophys. J. Int.*, *148*, 201–213, 2002.

Woodhouse, J., and F. Dahlen, The effect of a general aspherical perturbation on the free oscillations of the earth, *Geophys. J. R. Astron. Soc.*, *53*, 335–354, 1978.

Zürn, W., and R. Widmer, On noise reduction in vertical seismic records below 2 mHz using local barometric pressure, *Geophys. Res. Lett.*, *22*, 3537–3540, 1995.

Zürn, W., G. Laske, R. Widmer-Schnidrig, and J. Gilbert, Observation of Coriolis coupled modes below 1 mhz, *Geophys. J. Int.*, *143*, 113–118, 2000.

R. Widmer-Schnidrig, Black Forest Observatory, Institute of Geophysics, Stuttgart University, Heubach 206, D-77709 Wolfach, Germany

April 1, 2002; revised November 11, 2002; accepted December 25, 2002.

This preprint was prepared with AGU's LaTeX macros v4, with the extension package 'AGU++' by P. W. Daly, version from .

Preliminary Results of the Earth's Free Oscillations after Peru Earthquake Observed using a SG in China

Xiang'e LEI, Houze XU and Heping SUN

(Laboratory of Dynamic Geodesy, Institute of Geodesy and Geophysics, Chinese Academy of Sciences, Wuhan 430077, China, xiangelei@263.net)

Abstract: We investigated the Earth's normal modes excited after the June 23, 2001 Peru Earthquake recorded with the superconducting gravimeter at station Wuhan/China. After removing effectively the tidal gravity and pressure perturbation signals, all the base normal modes from ${}_0S_0$ to ${}_0S_{32}$, the splitting modes of the ${}_0S_2$ and ${}_0S_3$ and some of the harmonic modes are observed obviously.

1 Introduction

It is well known the large earthquake can not only excite the Earth's body and surface waves, but also the Earth's free oscillation (EFO). Comparing those in the theoretical prediction, the EFO can provide us with the information independently to the seismology in researching for the variation of the Earth's inner geophysical properties (Crossley and Hinderer, 1994). The first two successful observations of the EFO are based on the strainmeter (Benioff et al 1961) and spring gravimeter (Ness et al 1961), their results coincided with theoretical estimations.

The studies show that the gravity recording can embody the signals of the spheriodal modes of the EFO. The superconducting gravimeters (SG), which possesses a very wide linear dynamic range, low noise and instrumental drift, are now considered as the most reliable instruments in the investigation of the small change in the Earth's gravity field. The global network of the SG become now the main tool in the study of the geophysical and geodynamic problems around world (Sun and Xu, 1997). The basic normal and harmonic modes observed with the SG after the 1996 Irian and the 1998 Baleny large earthquakes have been investigated by Van Camp (Van Camp, 1999). In this paper, we will check all the basic normal modes of the EFO between ${}_0S_0$ and ${}_0S_{32}$, the splitting models of the ${}_0S_2$ and ${}_0S_3$ and some harmonic modes by analyzing the SG data at Wuhan station, after Peru Ms 7.9 earthquake at 20:33:16 on June 23, 2001 (latitude: 16.00°, longitude: 73.70°W).

2 Techniques of the data processing

The influence of long-term gravity variation might be neglected, when checking the EFO modes by using the SG data after the large earthquake. The sampling of the Wuhan SG observation is given as 20 s, the total numbers of the data used in this study is 23,500. The spline interpolation method at the order of 3 is used in order to obtain the pressure data rate of 20 s from origin 10 minutes sampling. Some perturbations as spikes and small earthquake events are corrected .

The former researchers (Ness et al, 1961 and Van Camp, 1999) removed the tidal gravity signals from observations by using digital filter, when the EFO modes are checked. However, in our study, the least square polynomial fitting is adopted to remove fragmentally gravity tides (Ding, 1997). We fit the data points in total of 4,000 (about 22 hours) once, by taking fitting polynomial at order of 20. The former 8,000 points are divided into two sections and the points between 10001 and 23500 are divided into four sections. The analysis shows that taking the polynomial at the order of 20 is enough for removing the two standing and two inflexion parts in the data section.

By integration theoretically the atmospheric gravity Green's function with the pressure around station, the pressure gravity admittance as of -0.3603 μGal/hPa is obtained (Sun, 1997). By taking a

regression between the SG tidal gravity residuals and the station pressure, a regression coefficient at station Wuhan is got as of -0.307 μGal/hPa (Xu et al 1999). The results show that the discrepancy is small when using the above two coefficients to correct pressure influence in the EFO band. Then an average value as of -0.326 μGal/hPa is adopted in our study. The results show that the tidal polynomial fitting could eliminate signals at the low frequency normal modes that will probably influence the resolution. The EFO modes are then calculated by applying the Discrete Fourtier Transform to tidal gravity residual.

The station noise is necessary to be taken into account before checking the EFO modes, it is reasonable to take the noise in a quite earthquake period as normal one and to remove them from the data set (Banka, 1998). If the checked EFO modes signals are larger than 3 time of the normal noise level, then these modes are adopted automatically in the computation procedure.

3 Results and discussions

The spectral results of the EFO modes are given in figures 1, 2 and 3, it is found that all the base modes from ${}_0S_0$ to ${}_0S_{32}$ are clearly shown, some numerical results are given in table 2. In order to comparison, the HB1 model and some results obtained by Benioff et al and Ness et al are also listed. In table 2 it is found that the splitting modes of the ${}_0S_2$ and ${}_0S_3$ are also observed obviously. All the base modes between ${}_0S_4$ and ${}_0S_{32}$ observed with our SG are in accordance with those given in the HB1 model and those observed with the strainmeter and the spring gravimeter. The discrepancy is generally not more than 2.0‰. Some harmonic modes observed with our SG are shown in Fig.2.

We successfully observed the spheriodal modes of the EFO by using SG C032 at station Wuhan/China. Different from the former researchers, the gravity tides are removed fragmentally by using with a polynomial fitting at order of 20. In the period between 140 to 250 s, the EFO modes with frequency higher than ${}_0S_{32}$ are observed. Many basic and harmonic modes are in good agreement with those in the publications, but some disagreement are probably related to the heterogeneity of earth mantle. It is believed that some satisfying answers for these problems will be obtained in the future Global Geodynamic Project.

Table2 Observational and theoretical periods of all normal modes form ${}_0S_0$ to ${}_0S_{32}$

modes	P(1) /m	P(2) /m	P(3) /m	P(4) /m	modes	P(1) /m	P(2) /m	P(3) /m	P(4) /m
${}_0S_0$		20.46	20.45	20.48	${}_0S_{17}$	6.48	6.488	6.490	6.495
${}_0S_2$	53.1-54.7	52.80-54.98	53.22-56.23	53.78	${}_0S_{18}$	6.23	6.232	6.237	6.237
${}_0S_3$	35.2-35.9	35.24-35.87	35.28-35.82	35.59	${}_0S_{19}$	6.01	6.002	6.003	6.002
${}_0S_4$	25.8	25.85	25.77	25.78	${}_0S_{20}$	5.78	5.778	5.790	5.790
${}_0S_5$	19.8	19.83	19.78	19.85	${}_0S_{21}$	5.59	5.608	5.599	5.597
${}_0S_6$	16.0	16.07	16.05	16.07	${}_0S_{22}$	5.39	5.423	5.417	5.420
${}_0S_7$	13.5	13.42	13.53	13.54	${}_0S_{23}$	5.26	5.255	5.250	5.255
${}_0S_8$	11.81	11.78	11.80	11.80	${}_0S_{24}$	5.10	5.104	5.107	5.103
${}_0S_9$	10.56	10.57	10.57	10.56	${}_0S_{25}$	4.96	4.959	4.961	4.962
${}_0S_{10}$	9.66	9.685	9.671	9.657	${}_0S_{26}$	4.83	4.828	4.823	4.828
${}_0S_{11}$	8.98	8.934	8.932	8.952	${}_0S_{27}$	4.69	4.703	4.708	4.705
${}_0S_{12}$	8.37	8.368	8.369	8.377	${}_0S_{28}$	4.59	4.585	4.578	4.587
${}_0S_{13}$	7.88	7.882	7.889	7.892	${}_0S_{29}$	4.47	4.476	4.461	4.475
${}_0S_{14}$	7.47	7.468	7.467	7.473	${}_0S_{30}$	4.37	4.366	4.376	4.370
${}_0S_{15}$	7.10	7.101	7.102	7.107	${}_0S_{31}$	4.27	4.270	4.274	4.270
${}_0S_{16}$	6.78	6.780	6.776	6.783	${}_0S_{32}$	4.18	4.167	4.171	4.175

Note: P(1) and observed by Benioff at el with strainmeter, P(2) given by Ness at el with spring gravimeter, P(3) investigated by us with SG C032 and P(4) provided by HB1 model

Acknowledgement This work is supported jointly by the National Natural Science Foundation of China (grant Nos. 40074018 and No. 49925411)

References

[1] Banka D, Jentzsch G, Crossley D. Investigations of superconducting gravimeter records in the frequency range of the free oscillations of the earth-the noise magnitude. In:Durcarme B, Paquet P, eds. Proc. 13th Symp. Earth Tides, Brussels, 1998: 641~648.

[2] Benioff H, Press F, Smith S. Excitation of the free Oscillations of the Earth by Earthquakes. J. Geophys. Res, 1961, 66 (2): 605~619.

[3] Crossley D J, Hinderer J. Global Geodynamics Project-GGP: status report 1994. In: Poitevin C, eds .Proceeding of the workshop on Non-tidal Gravity changes. Luxembourg: via Conseil de L'Europe Cahiers du Centre Européen de Géodynamique et de Séismologie, 1995(11): 244 ~269.

[4] Ding Y R. Processing method of astronomical data. Nanjing: Nanjing University Press, 1997,190~202.

[5] Haddon R A, Bullen K E. An earth model incorporating free earth oscillation data. Phys Earth and Plan Int., 1969(2): 35~42.

[6] Ness N R, Harrison C T, Slichter L B. Observation of the free oscillation of the earth. J.Geophys. Res., 1961, 66(2): 621~629.

[7] Sun H P, Xu H Z. Execution and prospect for the global geodynamics project cooperation. Advance in Earth Sciences, 1997,12(2): 152~157.

[8] Sun H P. Atmospheric gravity Green's function. Chinese Science Bulletin, 1997, 42(1): 712~1719.

[9] Van Camp M. Measuring Seismic normal modes with the GWR C021 Superconducting gravimeter. Phys. Earth and Plan Int., 1999 (116): 81~92.

[10] Xu J Q, Hao X H, Sun H P. Influence of atmospheric pressure on tidal gravity at Wuhan station. Acta.Geophysica. Sinica, (Chinese), 1999,28(1): 21~27.

[11] Zürn W, Widmer R. On noise reduction in vertical Seismic records below 2mHz using local barometric pressure. Geophys. Res Let. , 1995(22): 3537~3540.

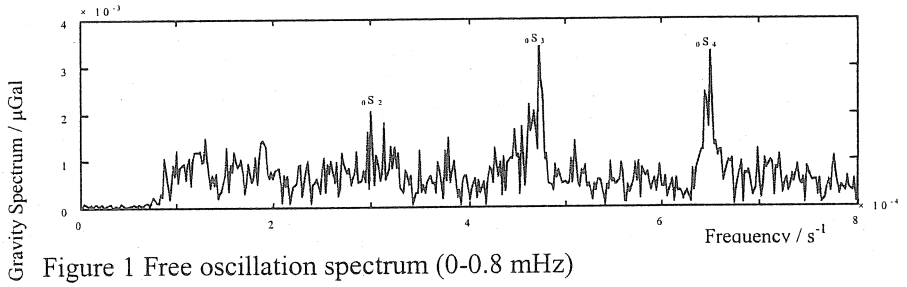

Figure 1 Free oscillation spectrum (0-0.8 mHz)

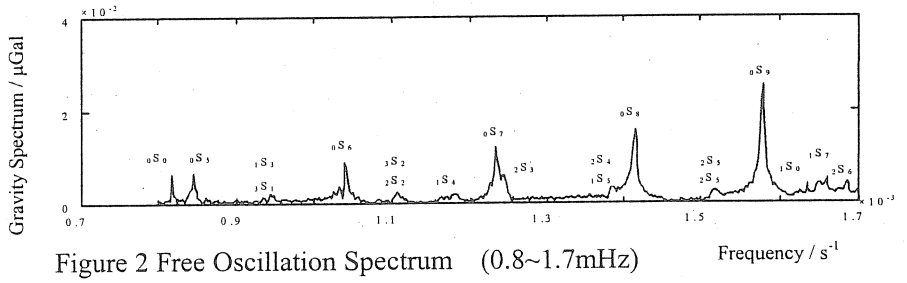

Figure 2 Free Oscillation Spectrum (0.8~1.7mHz)

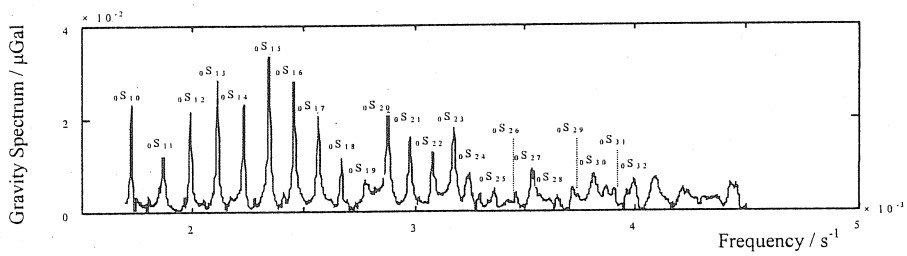

Figure 3 Free Oscillation Spectrum (1.7~4.5mHz)

A 3.7 mHz - gravity signal on June 10, 1991

by

Walter Zürn, Bettina Bayer and Rudolf Widmer-Schnidrig

Black Forest Observatory Schiltach (BFO), Universities Karlsruhe/Stuttgart
Heubach 206
D-77709 Wolfach, Germany

1 Introduction

The paroxysmal Mount Pinatubo eruption of June 15, 1991 excited Rayleigh waves which traveled around the globe (Kanamori and Mori, 1992; Widmer and Zürn, 1992; Kanamori et al., 1994; Zürn and Widmer, 1996). These waves were essentially bichromatic with frequencies of 3.68 and 4.44 mHz and were identified as vertical modes of the atmosphere (i. e. Lognonné et al., 1998) excited by the volcanic eruption. These oscillations in turn excited the observed Rayleigh waves.

Japanese scientists recently observed continuous vibrations of the earth ("hum" for short) in the frequency band between 2 and 7 mHz involving the fundamental spheroidal modes ${}_oS_l$ (e. g. Nawa et al. 1998, Suda et al. 1998, Kobayashi and Nishida 1998, Tanimoto et al. 1998). Atmospheric pressure fluctuations are the preferred source of excitation because seasonal variation of the amplitudes on one hand and higher amplitude of the modes near 3.68 mHz on the other were also observed and energy estimates corroborate this idea (e. g. Kobayashi and Nishida 1998; Tanimoto and Um 1999; Nishida and Kobayashi 1999; Ekström, 2001).

Among other observations Zürn and Widmer (1996) mention a harmonic signal with 3.68 mHz five days before the Pinatubo eruption. This will be described in more detail in the following.

2 Observations

On June 10, 1991 between 15:30 and 17:45 UTC a phase-coherent oscillation with a double amplitude of 40 nanogals was observed in the record of the LaCoste-Romberg Earth Tide gravimeter (ET-19, Richter et al. 1995) at BFO (Fig. 1).

The double amplitude of the Pinatubo Rayleigh waves at BFO was estimated to be about 500 nanogals, the incessantly excited modes have amplitudes of at most 1 nanogal. A magnitude 6.5 earthquake on the Northern Midatlantic ridge constrains the analysis at the end of the time window, but from the BFO record it appears as if the harmonic signal dies out shortly before the first arrivals from this event. Spectral analysis showed, that the frequency of this oscillation was 3.68 mHz (Fig. 2).

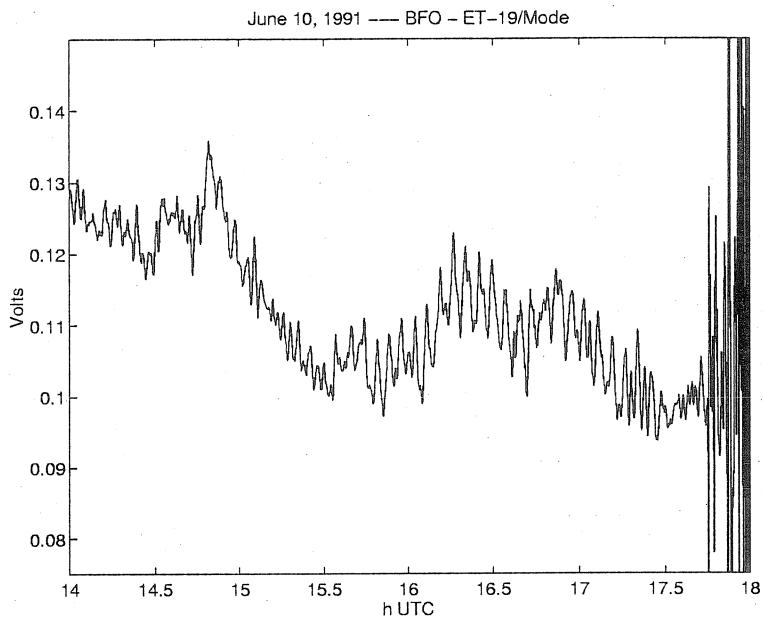

Figure 1: Record from mode-channel of the LaCoste-Romberg gravimeter ET-19 at BFO from 14:00 to 18:00 on June 10, 1991 (UTC). Note the oscillation between 15:30 and 17:30 which has a double amplitude of 40 nanogals. After 17:30 the waves from an earthquake on the Northern Midatlantic ridge arrive at BFO.

Subsequently records from seismic stations around the world were inspected for similar oscillations but signals could only be detected clearly in the records of vertical component STS-1 seismometers at ECH and SSB (GEOSCOPE) and at BNI (MedNet) in the same time period. Stations BFO, ECH and SSB are located on one side (northern and western) of the Alps, BNI lies centrally in the western Alps (Fig. 3).

While at SSB and ECH the oscillation was also phase-coherent, this was not the case at BNI, where a phase jump of $\pi/2$ occurred in the middle of the record. This is the reason for the deformed spectral peak for this record (Fig. 4).

All other instruments at BFO (STS-1 prototypes, strain- and tiltmeters) did not show this signal clearly above the noise. Since the 3.68 mHz pointed to an atmospheric connection, we also inspected barograms and magnetograms from several German and French stations but without success. Unfortunately a barometer record from SSB was not available for this time period.

3 Search for a possible source

Of course, our first suspects were the then active volcanoes Mount Pinatubo (Philippines) and Mount Unzen (Japan). However, no especially violent eruptions occurred on that day at either of these two and if one of them had been the source of these waves the rather quiet stations in Japan and China should have shown the oscillations very clearly, which is not the case. Although several volcanoes were active at the time, we were not able to identify an unusually violent phase at any of them. Note that a few

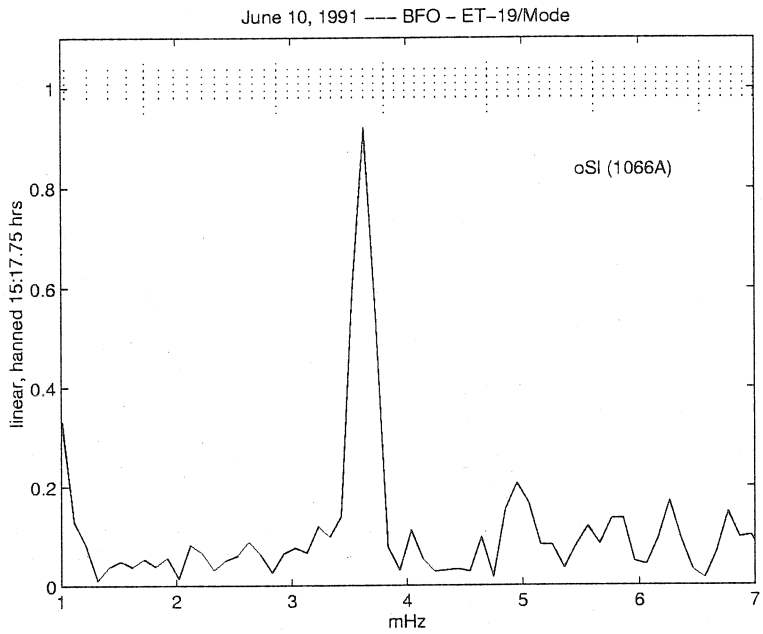

Figure 2: Spectrum of the part of record shown in Fig. 1 between 15:00 and 17:45 after application of a hanning window and padding with zeros. Theoretical frequencies of the fundamental spheroidal modes for 1066A are indicated at the top (longer lines belong to ${}_oS_{10}$, ${}_oS_{20}$ and so forth to ${}_oS_{60}$). The peak aligns well with ${}_oS_{28}$. Raw seismograms were used here.

violent eruptions at other times were checked for Pinatubo/El Chichón type signals as described in Zürn and Widmer (1996) but without success, while Kanamori et al. (1994) found a signal from Mount St. Helens in the nearfield of the volcano.

Since huge thunderstorms also produced oscillations with this frequency in the ionosphere (Georges, 1973) we had to look also for sources in the atmosphere. We tried to obtain information about unusual meteorological phenomena in Central Europe by phone calls and letters to meteorologists and atmospheric physicists at the universities of Karlsruhe, Frankfurt and Zrich, without finding anything unusual. According to meteorologists in Karlsruhe (Hoeschele, pers. comm.) there were a few thermal thunderstorms in the general area of the 4 stations, but none of them was especially powerful. Studies of weather maps also did not reveal anything special on this day.

We obtained satellite photos of Central Europe from EUMETEOSAT in the spectral bands 0.5 - 0.9 μm (visible spectra, VIS), 5.7 - 7.1 μm (water vapor, WV) and 10.5 - 12.5 μm (infrared, IR). The photos were taken every half hour. In the WV band (only) an interesting very weak plane-wave like feature with a wavelength of 94 km could be identified. The crests of these waves were oriented in EW direction and were about 300 km long, while the NS extent was about 1000 km. The center of the field lies between Paris and Strasbourg, i. e. west of station ECH. The possibility exists, that this is an acoustic-gravity wave with a horizontal wavelength of 94 km and a frequency of 3.7 mHz, but then why does it not show up on the high resolution

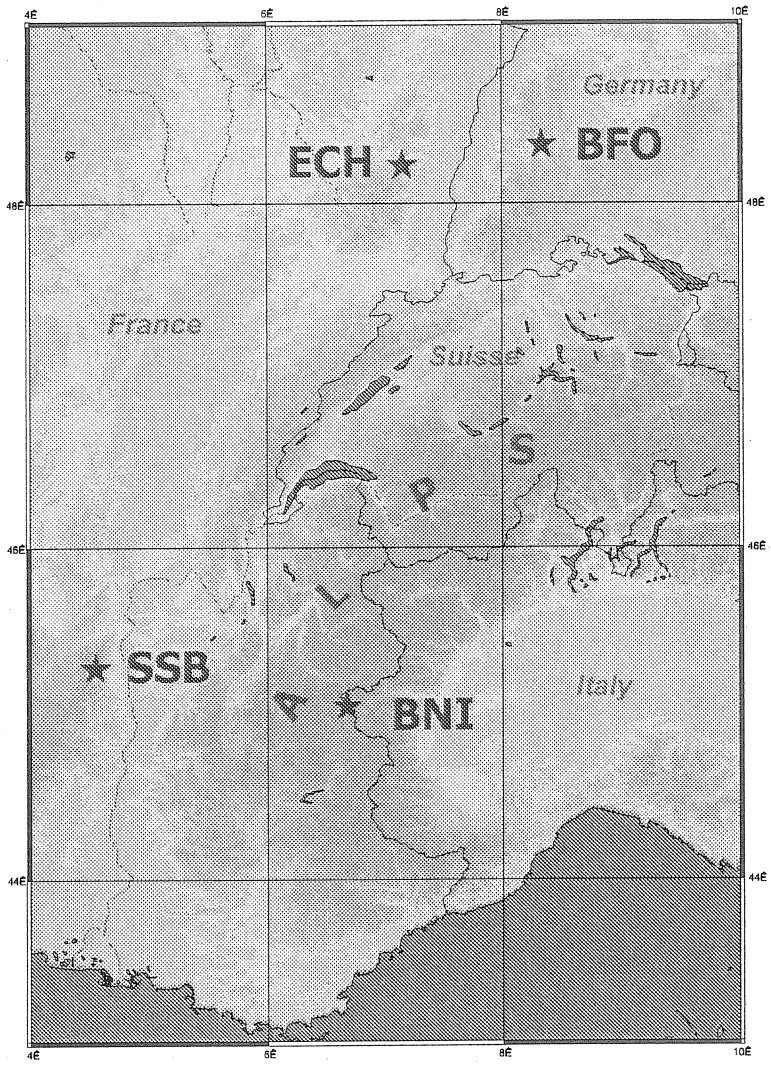

Figure 3: Map showing the locations of the 4 stations.

barograms of Strasbourg and BFO? For an isothermal atmosphere with a scale height of 9000 m the vertical wavenumber would be imaginary for these parameters, but an isothermal atmosphere is a poor approximation to the real one. Another question then would be why the frequency of this wave is a identical to the eigenfrequency of a vertical mode of the atmosphere while it is propagating horizontally. The feature in the satellite photos is so weak, that a propagation of the feature with time could not be determined. We have not yet ruled out the possibility that this feature is an artifact in the satellite pictures.

Lognonné (pers. comm. 1998) suggested a meteorite impact on the earth's atmosphere could have excited this mode of the atmosphere just like Shoemaker-Levy did on Jupiter in 1994, since the signal was observed during a summer afternoon in Central Europe nothing is known about such an event.

The atmospheric Lamb waves from Krakatoa, Mount St. Helens, the 1908 Tunguska event and atmospheric nuclear explosions were dispersed wave trains, not monochro-

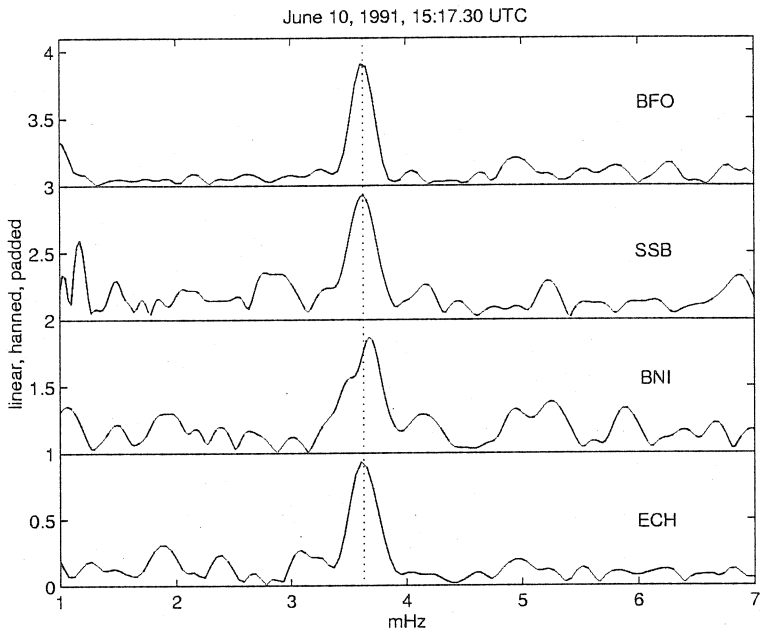

Figure 4: Spectra of the seismograms (15:00 - 17:30) of the 4 European stations. Note the deformation of the peak for BNI. Using a boxcar window results in a double peak for this station.

matic oscillations for nearly two hours. Just like in the cases of Mount Pinatubo and El Chichón the source was most likely an oscillatory one. We inspected the records from the BFO gravimeter for the years 1976 through 2001 for similar (or larger) harmonic signals without success outside of earthquakes and the volcanoes mentioned.

The only evidence pointing to a source in the atmosphere is the special frequency, nothing else. On the other hand, the frequency belongs to the fundamental spheroidal mode ${}_oS_{28}$ of the solid earth. Impulsive sources (e. g. earthquakes, including slow and silent ones) have a broad spectrum and cannot excite monochromatic oscillations. However, could this be a special (extremely strong) case of the "hum", once in 25 years? On the other hand, could signals like this (whatever the source) contaminate the hum studies and produce statistically the higher amplitude at this frequency?

4 Global signal after all ???

In desperation we looked at the seismograms of the Global Seismic Networks again after 10 years. IRIS and GEOSCOPE data of vertical component STS-1 seismometers were retrieved from the data center and hanned spectra were computed for overlapping 3 hour windows and inspected for energy at 3.7 mHz. We did not find conspicuous peaks in the majority of them. However, there were peaks in the spectra for stations RPN (Easter Island) and ESK (Scotland) but with smaller signal-to-noise ratios (SNR) than for the Central European stations. Then we inspected these time series again between 14:30 and 17:30 UTC and selected the 20 most quiet seismograms and separated those into two groups by quality. The 10 best were ANMO, CAN, COR, ESK, GSC, INU,

PAS, SBC, SUR and TAM, the nine of slightly lesser quality were ERM, HRV, HYB, ISA, KIP, MAJO, RPN and WFM. The raw time series were divided by the magnitude of the transfer-function at 3.7 mHz to get true acceleration spectra in the vicinity of our signal. Then the spectra were multiplied and the product spectrum showed an extremely clear peak at 3.68 mHz. In several steps we then removed the stations which appeared to reduce the SNR when included in the product and retained only the 10 "best": ANMO, COR, ESK, KIP, MAJO, PAS, RPN, SBC, SUR and WFM. This product spectrum is shown in Fig. 5. The only individual spectrum of the 10 showing a clear peak is from RPN, shown in Fig. 6.

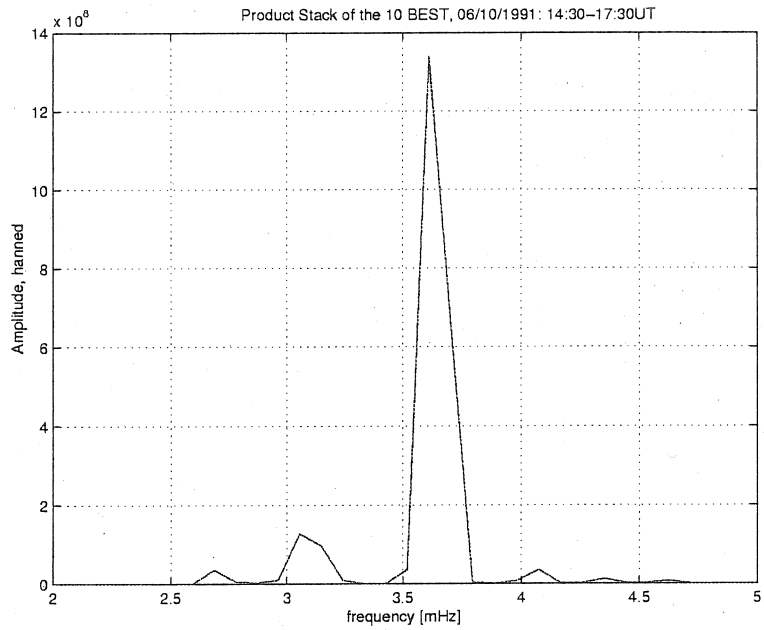

Figure 5: Product spectrum of the 10 quietest stations found for this time interval. These stations are: ANMO, COR, ESK, KIP, MAJO, PAS, RPN, SBC, SUR and WFM. Note that none of the spectra shown in Fig. 3 was used.

Acknowledgments: We thank Jacques Hinderer for providing pressure and gravity records from station J9 (near Strasbourg) and from Echéry. We obtained satellite photos from EUMETEOSAT free of charge, which is highly appreciated.

References

Ekström, G. (2001). Time domain analysis of Earth's long-period background seismic radiation. *J. geophys. Res.*, **106**: 26,483 - 26493.

Georges, T. M. (1973). Infrasound from Convective Storms: Examining the Evidence. *Rev. Geophys. Space Phys.*, **11**: 571 - 594.

Kanamori, H., Mori, J. (1992). Harmonic excitation of of mantle Rayleigh waves by the 1991 eruption of Mount Pinatubo, Philippines. *Geophys. Res. Lett.* **19**: 721 - 724.

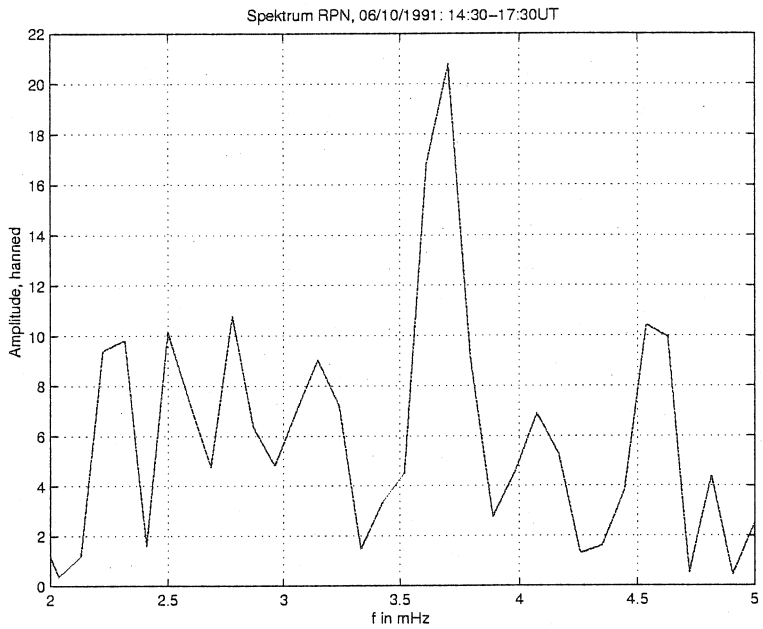

Figure 6: Spectrum of the seismogram (14:30 - 17:30) from RPN. Note that SNR is inferior to the ones in Fig. 4.

Kanamori, H., Mori, J., Harkrider, D. G. (1994). Excitation of atmospheric oscillation by volcanic eruptions. *J. Geophys. Res.*, **99**: 21,947 - 21,961.

Kobayashi, N., Nishida, K. (1998). Continuous excitation of planetary free oscillations by atmospheric disturbances. *Nature* **395**: 357 - 360.

Lognonné, P., Clévédé, E., Kanamori, H. (1998). Computation of seismograms and atmospheric oscillations by normal mode summation for a spherical earth model with realistic atmosphere. *Geophys. J. Int.*, **135**: 388 - 406.

Nawa, K., Suda, N., Fukao, Y., Sato, T., Aoyama, Y., Shibuya, K. (1998). Incessant excitation of the Earth's free oscillations. *Earth Planets Space*, **50**: 3 - 8.

Nishida, K., Kobayashi, N. (1999). Statistical features of Earth's continuous free oscillations. *J. geophys. Res.*, **104**: 28,741 - 28,750.

Richter, B., H.-G. Wenzel, W. Zürn and F. Klopping (1995). From Chandler wobble to free oscillations: comparison of cryogenic gravimeters and other instruments in a wide period range. *Phys. Earth planet. Inter.*, **91**, 131 - 148.

Suda, N., Nawa, K., Fukao, Y. (1998). Earth's Background Free Oscillations. *Science*, **279**: 2089 - 2091.

Tanimoto, T., Um, J. (1999). Cause of continuous oscillations of the Earth. *J. geophys. Res.*, **104**: 28,723 - 28739.

Tanimoto, T., Um, J., Nishida, K., Kobayashi, N. (1998). Earth's continuous oscillations observed on seismically quiet days. *Geophys. Res. Lett.* **25**: 1553 - 1556.

Widmer, R., Zürn, W. (1992). Bichromatic excitation of long-period Rayleigh and air waves by the Mount Pinatubo and El Chichón volcanic eruptions. *Geophys. Res. Lett.* **19**: 765 - 768.

Zürn, W., Widmer, R., 1996: World-Wide Observation of Bichromatic Long Period Rayleigh-waves Excited During the June 15, 1991 Eruption of Mt. Pinatubo. In: The 1991 Eruption of Mt. Pinatubo (C. Newhall and R. Punongbayan, Eds.), USGS, Washington, pp 615 - 624.